10484
NACA TN 4147

TECH LIBRARY KAFB, NM
0067042

NATIONAL ADVISORY COMMITTEE FOR AERONAUTICS

TECHNICAL NOTE 4147

MEASURED AND PREDICTED DYNAMIC RESPONSE CHARACTERISTICS OF A FLEXIBLE AIRPLANE TO ELEVATOR CONTROL OVER A FREQUENCY RANGE INCLUDING THREE STRUCTURAL MODES

By Henry A. Cole, Jr., and Euclid C. Holleman

Ames Aeronautical Laboratory
Moffett Field, Calif.

Washington
February 1958

AFMDC
TECHNICAL LIBRARY

TECH LIBRARY KAFB, NM

0067042

NATIONAL ADVISORY COMMITTEE FOR AERONAUTICS

TECHNICAL NOTE 4147

MEASURED AND PREDICTED DYNAMIC RESPONSE CHARACTERISTICS OF A FLEXIBLE AIRPLANE TO ELEVATOR CONTROL OVER A FREQUENCY RANGE INCLUDING THREE STRUCTURAL MODES

By Henry A. Cole, Jr., and Euclid C. Holleman

SUMMARY

The longitudinal frequency response of a large flexible swept-wing airplane, as determined from its measured response to elevator pulses, is presented over the operating Mach number range at altitudes from 15,000 to 35,000 feet. Response quantities for the nose, center of gravity, wing tip, and tail are shown for frequencies from the airplane short-period mode to the fuselage first-bending mode.

Comparisons are made between the measured responses and responses predicted by dynamical analyses with up to three structural degrees of freedom. The forms of transfer functions needed to simulate the response over several frequency bands are shown. The dynamic response measured in flight is interpreted in terms of lines of low response, and comparisons are made with predicted lines of low response and node lines predicted by free-free analysis and measured in ground vibration tests.

INTRODUCTION

The mass distribution and structural flexibility of some recent high-aspect-ratio swept-wing bombers and transports has resulted in airplanes with relatively low frequency structural modes. Consequently, the response of these airplanes to disturbances such as control inputs and gust loads consists of large structural deflections as well as motions of the airplane as a whole. Various parts of the airplane, then, are subjected to widely different accelerations. These accelerations not only affect the local structural stress, but also influence the operation of mechanical and electronic equipment. When the airplane is equipped with an automatic control system, the local dynamic response to control motion is of particular significance because structural vibration signals which are fed into the system by pickups (accelerometers, rate gyros, etc.) may either cause the system to become unstable or limit the gain allowable for system stability (refs. 1, 2, and 3).

In order to provide information on dynamic characteristics of flexible airplanes, the NACA has been evaluating measured and predicted dynamic responses of a Boeing B-47 airplane to control surface motions. The dynamic response at frequencies below the structural mode frequencies has been reported in references 1, 4, and 5. Also, a limited amount of measured responses at structural mode frequencies was presented in these reports, but the analysis was limited to frequencies below the natural frequencies of structural modes. In the present report, measured dynamic responses to elevator control at structural mode frequencies are presented for a wide range of flight conditions, and an analysis is developed which includes three structural modes, wing first bending, wing first torsion, and fuselage first bending. Other analyses including structural modes have been presented in references 6, 7, and 8.

In the first part of the report, the measured responses of widely separated points on the airplane are examined for effects of altitude, Mach number, and dynamic pressure. In the second part, equations of motion are developed for three structural degrees of freedom and two airplane degrees of freedom. Finally, comparisons are made between measured and predicted structural response characteristics and results are interpreted to locate optimum points for automatic control system pickups.

Data used in this report were obtained from flight tests conducted at the High Speed Flight Station of the NACA and the analysis and reduction of data was a cooperative effort of HSFS and Ames Aeronautical Laboratory.

Symbols used in this report are defined in Appendix A.

TEST EQUIPMENT

The test airplane was a Boeing B-47A with General Electric J47-GE-23 turbojets and with wing vortex generators as shown in figure 1. Wing deflections were measured by an optigraph mounted on top of the fuselage which recorded the movement of 100-watt target lights. Elevator angle was measured by an NACA resistance-type control-position indicator. The pitching velocity at center of gravity was measured by a magnetically damped NACA pitch turnmeter, the acceleration at the center of gravity and tail by NACA air-damped accelerometers, and the acceleration at the nose and wing tip by Statham linear accelerometers. The locations of the instruments used in this report are indicated in figure 2.

MEASURED FREQUENCY RESPONSE

Measured frequency responses were selected which would define the complete motion of the airplane over a wide range of flight conditions. The measured quantities are pitching velocity at the center of gravity, acceleration at the center of gravity, acceleration at the nose, acceleration at the wing tip, and acceleration at the tail. Although these few points are not sufficient to define structural deformations in detail, the most significant deflections which occur in the frequency range of interest are of the first-bending type and, hence, the principal deflections of in-between points can be approximated by use of the assumed cantilever modes which are introduced later in the analysis. The flight conditions covered are plotted in figure 3 and are listed in table I.

Frequency response data were obtained by the "pulse technique" which is described in detail in reference 4. Briefly, in this method, the pilot applies a pulse force to the controls and the resulting motions are recorded. The time histories of the elevator angle input and the output response quantity are transformed to frequency form by the Fourier integral. Corrections are made for the dynamic response of instruments and frequency response is cut off at frequencies where the level falls below values required for accurate results.

In order to document the response and to show how the response varies with different parameters held constant, frequency responses are plotted with altitude held constant in figures 4, 5, and 6, with the aeroelastic parameter q/β held constant in figure 7, and with Mach number held constant in figure 8. Discussion of these results follows.

Frequency Response At Constant Altitude

The frequency response is presented for three altitudes, 15,000 feet in figure 4, 25,000 feet in figure 5, and 35,000 feet in figure 6. Certain trends are apparent from these figures. The peak of the short-period mode at a frequency from 1 to 4 radians per second increases in amplitude and occurs at higher frequencies as Mach number is increased. This trend is explained in reference 4.

The peak in the acceleration responses due to the wing first-bending mode (approximately 9 radians/sec), which is most apparent in figures 4(d), 5(d), and 6(d), decreases with increasing Mach number. Also, the valley or dip in the response which follows the short-period mode peak shifts to higher frequencies as Mach number is increased.

The response is very complex at frequencies higher than the wing first-bending mode, partly because of inaccuracies in the data by the pulse technique and partly because of many vibrations, insignificant for present purposes, which are picked up by the accelerometers. However, the peaks which reach fairly high amplitudes are considered to be accurate indications of structural modes and only peaks which rise above 10g's per radian on acceleration responses will be considered to be significant here.

The next significant peak appears at frequencies from 14 to 17 radians per second. On the basis of ground vibration tests (ref. 9) and analysis (ref. 10), this mode is believed to be of a wing second-bending type coupled with body translation and pitch.

A very definite high peak is in evidence on all of the responses near a frequency of 30 radians per second, which, according to ground vibration tests, is a mode consisting primarily of fuselage first bending. Unfortunately, the frequency content of the pulse inputs was not high enough to define this peak clearly in every case, but the peak amplitudes appear to increase with Mach number and tend to become less severe as altitude is increased.

A small blip or side band occurs in many cases at a high level of amplitude from 20 to 25 radians per second on the acceleration responses of the wing tip. This is believed to be due to the wing first-torsion mode as indicated by ground vibration tests and analysis. Because of the very close proximity of the wing first-torsion mode to the fuselage first-bending mode it is difficult to note any separate effects.

Frequency Response With Aeroelastic Parameter q/β Constant

Frequency responses with aeroelastic parameter, q/β, equal to 280 pounds per square foot are plotted in figure 7 for the range of test altitudes as indicated in figure 3. All of the responses fall fairly close together in both amplitude and phase. The differences which do occur, near the short-period mode frequency, are explained by the pseudostatic theory (refs. 1 and 4) when differences in weight are included. The results in reference 1 show that the steady-state gain of the ratio of acceleration to elevator angle and the damping ratio of the short-period mode both decrease with an increase in altitude at constant q/β. These trends have opposite effects on the amplitude of the frequency response curves and tend to cancel each other when the frequency is raised to the short-period mode frequency. However, with the exception of the steady-state gain, it appears that the response could be considered essentially unchanged for some practical purposes when q/β is held constant and other parameters are varied.

Frequency Response At Constant Mach Number

Curves for a Mach number of 0.7 (fig. 3) are plotted in figure 8. As altitude is decreased at constant Mach number, the aeroelastic parameter q/β increases and, therefore, the frequency of the short-period mode peak and the general level of the amplitudes increase.

The peak of the wing first-bending mode at a frequency of 8 to 9 radians per second which is seen most clearly in figure 8(d) tends to disappear as q/β is increased. Although peaks are not well defined at higher frequencies, an opposite trend appears for the modes at 16 radians per second and 30 radians per second. These peaks tend to increase with q/β. It should be noted here that in forced oscillation tests the height of the peak in the frequency response depends on the manner in which the driving force is coupled to the mode as well as on the damping of the unforced mode itself. Hence, in the interpretation of peak-amplitude trends, consideration should be given to changes in the coupling of the modes with the forcing as well as to changes in aerodynamic damping and spring forces.

ANALYTICAL METHODS FOR PREDICTION OF DYNAMIC RESPONSE

In the previous section, measured dynamic responses of the airplane were presented to document the response and to show the effects of various parameters. Of course, it is desirable to be able to predict these response characteristics for use in rational design of the airplane and its control system. In the following section, methods of analysis including structural degrees of freedom are developed.

Equations of Motion

Equations of motion of a flexible airplane for frequencies below the structural mode frequencies were developed in reference 4. Also, equations of motion including structural modes have been presented in references 6, 7, and 8. In the analysis here, the equations are developed for two airplane degrees of freedom and three structural degrees of freedom in a form which lends itself to digital machine computing or hand calculations. The equations of motion of the airplane may be simply stated by Lagrange's equation:

$$\frac{d}{dt}\frac{\partial KE}{\partial \dot{q}_i} + \frac{\partial PE}{\partial q_i} = Q_i \tag{1}$$

where KE is the kinetic energy, PE the potential energy, q_i the generalized coordinates, and Q_i the generalized forces. To completely describe the complex dynamic system of a flexible airplane, an infinite number of coordinates (q_i) are needed. However, in most practical problems, the motions of the airplane occur within a finite frequency range, and these motions can be adequately described with a finite number of coordinates. The trick is to select the minimum number of coordinates which are needed for the frequency range of interest.

Selection of coordinates.- The mode of deformation of the structure at an instant of time represents a condition in which the structural spring forces are in equilibrium with the combined forces of all the loads. The individual loads, which include inertial, aerodynamic, and structural damping loads due to motions of the airplane as a whole and structural deflections, vary in accordance with the frequency range considered. At low frequencies, loads due to motions of the airplane as a whole are of primary importance, while at higher frequencies, loads due to motion of the structure are of primary importance. Since the total deflection results from various combinations of the individual loads, an insight to the coordinates needed to define the total deflection is gained if the deflections due to the individual loads are known.

To study the low-frequency range, pseudostatic deformations of the wing resulting from loads due to α, $\dot{\theta}$, n, and $\ddot{\theta}$ were calculated through use of aerodynamic and structural influence coefficients (see Appendixes B and C). The deflection of the wing from the reference plane shown in figure 9 is presented in figure 10 in components of bending of the elastic axis (38-percent chord) and streamwise twist. All of the curves are of the wing first-bending type with various amounts of twist of the wing first-torsion type. Although fuselage bending is not shown on the figure, it occurs in various amounts in the same direction as the wing bending.

At structural mode frequencies, the inertial forces due to structural motion are apt to be of greatest importance. The individual effect of these inertial forces was evaluated by calculating the vacuum vibration modes of the airplane as described in Appendix B. These modes are plotted about the space axes in figure 11, but the deflections will be discussed as viewed from the deflection reference plane on the fuselage.

The dominant mode is of the wing first-bending mode type. The first subdominant mode is primarily wing first torsion with some wing second bending. The second subdominant mode is primarily fuselage bending with a curve of wing first-bending type in the wing. At this frequency it is noted that there is little or no bending of the inboard portion of the wing which indicates a component of wing second bending is present.

The individual deformations in figures 10 and 11 indicate the principle deformations to be expected for frequencies up to 25 radians per second. In order to satisfy both the conditions of the pseudostatic frequency range (various amounts of wing torsion and fuselage bending occurring with wing first bending) and the structural mode frequency range (various amounts of fuselage bending with different types of wing bending curves), it is necessary to break up the deflection curves into components. This was done by selecting wing first bending, fuselage first bending, and wing first torsion for degrees of freedom (fig. 12 and table II). Although wing second bending is evident in some deflections, it was neglected to simplify the analysis. It should be noted that the deflection coordinates in figure 12 are deflections relative to the deflection reference plane in figure 9 which represent the structural deflections which an observer would see from the rigid airplane center-of-gravity location. Also, coordinates of displacement of rigid airplane center-of-gravity location and pitch angle of the deflection reference plane were included to take into account motions of the airplane as a whole.

There are other combinations of coordinates which could be used to describe these motions, but the component deflection breakdown used here has many advantages. The equations are put in a form which allows direct application of the pseudostatic principle in any of the structural degrees of freedom. The calculation of generalized forces is simplified. The structural degrees of freedom correspond to deflections seen by an observer on the airplane and, hence, correspond to the optigraph measurements.

APPLICATION OF LAGRANGE'S EQUATION

By means of equation (1) and coordinates, displacement of center of gravity (Z_{cg}), pitch angle of center of gravity (θ), wing first bending (y), fuselage first bending (h), and wing first torsion (l), the equations of motion as derived in Appendix C are:

$$\begin{bmatrix} K_1M + \frac{C_{L_{\dot{\alpha}}}}{V} & 0 & K_1\Sigma m_i a_i & K_1\Sigma m_i b_i & K_1\Sigma m_i c_i \\ \frac{-C_{m_{\dot{\alpha}}}}{V} & K_2I_y & K_2\Sigma m_i a_i x_i & K_2\Sigma m_i b_i x_i & K_2\Sigma m_i c_i x_i \\ K_1\Sigma m_i a_i & K_1\Sigma m_i a_i x_i & K_1\Sigma m_i a_i^2 & 0 & K_1\Sigma m_i a_i c_i \\ K_1\Sigma m_i b_i + \frac{\Sigma C_{L_{\dot{\alpha}_i}} b_i}{V} & K_1\Sigma m_i b_i x_i & 0 & K_1\Sigma m_i b_i^2 & 0 \\ K_1\Sigma m_i c_i & K_1\Sigma m_i c_i x_i & K_1\Sigma m_i a_i c_i & 0 & K_1\Sigma m_i c_i^2 \end{bmatrix} D^2 +$$

$$\begin{bmatrix} \frac{C_{L_\alpha}}{V} & C_{L_{\dot{\alpha}}} + C_{L_{\dot{\theta}}} & C_{L_{\dot{y}}} & C_{L_{\dot{h}}} & C_{L_{\dot{l}}} \\ \frac{-C_{m_\alpha}}{V} & -\left(C_{m_{\dot{\alpha}}} + C_{m_{\dot{\theta}}}\right) & -C_{m_{\dot{y}}} & -C_{m_{\dot{h}}} & -C_{m_{\dot{l}}} \\ \frac{\Sigma C_{L_{\alpha_i}} a_i}{V} & \Sigma C_{L_{\dot{\theta}_i}} a_i & \Sigma C_{L_{\dot{y}_i}} a_i & 0 & \Sigma C_{L_{\dot{l}_i}} a_i \\ \frac{\Sigma C_{L_{\alpha_i}} b_i}{V} & \Sigma\left(C_{L_{\dot{\alpha}_i}} + C_{L_{\dot{\theta}_i}}\right) b_i & 0 & \Sigma C_{L_{\dot{h}_i}} b_i & 0 \\ \frac{\Sigma C_{L_{\alpha_i}} c_i}{V} & \Sigma C_{L_{\dot{\theta}_i}} c_i & \Sigma C_{L_{\dot{y}_i}} c_i & 0 & \Sigma C_{L_{\dot{l}_i}} c_i \end{bmatrix} D +$$

$$\begin{bmatrix} 0 & C_{L_\alpha} & C_{L_y} & C_{L_h} & C_{L_l} \\ 0 & -C_{m_\alpha} & -C_{m_y} & -C_{m_h} & -C_{m_l} \\ 0 & \Sigma C_{L_{\alpha_i}} a_i & \begin{matrix} K_1\omega_{n_a}{}^2\Sigma m_i a_i{}^2 + \\ \Sigma C_{L_{y_i}} a_i \end{matrix} & 0 & \Sigma C_{L_{l_i}} a_i \\ 0 & \Sigma C_{L_{\alpha_i}} b_i & 0 & \begin{matrix} K_1\omega_{n_b}{}^2\Sigma m_i b_i{}^2 + \\ \Sigma C_{L_{h_i}} b_i \end{matrix} & 0 \\ 0 & \Sigma C_{L_{\alpha_i}} c_i & \Sigma C_{L_{y_i}} c_i & 0 & \begin{matrix} K_1\omega_{n_c}{}^2\Sigma m_i c_i{}^2 + \\ \Sigma C_{L_{l_i}} c_i \end{matrix} \end{bmatrix} \begin{Bmatrix} Z_{cg} \\ \theta \\ y \\ h \\ l \end{Bmatrix} = \begin{Bmatrix} -C_{L_\delta} \\ C_{m_\delta} \\ 0 \\ -C_{L_\delta} \\ 0 \end{Bmatrix} \delta \qquad (2)$$

Symbols are defined in Appendix A. Aerodynamic coefficient terms (e.g., $\Sigma C_{L_{\alpha_i}} a_i$) were evaluated from aerodynamic influence coefficients which were based on steady-state lifting line theory. The aerodynamic influence coefficients were further modified to include weighting terms so that the summations performed are quadrature solutions of the integral of the product of the spanwise lift function and the deflection function.

Equation (2) may be solved for transfer functions Z_{cg}/δ, θ/δ, y/δ, h/δ, and l/δ. From these solutions the motion of any point on the airplane may be determined. The acceleration at a point (i) for example is given by:

$$\frac{n_i}{\delta} = \frac{D^2}{32.2}\left(\frac{Z_{cg}}{\delta} + x_i \frac{\theta}{\delta} + a_i \frac{y}{\delta} + b_i \frac{h}{\delta} + c_i \frac{l}{\delta}\right) \tag{3}$$

Equation (2) may be easily extended to include more degrees of freedom. Coordinates should be selected which are normal or nearly normal to avoid ill-conditioned equations. In other words, the cross terms such as $\Sigma m_i a_i c_i$ should be approximately zero. If a suitable digital computing machine is available, then a large number of normal coordinates could be included in the equations of motion. However, for preliminary design use and for interpretation of the dynamic response, the simplifications attendant with a few degrees of freedom are desirable.

The adequacy of the degrees of freedom selected can always be checked at a given frequency by comparing the deflections predicted by the equations with the deflections computed from the applied loads (Appendix C).

The Pseudostatic Method

When only the dynamic response below structural mode frequencies is needed, equation (2) may be simplified by eliminating terms in D^2 and D which occur with the variables y, h, and l. This assumes that the inertial and damping forces arising from structural motion are negligible. This is sometimes called the pseudostatic method because only the spring terms of the structural modes are included, but all of the dynamic effects of the rigid body degrees of freedom are included. Equation (2) may be written in matrix form as follows:

$$\begin{bmatrix} c_{ij} \end{bmatrix} \begin{Bmatrix} Z_{cg} \\ \theta \\ y \\ h \\ l \end{Bmatrix} = \begin{Bmatrix} -C_{L_\delta} \\ C_{m_\delta} \\ 0 \\ -C_{L_\delta} \\ 0 \end{Bmatrix} \delta \tag{4}$$

in which the elements of $\left[C_{ij}\right]$ are quadratic polynomials in D, that is, $c_{11} = \left(K_1 M + \frac{C_{L_{\dot{\alpha}}}}{V}\right) D^2 + \frac{C_{L_\alpha}}{V} D$. Equation (4) may be partitioned into equations:

$$\begin{bmatrix} c_{11} & c_{12} \\ c_{21} & c_{22} \end{bmatrix} \begin{Bmatrix} Z_{cg} \\ \theta \end{Bmatrix} + \begin{bmatrix} C_{L_y} & C_{L_h} & C_{L_l} \\ -C_{m_y} & -C_{m_h} & -C_{m_l} \end{bmatrix} \begin{Bmatrix} y \\ h \\ l \end{Bmatrix} = \begin{Bmatrix} -C_{L_\delta} \\ C_{m_\delta} \end{Bmatrix} \delta \tag{5}$$

and

$$\begin{bmatrix} c_{31} & c_{32} \\ c_{41} & c_{42} \\ c_{51} & c_{52} \end{bmatrix} \begin{Bmatrix} Z_{cg} \\ \theta \end{Bmatrix} + \begin{bmatrix} K_1 \omega_{n_a}{}^2 \Sigma m_i a_i{}^2 + \Sigma C_{L_{y_i}} a_i & 0 & \Sigma C_{L_{l_i}} a_i \\ 0 & K_1 \omega_{n_b}{}^2 \Sigma m_i b_i{}^2 + \Sigma C_{L_{h_i}} b_i & 0 \\ \Sigma C_{L_{y_i}} c_i & 0 & K_1 \omega_{n_c}{}^2 \Sigma m_i c_i{}^2 + \Sigma C_{L_{l_i}} c_i \end{bmatrix} \begin{Bmatrix} y \\ h \\ l \end{Bmatrix} = \begin{Bmatrix} 0 \\ -C_{L_\delta} \\ 0 \end{Bmatrix} \delta \tag{6}$$

In the pseudostatic method, equation (6) is solved for $\begin{Bmatrix} y \\ h \\ l \end{Bmatrix}$ and substituted in equation (5). The resulting equation then is only a function of Z_{cg}, θ, and δ. The important condition in using equations (5) and (6) for pseudostatic calculations is that

$$\begin{vmatrix} K_1 \omega_{n_a}{}^2 \Sigma m_i a_i{}^2 + \Sigma C_{L_{y_i}} a_i & 0 & \Sigma C_{L_{l_i}} a_i \\ 0 & K_1 \omega_{n_b}{}^2 \Sigma m_i b_i{}^2 + \Sigma C_{L_{h_i}} b_i & 0 \\ \Sigma C_{L_{y_i}} c_i & 0 & K_1 \omega_{n_c}{}^2 \Sigma m_i c_i{}^2 + \Sigma C_{L_{l_i}} c_i \end{vmatrix} \neq 0 \tag{7}$$

for this is the condition for existence of the inversion used in solving equation (6) for $\begin{Bmatrix} y \\ h \\ l \end{Bmatrix}$. The determinant, equation (7), becomes very small and approaches zero if two similar modes are selected as degrees of freedom. The best conditioning of equation (6) is obtained when modes are selected which are normal ($\Sigma m_i a_i c_i = 0$). The pseudostatic analysis, as used in reference 4, used each of the control points on the wing as a separate degree of freedom. All of these degrees of freedom could be used in the dynamical analysis by expanding equations (2) to include more degrees of freedom, but this procedure is usually impractical.

Pseudostatic method techniques can also be applied to the equations which include dynamic effects of structural modes. In these cases, the modes in the frequency range of interest are included as dynamic degrees of freedom, and the higher frequency modes as pseudostatic. For example, if the frequency response were needed through the wing first-bending mode frequency, then only terms in D^2 and D associated with variables h and l would be neglected.

COMPARISON OF MEASURED AND PREDICTED RESPONSES

In the previous two sections, measured dynamic responses were presented to document the dynamic response for systems design, and analytical means of prediction of the dynamic response were developed. Comparison of the measured and predicted responses will now be presented to show how well the analysis represents the measured frequency response characteristics of the airplane (i.e., which forms of transfer functions are needed to simulate the dynamic response in systems design) and how well the node lines or points of low response can be predicted by analysis or ground vibration tests.

Frequency Response Curves and Related Transfer Function Forms

Near the short-period frequency.- If the response is only needed at frequencies near the airplane short-period mode frequency, then the pseudostatic method should provide adequate predictions. In order to verify this, measured responses of wing tip deflection at several altitudes are compared with the predicted response in figure 13. Wing tip deflection is used here for comparison because it is the most direct and accurate measurement of aeroelastic effects on the airplane. From equation (6), solutions of y and l are combined in accordance with equation (C33) in Appendix C to form the transfer function for wing tip deflection which has the form

$$\frac{z_{wt}}{\delta} = \frac{K\left(1 + \frac{2\zeta}{\omega_n} D + \frac{1}{{\omega_n}^2} D^2\right)_1}{\left(1 + \frac{2\zeta}{\omega_n} D + \frac{1}{{\omega_n}^2} D^2\right)_2} \tag{8}$$

where the numerical values for ζ and ω_n are determined from the equations of motion for a given flight condition. The subscripts 1, 2, . . . are used to indicate that the ζ and ω_n are different in the second-order transfer function terms.

The forms of transfer functions of other quantities $\dot{\theta}/\delta$, n/δ are the same as for a rigid airplane and are given in reference 4. Solutions in the form of equation (8) were obtained for flight conditions at a Mach number of 0.7 and altitudes of 35,000 and 15,000 feet for the airplane weight configuration. These were then plotted in frequency response form through use of dynamic response templates presented in reference 11. The frequency response function may also be obtained by substituting $i\omega$ for D in equation (8).

The agreement between experiment and the pseudostatic predictions is quite good up to a frequency of 4 radians per second. At higher frequencies, the response rises sharply in a dynamic peak due to the wing first-bending mode which is especially noticeable at the higher altitude of 35,000 feet.

Including the short-period and wing first-bending frequencies.- In order to take account of the dynamic effects of the lowest structural mode the wing first-bending mode needs to be included as a dynamic degree of freedom in the equations of motion. This is done by only neglecting the D^2 and D terms associated with h and l in equation (2). The transfer function for z/δ then takes on the form:

$$\frac{z}{\delta} = \frac{K\left(1 + \frac{2\zeta}{\omega_n} D + \frac{1}{{\omega_n}^2} D^2\right)_1}{\left(1 + \frac{2\zeta}{\omega_n} D + \frac{1}{{\omega_n}^2} D^2\right)_2\left(1 + \frac{2\zeta}{\omega_n} D + \frac{1}{{\omega_n}^2} D^2\right)_4} \tag{9}$$

Responses predicted by this method are also shown in figure 13, and it may be seen that the dynamic response peaks agree well with the experimental ones. The deflection check, as described in Appendix C, indicated that the selection of coordinates was excellent for describing the structural deflections in this frequency range (up to 15 radians per second).

An interesting result in figure 13 is the disappearance of the large dynamic response peak of the wing first-bending mode at an altitude of 15,000 feet. When the airplane undergoes forced oscillation, there is a frequency for which the generalized forces of inertial loads and aerodynamic loads nearly cancel. This frequency is marked by the valley in the frequency response which occurs around 5 radians per second at an altitude of 35,000 feet. At 15,000 feet, this condition occurs at nearly the same frequency as the wing first-bending mode frequency and hence little or no driving force is transmitted to the wing and the dynamic response peak remains small.

The forms of other transfer functions for dynamic y and pseudostatic h and l are:

$$\frac{\dot{\theta}}{\delta} = \frac{K_{\dot{\theta}}\left(1 + T_{\dot{\theta}}D\right)\left(1 + \frac{2\zeta}{\omega_n} D + \frac{1}{\omega_n^2} D^2\right)_1}{\left(1 + \frac{2\zeta}{\omega_n} D + \frac{1}{\omega_n^2} D^2\right)_2\left(1 + \frac{2\zeta}{\omega_n} D + \frac{1}{\omega_n^2} D^2\right)_4} \tag{10}$$

and

$$\frac{n_{cg}}{\delta} = \frac{K_n\left(1 + \frac{2\zeta}{\omega_n} D + \frac{1}{\omega_n^2} D^2\right)_1\left(1 + \frac{2\zeta}{\omega_n} D + \frac{1}{\omega_n^2} D^2\right)_3}{\left(1 + \frac{2\zeta}{\omega_n} D + \frac{1}{\omega_n^2} D^2\right)_2\left(1 + \frac{2\zeta}{\omega_n} D + \frac{1}{\omega_n^2} D^2\right)_4} \tag{11}$$

Including the short-period, wing first-bending, and fuselage first-bending frequencies.- The predicted response may be extended to cover a wider range of frequencies by including another dynamic degree of freedom. In selecting additional degrees of freedom, consideration must be given to the importance of the modes on the over-all response. In looking at the free-free modes in figure 11, it may be seen that the first subdominant mode consists primarily of deflection of the inboard nacelle mass whereas the second subdominant mode consists primarily of deflection of the tail mass. Fuselage bending was selected as the next most important degree of freedom because it would be expected to have the largest influence on local fuselage responses.

Because of the small deflections involved at the higher frequencies, structural deflection measurements, particularly of the fuselage, were not of sufficient accuracy to use for comparison with theory. However, the accelerometer measurements were of sufficient accuracy over the entire frequency range of interest, and hence will be used for comparison here.

Equation (2) was solved for $\dot{\theta}$, Z_{cg}, y, and h with the torsion-mode variable l neglected. Acceleration responses at the nose, center of gravity, wing tip, and tail were obtained through use of equation (3) and are plotted in figure 14. The form of these acceleration responses is

$$\frac{n_{(\ )}}{\delta} = \frac{K_{(\ )}\left(1 + \frac{2\zeta}{\omega_n} D + \frac{1}{\omega_n^2} D^2\right)_1\left(1 + \frac{2\zeta}{\omega_n} D + \frac{1}{\omega_n^2} D^2\right)_3\left(1 + \frac{2\zeta}{\omega_n} D + \frac{1}{\omega_n^2} D^2\right)_5}{\left(1 + \frac{2\zeta}{\omega_n} D + \frac{1}{\omega_n^2} D^2\right)_2\left(1 + \frac{2\zeta}{\omega_n} D + \frac{1}{\omega_n^2} D^2\right)_4\left(1 + \frac{2\zeta}{\omega_n} D + \frac{1}{\omega_n^2} D^2\right)_6} \tag{12}$$

and the form of pitching velocity at the center of gravity is

$$\frac{\dot{\theta}}{\delta} = \frac{K_{\dot{\theta}}\left(1 + T_{\dot{\theta}}D\right)\left(1 + \frac{2\zeta}{\omega_n} D + \frac{1}{\omega_n^2} D^2\right)_1\left(1 + \frac{2\zeta}{\omega_n} D + \frac{1}{\omega_n^2} D^2\right)_3}{\left(1 + \frac{2\zeta}{\omega_n} D + \frac{1}{\omega_n^2} D^2\right)_2\left(1 + \frac{2\zeta}{\omega_n} D + \frac{1}{\omega_n^2} D^2\right)_4\left(1 + \frac{2\zeta}{\omega_n} D + \frac{1}{\omega_n^2} D^2\right)_6} \tag{13}$$

Comparable measured acceleration responses are shown in figure 15. The portion of the measured wing-tip response has been deleted between frequencies of 12 and 25 radians per second because the scatter in this region obscures the other response curves. It may be seen that the pattern of predicted (fig. 14) and measured responses (fig. 15) are very similar in both amplitude and phase angle which indicates that the equations are of the correct form. Hence, transfer functions of the form of equations (12) and (13) should be adequate for simulation of the dynamic response over this frequency range.

A closer comparison of the responses can be obtained by plotting the accelerations at peaks of the various modes on an amplitude-phase plane. Discussion of the results at the wing first-bending mode and the fuselage first-bending mode peaks follows. When values are compared, it should be kept in mind that errors should be evaluated on the basis of absolute differences rather than percentages because amplitude ratios which are small and phase angles at points with a steep slope are difficult to measure accurately.

The amplitude and phase angle of the various accelerations at the wing first-bending mode frequency are plotted in figure 16. The agreement between measured and predicted values is considered to be good. The deflection check of Appendix C is shown in figure 17. The deflections in phase with the wing tip are plotted in bending and streamwise twist components for comparison. The close agreement indicates that the degrees of freedom were adequate to describe the mode shape.

Comparison of the peak amplitudes at the fuselage first-bending mode frequency near 30 radians per second in figures 14 and 15 shows a large difference between measured and predicted values. However, in both cases the damping ratio is very low and the height of this peak is extremely sensitive to small changes in damping ratio. Physically this means that the exact values of the peak are dependent on very small forces which are beyond the accuracy of the analysis. It is quite possible that better agreement would be obtained if structural damping and unsteady lift forces were included in the analysis. However, since the structural and mass characteristics of the fuselage are not known accurately (see Appendix B), it is felt that further refinements would be futile unless structural properties of the fuselage were measured.

In order to compare the modes of deformation, the accelerations at the fuselage first-bending mode frequency were normalized to the tail acceleration and are plotted in figure 18. It may be seen that there are phase-angle differences between measured and predicted values as high as 45° and that the relative wing-tip amplitude measured is much larger than predicted. Hence, the coordinates of wing first bending and fuselage first bending are not adequate to define the motion with precision at the peak frequency, but are close enough to give the correct general form of the frequency response over the entire range under consideration. For an analog simulation, the damping of the fuselage first-bending mode would have to be increased to match flight values.

The deflection check of Appendix C is plotted in figure 19. Here, the deflections in phase with tail deflection are plotted in wing bending and streamwise twist components. It may be seen that the applied loads in this condition cause much higher wing-tip deflections and more wing torsion than is predicted with simple wing first bending and fuselage first bending. A solution of the complete equations with dynamic y, h, and l was also made and the results indicated that the correct amount of torsion was obtained, but that wing-tip deflection was still too small. As seen in figure 17, the experimental values also indicate higher wing deflections than predicted by the simple wing-bending analysis. A wing first-bending type curve with more curvature near the root could be used in place of the wing first-bending curve used in the analysis, but this would compromise the results in the low-frequency range. If a wing first-bending curve with more curvature near the root were included as an additional degree of freedom, then the equations would probably be ill-conditioned. Hence, it appears that a wing second-bending degree of freedom would have to be added to predict the wing deflections accurately over the frequency range considered here.

Node Lines and Lines of Low Response

In many applications the adverse effects of a structural mode can be eliminated by locating control system elements on node lines, that is, points of zero displacement. Also the stability of a system or the effectiveness of a mass balance weight often depends on which side of the node line the pickup or mass is located. The existence of node lines requires that all points on the structure vibrate either in phase or 180° out of phase. This condition is satisfied in the free-free analysis and approximately in ground vibration tests.

Wing first-bending mode.- It may be seen in figure 16 that the nose, center of gravity, wing tip, and tail accelerations do not fall on a straight line through the origin, but are close enough to determine points of low response in flight. Through the use of the assumed fuselage mode of deformation, parabolic bending to the rear of the center of gravity, points of low response on the fuselage were calculated for the measured and predicted values in figure 16 and are shown in figure 20 together with node lines from ground vibration tests and from the free-free analysis.

The fuselage node lines or lines of low response from flight, free-free analysis, and dynamical analysis are in approximate agreement, but the ground vibration values obtained from reference 9 are considerably farther to the rear. Hence, support of the airplane on air bags is not representative of the manner in which the airplane is supported in flight at this frequency. A possible means of supporting the airplane on the ground to simulate coupling effects of the short-period flight mode is suggested by the moment of inertia tests described in reference 10. The spring and knife edges support the airplane in a manner which very nearly corresponds to the mechanics of the short-period mode at frequencies near the wing first-bending mode frequency. As a result, the oscillations of the airplane on the moment-of-inertia rig correspond very nearly to those which occur in flight, except for the phase lag of the wing which results from aerodynamic damping forces in flight.

Fuselage first-bending mode.- From figure 18 it may be seen that the predicted accelerations at the nose, center of gravity, and tail fall nearly in a straight line, and since nose and tail values are 180° out of phase with the center of gravity, two node lines exist on the fuselage. The experimental points do not fall on a straight line, but are close enough to locate points of low response. The node lines are shown in figure 21 and it may be seen that they are in approximate agreement.

It should be noted that the forward flight node line is somewhat farther forward than the others. In the evaluation of flight node lines it was found that considerable nose bending was taking place. As seen in figure 18, the phase of the nose acceleration is shifted toward that of the wing tip which indicates that nose bending would have to be treated as a separate degree of freedom to duplicate the motion accurately.

CONCLUSIONS

The evaluation of the dynamic response of a large flexible airplane to elevator pulses over a wide range of flight conditions including Mach numbers of 0.5 to 0.8 and altitudes of 15,000 to 35,000 feet and comparisons with predicted dynamic response at selected locations have led to the following conclusions:

1. For practical purposes the dynamic response of a flexible airplane is invariant with the aeroelastic parameter q/β.

2. At constant Mach number, the dynamic response peak of the wing first-bending mode tends to increase in amplitude as altitude is increased.

3. Dynamical analysis with one structural degree of freedom (wing first bending) and steady-state aerodynamic theory adequately predicts the response through the frequency of the wing first-bending mode.

4. Dynamical analysis with two structural degrees of freedom (wing first bending and fuselage first bending) and with steady-state aerodynamic theory gives a form of frequency response which approximately corresponds with measured frequency responses through the frequency of the fuselage first-bending mode.

5. Dynamical analysis with three structural degrees of freedom (wing first bending, wing first torsion, and fuselage first bending) gives better predictions of the wing distortion than the analysis with two structural degrees of freedom, but components of wing second bending and fuselage nose bending will have to be taken into account to obtain more accurate predictions of the response at frequencies above the wing first-bending mode frequency.

6. Lines of small response of the wing first-bending mode and the fuselage first-bending mode measured in flight show fair correlation with those predicted by dynamical analysis.

7. Node lines measured in ground vibration tests with the particular airplane support used did not agree with the lines of small response measured in flight.

Ames Aeronautical Laboratory
National Advisory Committee for Aeronautics
Moffett Field, Calif., Oct. 7, 1957

APPENDIX A

LIST OF SYMBOLS

C_L	lift coefficient
C_{L_i}	weighted lift coefficient at station i
C_m	pitching-moment coefficient
D	differential operator, $\frac{d}{dt}$
F_j	applied force at station j, positive downward
I_y	longitudinal moment of inertia, slug-ft^2
$K_{(\ )}$	gain of subscript quantity
M	total mass of airplane, slugs, or Mach number
S	wing area, sq ft
$T_{\dot{\theta}}$	pitching velocity time constant, sec
V	velocity, ft/sec
W	airplane gross weight, lb
$Z_{(\ )}$	vertical displacement of subscript station relative to space reference plane, positive downward, ft
a_i	normalized coordinate of first structural mode
a_{ij}	aerodynamic influence coefficient, weighted lift coefficient at station i due to a unit angle of attack at station j
b	wing span, ft
b_i	normalized coordinate of second structural mode
b_{ij}	structural influence coefficient, deflection at station i, relative to reference plane, due to load at station j, ft/lb (Because of symmetry, stiffness of both wings is included.)

c	wing chord, ft
c_i	normalized coordinate of third structural mode
$\bar{c}$	wing mean aerodynamic chord, M.A.C., $\frac{2}{S}\int_0^{b/2} c^2 dy$
c.g.	center of gravity, percent $\bar{c}$
g	acceleration due to gravity, 32.2 ft/sec^2
h	deflection coordinate of second structural mode relative to reference plane, positive downward, ft
l	deflection coordinate of third structural mode relative to reference plane, positive downward, ft
$m_{( )}$	mass at subscript station, slugs (Because of symmetry, mass of both wings at each wing station is used.)
$n_{( )}$	normal acceleration at subscript station, positive downward, gravity units
q	dynamic pressure, lb/sq ft
$x_{( )}$	longitudinal distance from center of gravity to subscript quantity, positive when center of gravity is forward of subscript quantity location, ft
y	deflection coordinate of first structural mode relative to reference plane, positive downward, ft
$z_{( )}$	total deflection of subscript station relative to reference plane, positive downward, ft
α	angle of attack, radians
β	ratio of rigid wing lift-curve slope at $M = 0$ to the rigid wing slope at M, $(\beta \cong \sqrt{1 - M^2\cos^2\Lambda})$
δ	elevator control deflection, positive downward, radians
ζ	damping ratio, dimensionless
η	spanwise coordinate, fraction of wing semispan
θ	pitch angle at center of gravity, radians

Λ	angle of sweepback
ρ	mass density of air, slugs/cu ft
$\Phi\left(\frac{\text{output}}{\text{input}}\right)$	phase angle of output quantity minus phase angle of input quantity
ω	frequency, radians/sec
$\omega_{f(\ )}$	undamped natural frequency of subscript free-free mode, radians/sec
$\omega_{n(\ )}$	undamped natural frequency of subscript pseudocantilever mode used as coordinate, radians/sec

Subscripts

a	first structural mode
b	second structural mode
c	third structural mode
cg	center of gravity
n	nose
t	tail
wt	wing tip

Dots are used to indicate differentiation with respect to time; for example $\dot{Z} = \frac{dz}{dt}$.

MATRICES

$\{\ \}$	column matrix
$[\ ]$	square matrix

$\overset{\circ}{\begin{bmatrix}\ \end{bmatrix}}$	square matrix with all except diagonal elements equal to zero
$\left\lfloor\ \right\rfloor$	row matrix
$\begin{bmatrix}\ \end{bmatrix}'$	transposed matrix
$\left\{1\right\}$	column matrix with all elements equal to unity
$\begin{bmatrix}I\end{bmatrix}$	unit matrix
$\begin{bmatrix}\ \end{bmatrix}^{-1}$	inverse matrix

APPENDIX B

CALCULATION OF FREE-FREE MODES

When an airplane vibrates at structural mode frequencies in flight, the aerodynamic and structural damping forces are ordinarily small compared to the inertial forces. For this reason, it might be expected that the modes in flight would not differ greatly from those of the airplane suspended in a vacuum (the free-free modes). Hence, a knowledge of the free-free modes is valuable in selecting degrees of freedom in the equations of motion.

Equations for free-free modes are also derived in reference 12, but the form obtained here is a particularly useful form. In figure 9, the vertical position of the ith discrete mass is given by:

$$Z_i = Z_{cg} + \theta x_i + z_i \qquad \text{(B1)}$$

where the center of gravity is taken as the reference point and small angles are assumed ($\theta = \sin \theta$).

If it is assumed that the airplane is vibrating sinusoidally in a natural free mode, the force due to inertia of the jth discrete mass is:

$$F_j = \omega_f^2 m_j Z_j \qquad \text{(B2)}$$

Then, at an instant of time in accordance with D'Alembert's principle, the system must be in a state of equilibrium as expressed by the following equations: The sum of vertical forces must be equal to zero,

$$\sum_{j=1}^{n} m_j Z_j + m_{cg} Z_{cg} + m_a(Z_{cg}+\theta x_a) = 0 \qquad \text{(B3)}$$

and the sum of moments must be equal to zero,

$$\sum_{j=1}^{n} m_j Z_j x_j + m_a(Z_{cg}+\theta x_a)x_a = 0 \qquad \text{(B4)}$$

where moments are taken about the center of gravity and the masses m_{cg} and m_a are introduced to take account of mass at the center of gravity and any rigidly attached mass m_a. The masses m_{cg} and m_a are separated from Σm_j. . . for convenience. In the example airplane, the influence coefficients of the nose of the airplane were not known. Hence the part of the fuselage forward of the center of gravity was assumed to be rigid. The masses m_{cg} and m_a are selected to satisfy mass and moment of inertia of the airplane as follows:

$$M = \sum_{j=1}^{n} m_j + m_{cg} + m_a \tag{B5}$$

$$I_y = \sum_{j=1}^{n} m_j x_j^2 + m_a x_a^2 \tag{B6}$$

$$\sum_{j=1}^{n} m_j x_j + m_a x_a = 0 \tag{B7}$$

The deflection of the system of masses is given by the structural influence coefficient matrix which was obtained from load-deflection measurements of the wing (ref. 13) and an estimate of fuselage stiffness which was made from the results of the ground vibration tests (ref. 9) and the known mass distribution of the fuselage;

$$\left\{z_i\right\} = \left[b_{ij}\right] \left\{F_j\right\} \tag{B8}$$

where $i,j = 1,2,\ldots,n$.

The structural deflections in the free-free mode are obtained by substituting the applied forces from equation (B2) into equation (B8)

$$\left\{z_i\right\} = \omega_f^2 \left[b_{ij}\right] \overset{\circ}{\left[m_j\right]} \left\{Z_j\right\} \tag{B9}$$

Using equations (B1) and (B9), one obtains:

$$\left\{Z_i\right\} - Z_{cg}\left\{1\right\} - \theta\left\{x_i\right\} = \omega_f^2 \left[b_{ij}\right] \overset{\circ}{\left[m_j\right]} \left\{Z_j\right\} \tag{B10}$$

If equation (B10) is premultiplied by $\left\lfloor m_i \right\rfloor$ and combined with equations (B3), (B5), and (B7), the following equation may be obtained

$$Z_{cg} = -\frac{\omega_f^2}{M} \left\lfloor m_i \right\rfloor \left[b_{ij} \right] \overset{\circ}{\left[m_j \right]} \left\{ Z_j \right\} \qquad \text{(B11)}$$

Also, if equation (B10) is premultiplied by $\left\lfloor m_i x_i \right\rfloor$ and combined with equations (B4), (B6), and (B7), the following equation may be obtained

$$\theta = -\frac{\omega_f^2}{I_y} \left\lfloor m_i x_i \right\rfloor \left[b_{ij} \right] \overset{\circ}{\left[m_j \right]} \left\{ Z_j \right\} \qquad \text{(B12)}$$

Substituting equations (B11) and (B12) into equation (B10), one obtains

$$\left\{ Z_i \right\} = \omega_f^2 \left[\left[I \right] - \frac{1}{M} \left\{ 1 \right\} \left\lfloor m_i \right\rfloor - \frac{1}{I_y} \left\{ x_i \right\} \left\lfloor m_i x_i \right\rfloor \right] \left[b_{ij} \right] \overset{\circ}{\left[m_j \right]} \left\{ Z_j \right\} \qquad \text{(B13)}$$

which is the equation desired. The modal columns $\left\{ Z_i \right\}$ and natural frequencies ω_f are the free-free modes of the airplane when $\left\{ Z_i \right\} = \left\{ Z_j \right\}$. This result may be achieved by iteration. When $\left\{ Z_i \right\}$ is known, then the position of the reference plane through the original center of gravity may be determined from equations (B3) through (B7) with the following result:

$$Z_{cg} = \frac{\Sigma m_j Z_j x_j - x_a \Sigma m_j Z_j}{m_{cg} x_a} \qquad \text{(B14)}$$

$$\theta = \frac{m_a x_a \Sigma m_j Z_j - (m_{cg} + m_a) \Sigma m_j Z_j x_j}{m_{cg} m_a x_a^2} \qquad \text{(B15)}$$

where $j = 1, 2, \ldots, n$.

APPENDIX C

DERIVATION OF EQUATIONS OF MOTION

The equations of motion of a flexible airplane in forced oscillations about an equilibrium condition may be formulated through use of Lagrange's equation:

$$\frac{d}{dt}\left(\frac{\partial KE}{\partial \dot{q}_i}\right) + \frac{\partial PE}{\partial q_i} = Q_i \tag{C1}$$

The airplane is assumed to be flying at constant velocity, and all motions about this state of equilibrium are assumed to be small. In order to calculate the kinetic and potential energies in equation (C1), the mass distribution and elastic properties of the airplane must be known. It is assumed that these properties are known in the form of discrete masses and structural influence coefficients.

The generalized forces (Q_i) in the case of an airplane are the aerodynamic forces arising from motions about equilibrium. The forces due to gravity, initial angle of attack, and initial structural deflection do not enter into the problem because they are in equilibrium and hence do no work. The generalized coordinates q_i represent the degrees of freedom of the dynamic system. In a specific application, the minimum number of coordinates which adequately describe the motion are selected. In this analysis, it is assumed that the motion of the flexible airplane can be described by the usual rigid airplane degrees of freedom, and three structural degrees of freedom measured in the axis system of figure 9. Any arbitrary deflection of the structure $\left\{z_i\right\}$ from the equilibrium position is given by:

$$\left\{z_i\right\} = \left\{a_i\right\} y + \left\{b_i\right\} h + \left\{c_i\right\} l \tag{C2}$$

where $\left\{a_i\right\}$, $\left\{b_i\right\}$, and $\left\{c_i\right\}$ are the normalized deflections at the mass stations of the three structural modes, y, h, and l, respectively.

In accordance with the coordinate system in figure 9, if the small angle assumption $\theta = \sin \theta$ is made, the vertical velocity of a discrete mass, m_i, is:

$$\dot{Z}_i = \dot{Z}_{cg} + x_i\dot{\theta} + a_i\dot{y} + b_i\dot{h} + c_i\dot{l} \tag{C3}$$

Expression for Airplane Inertial Forces in Terms of Coordinates

The kinetic energy of the system of discrete masses about the equilibrium position is:

$$KE = \frac{1}{2}\sum_{i=1}^{n} m_i \dot{z}_i^2 + \frac{1}{2} m_{cg}\dot{z}_{cg}^2 + \frac{1}{2} m_a\left(\dot{z}_{cg} + x_a\dot{\theta}\right)^2 \tag{C4}$$

where the masses m_{cg} and m_a have been introduced to satisfy equations (B5), (B6), and (B7).

Using equations (C3) and (C4) and taking the partial derivatives of KE with respect to coordinate velocities, and also the time derivative, one may obtain

$$\frac{d}{dt}\begin{Bmatrix} \partial KE/\partial \dot{z}_{cg} \\ \partial KE/\partial \dot{\theta} \\ \partial KE/\partial \dot{y} \\ \partial KE/\partial \dot{h} \\ \partial KE/\partial \dot{\imath} \end{Bmatrix} = \begin{bmatrix} M & 0 & \Sigma m_i a_i & \Sigma m_i b_i & \Sigma m_i c_i \\ 0 & I_y & \Sigma m_i a_i x_i & \Sigma m_i b_i x_i & \Sigma m_i c_i x_i \\ \Sigma m_i a_i & \Sigma m_i a_i x_i & \Sigma m_i a_i^2 & \Sigma m_i a_i b_i & \Sigma m_i a_i c_i \\ \Sigma m_i b_i & \Sigma m_i b_i x_i & \Sigma m_i a_i b_i & \Sigma m_i b_i^2 & \Sigma m_i b_i c_i \\ \Sigma m_i c_i & \Sigma m_i c_i x_i & \Sigma m_i a_i c_i & \Sigma m_i b_i c_i & \Sigma m_i c_i^2 \end{bmatrix} \begin{Bmatrix} \ddot{z}_{cg} \\ \ddot{\theta} \\ \ddot{y} \\ \ddot{h} \\ \ddot{\imath} \end{Bmatrix} \tag{C5}$$

Expression for Airplane Spring Forces

The potential energy of the deflected airplane is given by:

$$PE = \frac{1}{2}\left\lfloor z_j \right\rfloor \left[b_{ij}\right]^{-1}\left\{z_i\right\} \tag{C6}$$

which becomes

$$PE = \frac{1}{2}\left\lfloor a_i \right\rfloor \left[b_{ij}\right]^{-1}\left\{a_i\right\} y^2 \tag{C7}$$

for the particular deflection in coordinate y. Taking the partial derivative with respect to y, one obtains:

$$\frac{\partial PE}{\partial y} = \left\lfloor a_i \right\rfloor \left[b_{ij} \right]^{-1} \left\{ a_i \right\} y \tag{C8}$$

Since potential energy as used herein must depend only on relative displacements within an uncoupled mode, equation (C8) can be written in terms of the undamped natural frequency of a particular degree of freedom. From equations (C1), (C5), and (C8), the equation for free vibration in the coordinate y is:

$$\Sigma m_i {a_i}^2 \ddot{y} + \left\lfloor a_i \right\rfloor \left[b_{ij} \right]^{-1} \left\{ a_i \right\} y = 0 \tag{C9}$$

which has solutions $y = A \sin \omega_{n_a} t$. Solving for ω_{n_a} in equation (C9) and combining with equation (C8), one obtains:

$$\frac{\partial PE}{\partial y} = {\omega_{n_a}}^2 \Sigma m_i {a_i}^2 y \tag{C10}$$

Similar expressions for potential energy may be found for the other degrees of freedom.

Use of Free-Free Mode in Calculation of ω_{n_a}

The natural frequency ω_{n_a} in equation (C10) may be calculated without resorting to $\left[b_{ij} \right]^{-1}$ if the structural degree of freedom $\left\{ a_i \right\} y$ is obtained from the structural deformation of a free-free mode such as described in Appendix B. In this case the potential energy of the free-free mode is given by:

$$PE = \frac{1}{2} {\omega_{f_a}}^2 \left[\Sigma m_i {Z_i}^2 + m_{cg} {Z_{cg}}^2 + m_a (Z_{cg} + x_a \theta)^2 \right] \tag{C11}$$

where the Z_i, Z_{cg}, and θ are solutions of the ath free-free mode. The deflection about the deflection reference plane (fig. 9) is:

$$\left\{a_i\right\} y = \left\{Z_i\right\} - Z_{cg}\left\{1\right\} - \theta\left\{x_i\right\} \tag{C12}$$

where y is the deflection given by $y = Z_{3R} - Z_{cg} - \theta x_{3R}$. If the structure is constrained to vibrate in the form $\left\{a_i\right\}$ with the deflection reference plane fixed in space, then the potential energy is:

$$PE = \frac{1}{2} \omega_{n_a}{}^2 \Sigma m_i a_i{}^2 y_i{}^2 \tag{C13}$$

When equation (C12) is satisfied, the potential energy is the same whether the airplane is vibrating in the free-free mode or with the deflection reference plane fixed. Equating (C11) and (C13) and solving for ω_{n_a} gives:

$$\omega_{n_a} = \omega_{f_a}\sqrt{\frac{\Sigma m_i Z_i{}^2 + m_{cg} Z_{cg}{}^2 + m_a(Z_{cg} + x_a\theta)^2}{\Sigma m_i a_i{}^2 y^2}} \tag{C14}$$

This equation expresses the characteristic difference in frequency of a free-free and a cantilever mode. Ordinarily, the free-free vibration of a given mode of deformation occurs at a much higher frequency than the cantilever one. When the fuselage bending is used as a separate degree of freedom, then the potential energy of fuselage bending in the free-free mode should be subtracted out of equation (C14) as follows:

$$\omega_{n_a} = \omega_{f_a}\sqrt{\frac{\Sigma m_i Z_i{}^2 + m_{cg} Z_{cg}{}^2 + m_a(Z_{cg} + x_a\theta)^2 - \frac{2PE_f}{\omega_{f_a}}}{\Sigma m_i a_i{}^2 y^2}} \tag{C15}$$

where PE_f is the potential energy of the fuselage in the free-free mode which satisfies equation (C12).

Equations of Motion With Air Forces Unspecified

Using equations (C1), (C5), and (C10), one may obtain

$$\begin{bmatrix} MD^2 & 0 & \Sigma m_i a_i D^2 & \Sigma m_i b_i D^2 & \Sigma m_i c_i D^2 \\ 0 & I_y D^2 & \Sigma m_i a_i x_i D^2 & \Sigma m_i b_i x_i D^2 & \Sigma m_i c_i x_i D^2 \\ \Sigma m_i a_i D^2 & \Sigma m_i a_i x_i D^2 & \Sigma m_i a_i^2 (D^2 + \omega_{n_a}^2) & \Sigma m_i a_i b_i D^2 & \Sigma m_i a_i c_i D^2 \\ \Sigma m_i b_i D^2 & \Sigma m_i b_i x_i D^2 & \Sigma m_i a_i b_i D^2 & \Sigma m_i b_i^2 (D^2 + \omega_{n_b}^2) & \Sigma m_i b_i c_i D^2 \\ \Sigma m_i c_i D^2 & \Sigma m_i c_i x_i D^2 & \Sigma m_i a_i c_i D^2 & \Sigma m_i b_i c_i D^2 & \Sigma m_i c_i^2 (D^2 + \omega_{n_c}^2) \end{bmatrix} \begin{Bmatrix} Z_{cg} \\ \theta \\ y \\ h \\ l \end{Bmatrix} = \begin{Bmatrix} Q_{Z_{cg}} \\ Q_\theta \\ Q_y \\ Q_h \\ Q_l \end{Bmatrix} \tag{C16}$$

Expression for Aerodynamic Forces

The generalized forces Q_i in equation (C16) consist of the aerodynamic forces. For convenience in calculation of these forces, the angle-of-attack coordinate, α, (fig. 9) is introduced here, and later in the report it is transformed to the coordinates of the preceding equations. The mass stations were originally selected to be compatible with the aerodynamic lifts. From reference 14, which is a development from Weissinger's steady-state lifting line theory, the aerodynamic influence coefficients may be obtained as follows

$$\left\{\alpha_\nu\right\} = \left[a_{\nu n}\right] \left\{G_n\right\}, \qquad \nu, n = 1,2,3,4 \tag{C17}$$

Solving for $\left\{G_n\right\}$ gives

$$\left\{G_n\right\} = \left[a_{\nu n}\right]^{-1} \left\{\alpha_\nu\right\} \tag{C18}$$

The elements of $\left\{G_n\right\}$ are the loading coefficients $c_l c/2b$ at stations 1, 2, 3, and 4, respectively, due to any arbitrary angle-of-attack distribution. The total lift on the wing is given by:

$$L = b^2 q \int_0^1 G(\eta) d\eta \tag{C19}$$

where $G(\eta)$ is the function taking on the value of G_n at the nth station.

This integration may be performed by Multhopp's quadrature method. In matrix form, the integration is performed by premultiplying equation (C18) by a weighting matrix. Also, dividing by qS to obtain a coefficient form gives

$$\left\{C_{L_n}\right\} = \left(\frac{b^2}{S}\right)\begin{bmatrix} 0.1502 & 0 & 0 & 0 \\ 0 & 0.2776 & 0 & 0 \\ 0 & 0 & 0.3628 & 0 \\ 0 & 0 & 0 & 0.1964 \end{bmatrix}\left[a_{\nu n}\right]^{-1}\left\{\alpha_\nu\right\} \tag{C20}$$

The column $\left\{C_{L_n}\right\}$ is thus weighted so that a summation with deflection coefficients gives a quadrature solution of the integral of the product of the spanwise lift function and the deflection function. Also the summation of the elements of $\left\{C_{L_n}\right\}$ gives the lift coefficient of the wing due to the angle-of-attack distribution $\left\{\alpha_\nu\right\}$.

In order to take account of chordwise loadings, the lift was divided into two components at each spanwise station, one component at the front spar and one at the rear spar. These were selected in such a manner as to place the chordwise center of pressure at the 25-percent chord line. This puts 80 percent of the lift on the front spar and 20 percent on the rear spar. Equation (C20) may then be written as

$$\left\{C_{L_i}\right\} = \left[a_{ij}\right]\left\{\alpha_j\right\} \tag{C21}$$

$j = 1,2,3,4$

$i = 1F,1R,2F,2R,3F,3R,4F,4R$

where

$$\left[a_{ij}\right] = \left(\frac{b^2}{S}\right)\begin{bmatrix} 0.8 & 0 & 0 & 0 \\ .2 & 0 & 0 & 0 \\ 0 & 0.8 & 0 & 0 \\ 0 & .2 & 0 & 0 \\ 0 & 0 & 0.8 & 0 \\ 0 & 0 & .2 & 0 \\ 0 & 0 & 0 & 0.8 \\ 0 & 0 & 0 & .2 \end{bmatrix}\begin{bmatrix} 0.1502 & 0 & 0 & 0 \\ 0 & 0.2776 & 0 & 0 \\ 0 & 0 & 0.3628 & 0 \\ 0 & 0 & 0 & 0.1964 \end{bmatrix}\left[a_{\nu n}\right]^{-1}$$

which is the aerodynamic influence coefficient matrix in a form suitable for calculation of generalized forces. Mach number effects in accordance with the Prandtl-Glauert rule are included in the values of $a_{\nu n}$ from reference 14. This means that an aerodynamic influence coefficient matrix should be calculated for each Mach number. However, in many cases, Mach number effects may be adequately taken into account by multiplying $\left[a_{ij}\right]$ for a Mach number of zero by $1/\beta$.

The moment coefficients are given by:

$$\left\{C_{m_i}\right\} = \frac{1}{\bar{c}}\overset{\circ}{\left[x_i\right]}\left\{C_{L_i}\right\} \tag{C22}$$

A generalized force is the work done per unit displacement when the system undergoes a virtual displacement of one of the degrees of freedom. In the following equations for generalized forces, small angles are assumed so that lift forces can be regarded as acting in the direction of the displacements. In a displacement of the Z_{cg} coordinate, all of the lift forces do work. Hence:

$$Q_{Z_{cg}} = -\left[\left(C_{L_{\dot{\alpha}}}D + C_{L_{\alpha}}\right)\alpha + C_{L_{\dot{\theta}}}\dot{\theta} + \left(C_{L_{\dot{y}}}D + C_{L_{y}}\right)y + \left(C_{L_{\dot{h}}}D + C_{L_{h}}\right)h + \left(C_{L_{\dot{l}}}D + C_{L_{l}}\right)l + C_{L_{\delta}}\delta\right]qS \tag{C23}$$

where the terms $C_{L_{\dot{\alpha}}}$, $C_{L_{\alpha}}$, $C_{L_{\dot{\theta}}}$, $C_{L_{\delta}}$ are the rigid airplane derivatives. The terms $C_{L_{\dot{y}}}$, $C_{L_{y}}$, $C_{L_{\dot{h}}}$, $C_{L_{h}}$, $C_{L_{\dot{l}}}$, $C_{L_{l}}$ were obtained by summing $\left\{C_{L_i}\right\}$ in equation (C21) where $\left\{\alpha_{\nu}\right\}$ is the angle of attack at control points due to displacements $\left\{a_i\right\}$, $\left\{b_i\right\}$, and $\left\{c_i\right\}$, respectively.

In a θ displacement, work is done by all of the moments. Hence:

$$Q_{\theta} = \left[(C_{m_{\dot{\alpha}}}D+C_{m_{\alpha}})\alpha + C_{m_{\dot{\theta}}}D\theta + (C_{m_{\dot{y}}}D+C_{m_{y}})y + (C_{m_{\dot{h}}}D+C_{m_{h}})h + (C_{m_{\dot{l}}}D+C_{m_{l}})l + C_{m_{\delta}}\delta\right]qS\bar{c} \tag{C24}$$

where $C_{m_{\dot{\alpha}}}$, $C_{m_{\alpha}}$, $C_{m_{\dot{\theta}}}$, $C_{m_{\delta}}$ are rigid airplane derivatives and the terms $C_{m_{\dot{y}}}$, $C_{m_{y}}$, $C_{m_{\dot{h}}}$, $C_{m_{h}}$, $C_{m_{\dot{l}}}$, $C_{m_{l}}$ are obtained by summing $\left\{C_{m_i}\right\}$ in equation (C22), using the appropriate respective angles of attack $\left\{\alpha_{\nu}\right\}$ as noted above.

In a displacement of the mode y, work is done by all of the forces which are displaced. For example, the work per unit of y done by the lift due to α is given by

$$\frac{\Delta w}{\Delta y} = qS\int_{0}^{1} c_l(\eta)a(\eta)\,d\eta \tag{C25}$$

where $c_l(\eta)$ and $a(\eta)$ are the distributed functions of lift coefficient and mode of deformation. This integral is similar to the one in equation (C19) and is also amenable to solution by Multhopp's quadrature method. Since the integrating factors are included in the aerodynamic influence coefficient matrix, then the work done by lift due to α is simply given by:

$$\frac{\Delta w}{\Delta y} = qS\left\lfloor a_i \right\rfloor\left[a_{ij}\right]\left\{1\right\}\alpha = qS\left\lfloor a_i \right\rfloor\left\{C_{L_{\alpha_i}}\right\}\alpha$$

or

$$\frac{\Delta w}{\Delta y} = qS\sum_{i=1f}^{3r} C_{L_{\alpha_i}}a_i\alpha \tag{C26}$$

The generalized force is

$$\begin{aligned} Q_y = -qS\Big[&\left(\Sigma C_{L_{\dot\alpha_i}} a_i\right)\dot\alpha + \left(\Sigma C_{L_{\alpha_i}} a_i\right)\alpha + \left(\Sigma C_{L_{\dot\theta_i}} a_i\right)\dot\theta + \left(\Sigma C_{L_{\dot y_i}} a_i\right)\dot y + \left(\Sigma C_{L_{y_i}} a_i\right)y + \\ &\left(\Sigma C_{L_{\dot h_i}} a_i\right)\dot h + \left(\Sigma C_{L_{h_i}} a_i\right)h + \left(\Sigma C_{L_{\dot\iota_i}} a_i\right)\dot\iota + \left(\Sigma C_{L_{\iota_i}} a_i\right)\iota + \left(\Sigma C_{L_{\delta_i}} a_i\right)\delta\Big] \end{aligned} \tag{C27}$$

and similarly for the other generalized forces

$$\begin{aligned} Q_h = -qS\Big[&\left(\Sigma C_{L_{\dot\alpha_i}} b_i\right)\dot\alpha + \left(\Sigma C_{L_{\alpha_i}} b_i\right)\alpha + \left(\Sigma C_{L_{\dot\theta_i}} b_i\right)\dot\theta + \left(\Sigma C_{L_{\dot y_i}} b_i\right)\dot y + \left(\Sigma C_{L_{y_i}} b_i\right)y + \\ &\left(\Sigma C_{L_{\dot h_i}} b_i\right)\dot h + \left(\Sigma C_{L_{h_i}} b_i\right)h + \left(\Sigma C_{L_{\dot\iota_i}} b_i\right)\dot\iota + \left(\Sigma C_{L_{\iota_i}} b_i\right)\iota + \left(\Sigma C_{L_{\delta_i}} b_i\right)\delta\Big] \end{aligned} \tag{C28}$$

$$\begin{aligned} Q_\iota = -qS\Big[&\left(\Sigma C_{L_{\dot\alpha_i}} c_i\right)\dot\alpha + \left(\Sigma C_{L_{\alpha_i}} c_i\right)\alpha + \left(\Sigma C_{L_{\dot\theta_i}} c_i\right)\dot\theta + \left(\Sigma C_{L_{\dot y_i}} c_i\right)\dot y + \left(\Sigma C_{L_{y_i}} c_i\right)y + \\ &\left(\Sigma C_{L_{\dot h_i}} c_i\right)\dot h + \left(\Sigma C_{L_{h_i}} c_i\right)h + \left(\Sigma C_{L_{\dot\iota_i}} c_i\right)\dot\iota + \left(\Sigma C_{L_{\iota_i}} c_i\right)\iota + \left(\Sigma C_{L_{\delta_i}} c_i\right)\delta\Big] \end{aligned} \tag{C29}$$

Again using the small angle assumption, one may relate the vertical acceleration to θ and α by the following transformation of coordinates.

$$\ddot Z = -V(\dot\theta - \dot\alpha) \tag{C30}$$

Equations (C16), (C23), (C24), (C27), (C28), (C29), and (C30) now define the equations of motion. Further development depends on the exact form in which the equations are desired.

Final Equations of Motion in Terms of Specific Coordinates

In the application to the B-47 airplane, the three structural degrees of freedom selected were wing bending (y), wing torsion (ι), and fuselage bending (h). The wing bending mode was obtained by removing the fuselage-bending component from the first free-free mode. The torsion mode was obtained by removing the fuselage- and wing-bending components from the second free-free mode. Hence, terms $\Sigma m_i b_i c_i$ and $\Sigma m_i a_i b_i$ become zero. Also, the terms $C_{L_{\dot{\alpha}_i}}$ and $C_{L_{\delta_i}}$, which represent forces at the tail, do not enter into equations in y and l. Downwash at the tail from the lift due to wing structural modes was found to be small and was neglected. Equations of motion used in the analysis are:

$$\left[\begin{array}{|c|c|c|c|c|}
\hline
\begin{gathered} K_1 M D^2 + \\ \frac{C_{L_{\dot{\alpha}}}}{V} D^2 + \frac{C_{L_{\alpha}}}{V} D \end{gathered} &
\begin{gathered} 0 \\ (C_{L_{\dot{\alpha}}} + C_{L_{\dot{\theta}}}) D + C_{L_{\alpha}} \end{gathered} &
\begin{gathered} K_1 \Sigma m_i a_i D^2 + \\ C_{L_{\dot{y}}} D + C_{L_y} \end{gathered} &
\begin{gathered} K_1 \Sigma m_i b_i D^2 + \\ C_{L_{\dot{h}}} D + C_{L_h} \end{gathered} &
\begin{gathered} K_1 \Sigma m_i c_i D^2 + \\ C_{L_{\dot{l}}} D + C_{L_l} \end{gathered} \\
\hline
\begin{gathered} 0 \\ -\frac{C_{m_{\dot{\alpha}}}}{V} D^2 - \frac{C_{m_{\alpha}}}{V} D \end{gathered} &
\begin{gathered} K_2 I_y D^2 - \\ (C_{m_{\dot{\alpha}}} + C_{m_{\dot{\theta}}}) D - C_{m_{\alpha}} \end{gathered} &
\begin{gathered} K_2 \Sigma m_i a_i x_i D^2 - \\ C_{m_{\dot{y}}} D - C_{m_y} \end{gathered} &
\begin{gathered} K_2 \Sigma m_i b_i x_i D^2 - \\ C_{m_{\dot{h}}} D - C_{m_h} \end{gathered} &
\begin{gathered} K_2 \Sigma m_i c_i x_i D^2 - \\ C_{m_{\dot{l}}} D - C_{m_l} \end{gathered} \\
\hline
\begin{gathered} K_1 \Sigma m_i a_i D^2 + \\ \frac{\Sigma C_{L_{\alpha_i}} a_i}{V} D \end{gathered} &
\begin{gathered} K_1 \Sigma m_i a_i x_i D^2 + \\ \Sigma C_{L_{\alpha_i}} a_i + \Sigma C_{L_{\dot{\theta}_i}} a_i D \end{gathered} &
\begin{gathered} K_1 \Sigma m_i a_i^2 (D^2 + \omega_{n_a}^2) + \\ \Sigma C_{L_{\dot{y}_i}} a_i D + \Sigma C_{L_{y_i}} a_i \end{gathered} &
0 &
\begin{gathered} K_1 \Sigma m_i a_i c_i D^2 + \\ \Sigma C_{L_{\dot{l}_i}} a_i D + \Sigma C_{L_{l_i}} a_i \end{gathered} \\
\hline
\begin{gathered} K_1 \Sigma m_i b_i D^2 + \\ \frac{\Sigma C_{L_{\dot{\alpha}_i}} b_i}{V} D^2 + \frac{\Sigma C_{L_{\alpha_i}} b_i}{V} D \end{gathered} &
\begin{gathered} K_1 \Sigma m_i b_i x_i D^2 + \\ \Sigma C_{L_{\dot{\alpha}_i}} b_i D + \\ \Sigma C_{L_{\alpha_i}} b_i + \Sigma C_{L_{\dot{\theta}_i}} b_i D \end{gathered} &
0 &
\begin{gathered} K_1 \Sigma m_i b_i^2 (D^2 + \omega_{n_b}^2) + \\ \Sigma C_{L_{\dot{h}_i}} b_i D + \Sigma C_{L_{h_i}} b_i \end{gathered} &
0 \\
\hline
\begin{gathered} K_1 \Sigma m_i c_i D^2 + \\ \frac{\Sigma C_{L_{\alpha_i}} c_i}{V} D \end{gathered} &
\begin{gathered} K_1 \Sigma m_i c_i x_i D^2 + \\ \Sigma C_{L_{\alpha_i}} c_i + \Sigma C_{L_{\dot{\theta}_i}} c_i D \end{gathered} &
\begin{gathered} K_1 \Sigma m_i a_i c_i D^2 + \\ \Sigma C_{L_{\dot{y}_i}} c_i D + \Sigma C_{L_{y_i}} c_i \end{gathered} &
0 &
\begin{gathered} K_1 \Sigma m_i c_i^2 (D^2 + \omega_{n_c}^2) + \\ \Sigma C_{L_{\dot{l}_i}} c_i D + \Sigma C_{L_{l_i}} c_i \end{gathered} \\
\hline
\end{array}\right]
\left\{\begin{matrix} z_{cg} \\ \theta \\ y \\ h \\ l \end{matrix}\right\}
=
\left\{\begin{matrix} -C_{L_{\delta}} \\ C_{m_{\delta}} \\ 0 \\ -C_{L_{\delta}} \\ 0 \end{matrix}\right\} \delta \qquad \text{(C31)}$$

where $1/qS = K_1$, $1/qS\bar{c} = K_2$ and all summations, Σ, are taken over stations 1F, 1R, 2F, 2R, 3F, 3R, 5, 6, and 7. The wing root stations, 4F and 4R, do not deflect in coordinates y, h, and l and, hence do not enter into the summations, but the lift at these stations is included in stability derivatives such as C_{L_y}, C_{L_h}, etc.

The acceleration at any point i on the airplane is given by:

$$n_i = \frac{D^2}{g}\left[Z_{cg} + x_i\theta + a_i y + b_i h + c_i l\right] \tag{C32}$$

Deflection check.- Because of the many terms involved, it is advisable to check the results obtained from the equations of motion. This can be done as follows: From solution of equation (C31), calculate the wing deflection for a particular frequency (make substitution $D = i\omega$). Usually a frequency corresponding to a peak in the frequency response is used because these are the most important points. The deflection is given by

$$\left\{z_i\right\} = \left\{a_i\right\} y + \left\{c_i\right\} l \tag{C33}$$

Through use of the structural and aerodynamic influence coefficient matrices, calculate deflections due to α, $\dot{\theta}$, $\ddot{\theta}$, n_{cg}, $\left\{z_i\right\}$, $\left\{\dot{z}_i\right\}$, $\left\{\ddot{z}_i\right\}$, and sum. The total deflections due to the loads should check with the initial deflection in equation (C33). Since the influence coefficient matrices are based on eight degrees of freedom, the deflection check indicates whether or not the three degrees of freedom selected are as adequate as eight degrees of freedom at the frequency considered.

REFERENCES

1. Cole, Henry A., Jr., Brown, Stuart C., and Holleman, Euclid C.: The Effects of Flexibility on the Longitudinal and Lateral-Directional Response of a Large Airplane. NACA RM A55D14, 1955.

2. Howard, Vincent W.: The Effects of Structural Elasticity on Aircraft Control Systems. WADC Tech. Rep. 56-166, June 1956.

3. Seamans, Robert C., Jr., Barnes, Frank A., Garber, Theodore B., and Howard, Vincent W.: Recent Developments in Aircraft Control. Jour. Aero. Sci., vol. 22, no. 3, Mar. 1955, pp. 145-164.

4. Cole, Henry A., Jr., Brown, Stuart C., and Holleman, Euclid C.: Experimental and Predicted Longitudinal Response Characteristics of a Large Flexible 35° Swept-Wing Airplane at an Altitude of 35,000 Feet. NACA RM A54H09, 1954.

5. Brown, Stuart C., and Holleman, Euclid C.: Experimental and Predicted Lateral-Directional Dynamic Response Characteristics of a Large Flexible 35° Swept-Wing Airplane at an Altitude of 35,000 Feet. NACA TN 3874, 1956.

6. McLaughlin, Milton D.: A Theoretical Investigation of the Short-Period Dynamic Longitudinal Stability of Airplane Configurations Having Elastic Wings of 0° to 60° Sweepback. NACA TN 3251, 1954.

7. Klawans, Bernard B., and Johnson, Harold I.: Some Effects of Fuselage Flexibility on Longitudinal Stability and Control. NACA TN 3543, 1956.

8. Budish, Nathan N.: Longitudinal Stability at High Airspeeds. (Model XB-47). Doc. No. D-8603, Boeing Airplane Co., Feb. 29, 1952.

9. Anon.: Flutter Inspection of Boeing XB-47 Airplane. Ser. MCR EXA5-4262-36-29, Air Materiel Command, Wright-Patterson AFB (E.D.M.R.), 1948.

10. Cole, Henry A., Jr., and Bennion, Frances L.: Measurement of the Longitudinal Moment of Inertia of a Flexible Airplane. NACA TN 3870, 1956.

11. Lees, Sidney: Graphical Aids for the Graphical Representation of Functions of the Imaginary Argument. Inst. Lab. Eng. Memo. E-25, M.I.T., Jan. 1952.

12. Scanlan, Robert H., and Rosenbaum, Robert: Introduction to the Study of Aircraft Vibration and Flutter. The MacMillan Co., 1951.

13. Mayo, Alton P., and Ward, John F.: Experimental Influence Coefficients for the Deflection of the Wing of a Full-Scale, Swept-Wing Bomber. NACA RM L53L23, 1954.

14. DeYoung, John, and Harper, Charles W.: Theoretical Symmetric Span Loading at Subsonic Speeds for Wings Having Arbitrary Plan Form. NACA Rep. 921, 1948.

TABLE I.- FLIGHT-TEST CONDITIONS

Flight number	Run number	Altitude	Mach number	Gross weight	$I_y \times 10^6$	c.g.	[1]β
18	6	14,900	0.50	103,400	1.23	22.8	0.91
18	7	15,000	.55	103,100	1.23	22.8	.88
18	8	15,100	.59	102,700	1.23	22.7	.86
18	10	15,100	.67	101,600	1.21	21.9	.82
18	11	15,100	.71	100,700	1.21	21.9	.80
18	12	15,200	.76	100,300	1.21	22.2	.76
11	19	20,000	.59	106,100	1.25	21.2	.86
17	15	20,500	.71	104,200	1.24	20.9	.80
15	7	25,500	.49	118,700	1.36	20.8	.91
15	5	25,200	.60	119,500	1.37	21.2	.86
15	4	25,100	.66	120,000	1.37	21.1	.83
17	10	24,800	.70	108,100	1.27	19.9	.80
17	12	25,380	.79	106,400	1.25	19.6	.74
3	6	29,900	.71	125,900	1.25	20.6	.80
5	18	34,400	.60	110,000	1.29	21.3	.86
5	15	36,000	.72	111,100	1.30	21.6	.79
5	13	35,300	.80	111,900	1.30	21.7	.74

[1] Based on $C_{L_{\alpha_{M=0}}}/C_{L_{\alpha_M}}$ from reference 14.

TABLE II.- PHYSICAL CHARACTERISTICS USED IN ANALYSIS

$$[a_{ij}] = \frac{1}{82.3}\begin{bmatrix} 18.4 & 8.9 & 3.1 & 1.8 \\ 4.6 & 2.2 & .8 & .4 \\ 3.12 & 54.8 & 24.4 & 4.4 \\ .78 & 13.7 & 6.1 & 1.1 \\ .96 & 6.8 & 96 & 29 \\ .24 & 1.7 & 24 & 7 \\ .4 & .62 & 12.8 & 54 \\ 1 & .15 & 3.2 & 13.4 \end{bmatrix}$$

$$C_{L_{\alpha_{tail}}} = 3.3$$

$$[b_{ij}] = \frac{1}{24,000}\begin{array}{ccccccccc} 1F & 1R & 2F & 2R & 3F & 3R & 5 & 6 & 7 \\ \hline 2.3486 & 2.3840 & 1.1943 & 1.2934 & 0.2302 & 0.2730 & 0.1717 & 1.6315 & 0 \\ 2.4598 & 2.5920 & 1.2430 & 1.4057 & .2330 & .2940 & .1497 & 1.6970 & 0 \\ 1.2134 & 1.2490 & .7419 & .7795 & .1769 & .2051 & .1383 & .9263 & 0 \\ 1.3309 & 1.4300 & .7881 & .9005 & .1804 & .2318 & .1102 & .9916 & 0 \\ .2447 & .2307 & .1765 & .1663 & .0659 & .0580 & .0767 & .2040 & 0 \\ .3057 & .3339 & .2116 & .2398 & .0705 & .0931 & .0396 & .2464 & 0 \\ .1614 & .0898 & .1286 & .0659 & .0596 & .0101 & .1273 & .1444 & 0 \\ 1.6137 & 1.6498 & .9208 & .9495 & .2025 & .2374 & .1528 & 1.1859 & 0 \\ 0 & 0 & 0 & 0 & 0 & 0 & 0 & 0 & 0.328 \end{array}$$

$$[m_i] = \begin{bmatrix} 20 & 20 & 61 & 61 & 130 & 130 & 484 & 206 & 264 \end{bmatrix}$$

$$[x_i] = \begin{bmatrix} 19.82 & 23.12 & 10.86 & 15.06 & -2.53 & 2.98 & -10.08 & 14.22 & 47 \end{bmatrix}$$

$$[a_i] = \begin{bmatrix} 0.953 & 1 & 0.576 & 0.623 & 0.141 & 0.174 & 0.096 & 0.718 & 0 \end{bmatrix}$$

$$[b_i] = \begin{bmatrix} 0 & 0 & 0 & 0 & 0 & 0 & 0 & 0 & 1 \end{bmatrix}$$

$$[c_i] = \begin{bmatrix} 0.32 & -.32 & 0.316 & -0.316 & 0.267 & -0.267 & 1 & 0.32 & 0 \end{bmatrix}$$

Change in stabilizer angle = 0.0342° per 1000 lb tail load

$I_y = 1,330,000$ slug-ft^2

$M = 3,580$ slugs

$m_a = 274$ slugs

$m_o = 1,930$ slugs

$x_a = 47.3$ feet

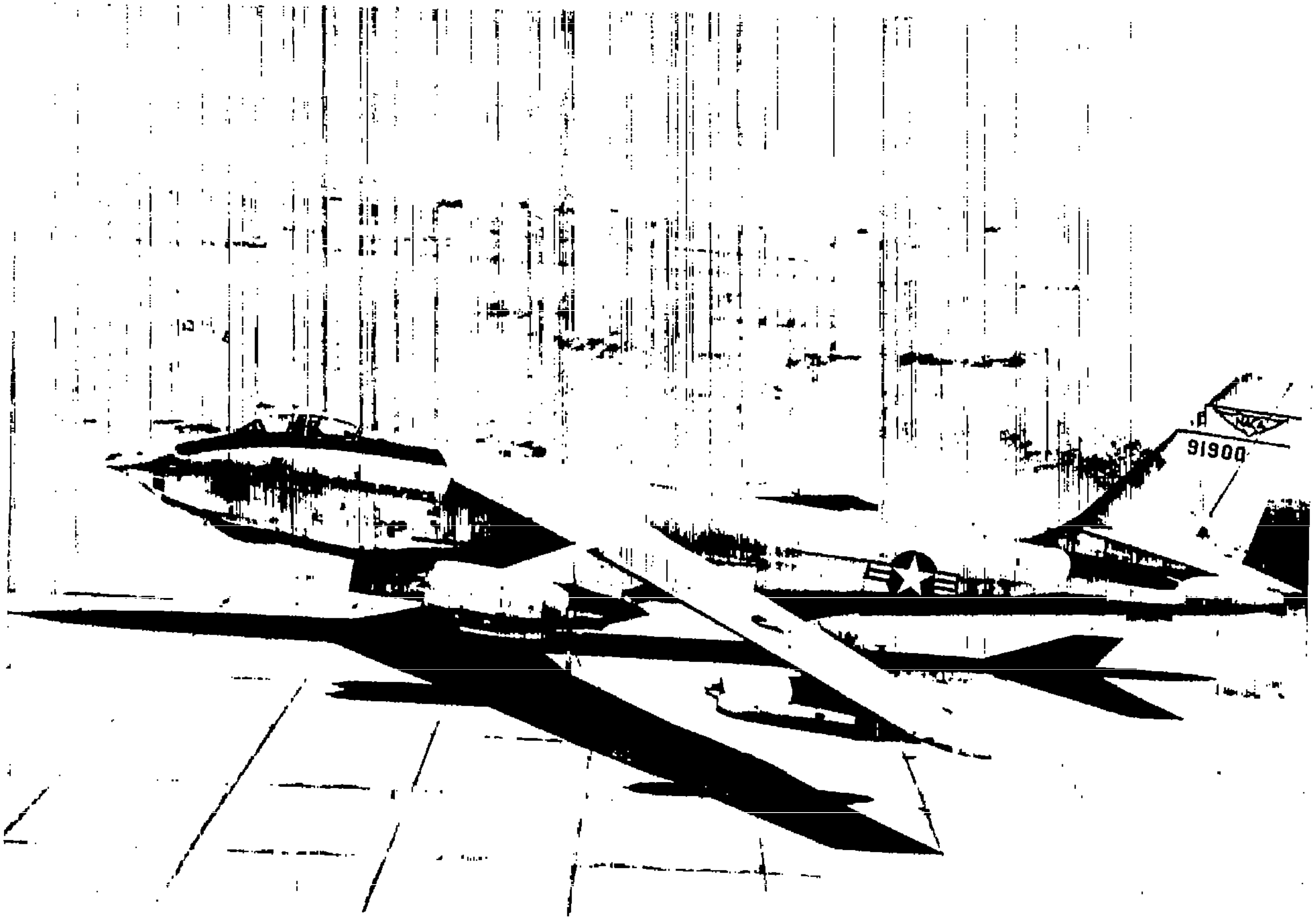

Figure 1.- Photograph of the test airplane.

A-19582

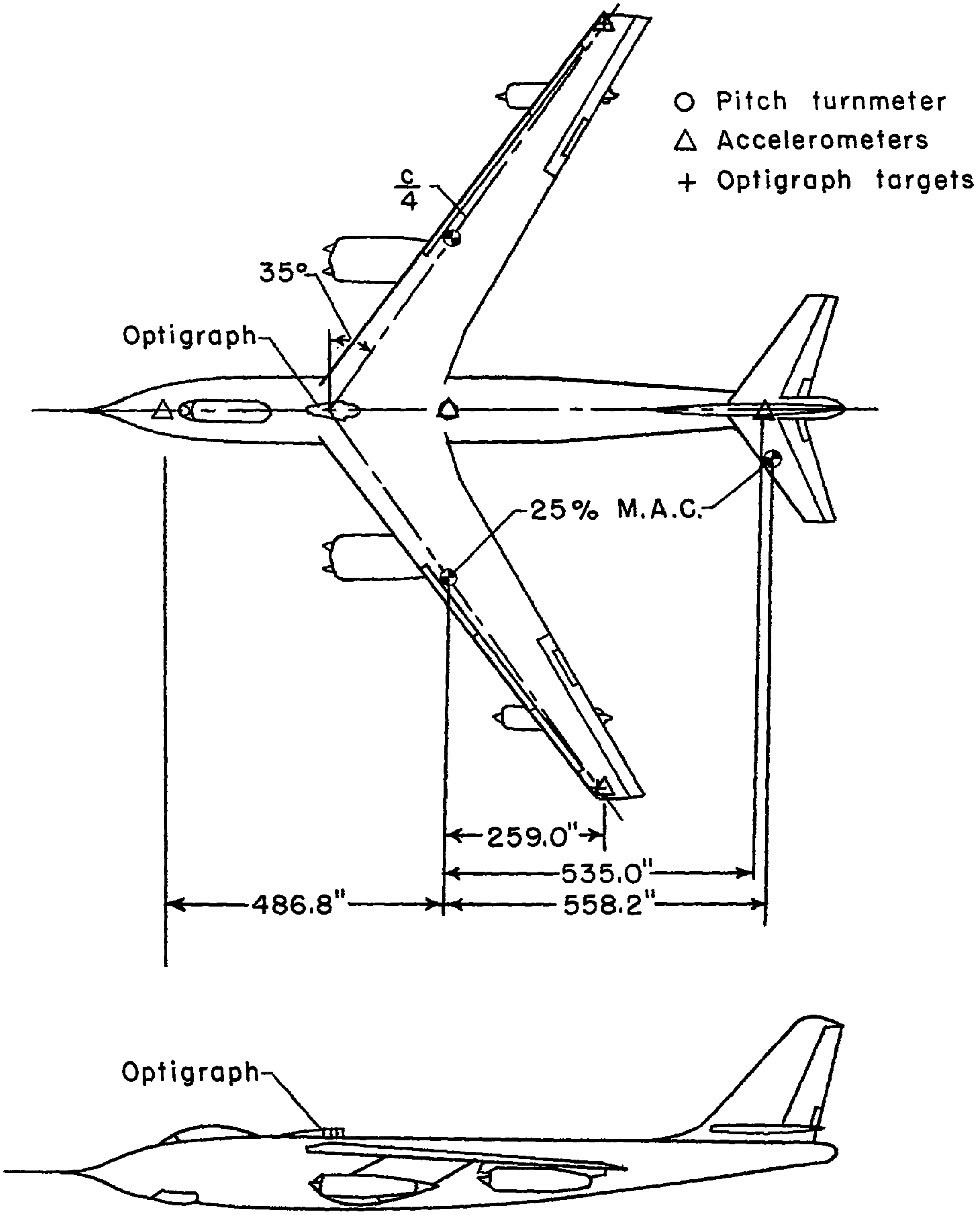
○ Pitch turnmeter
△ Accelerometers
+ Optigraph targets
$\frac{c}{4}$
35°
Optigraph
25% M.A.C.
259.0"
535.0"
486.8"
558.2"
Optigraph

Figure 2.- Two-view drawing of test airplane.

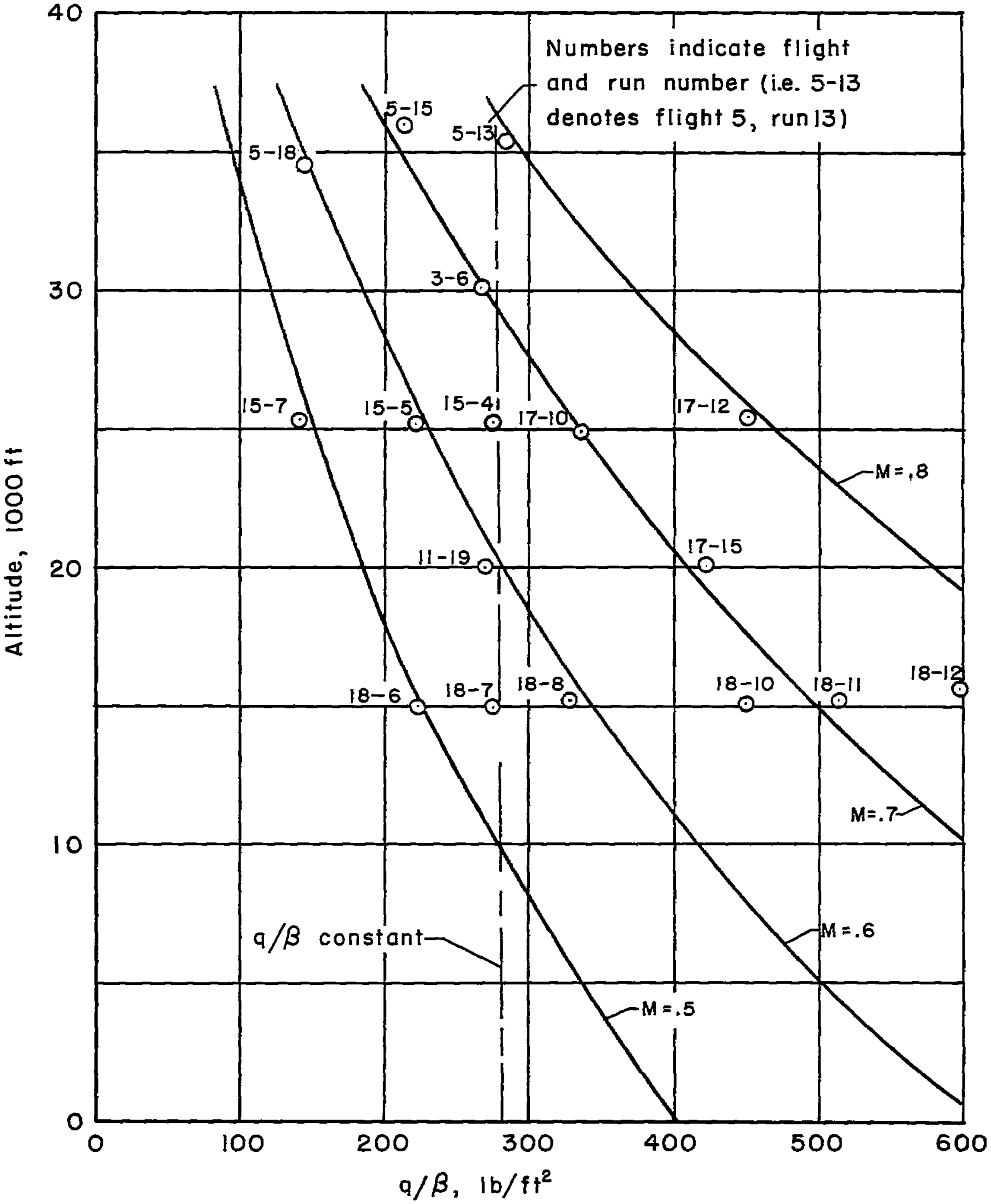

Figure 3.- Flight test conditions; 126,000 > W > 100,000 and center of gravity between 20 and 23 percent M.A.C.

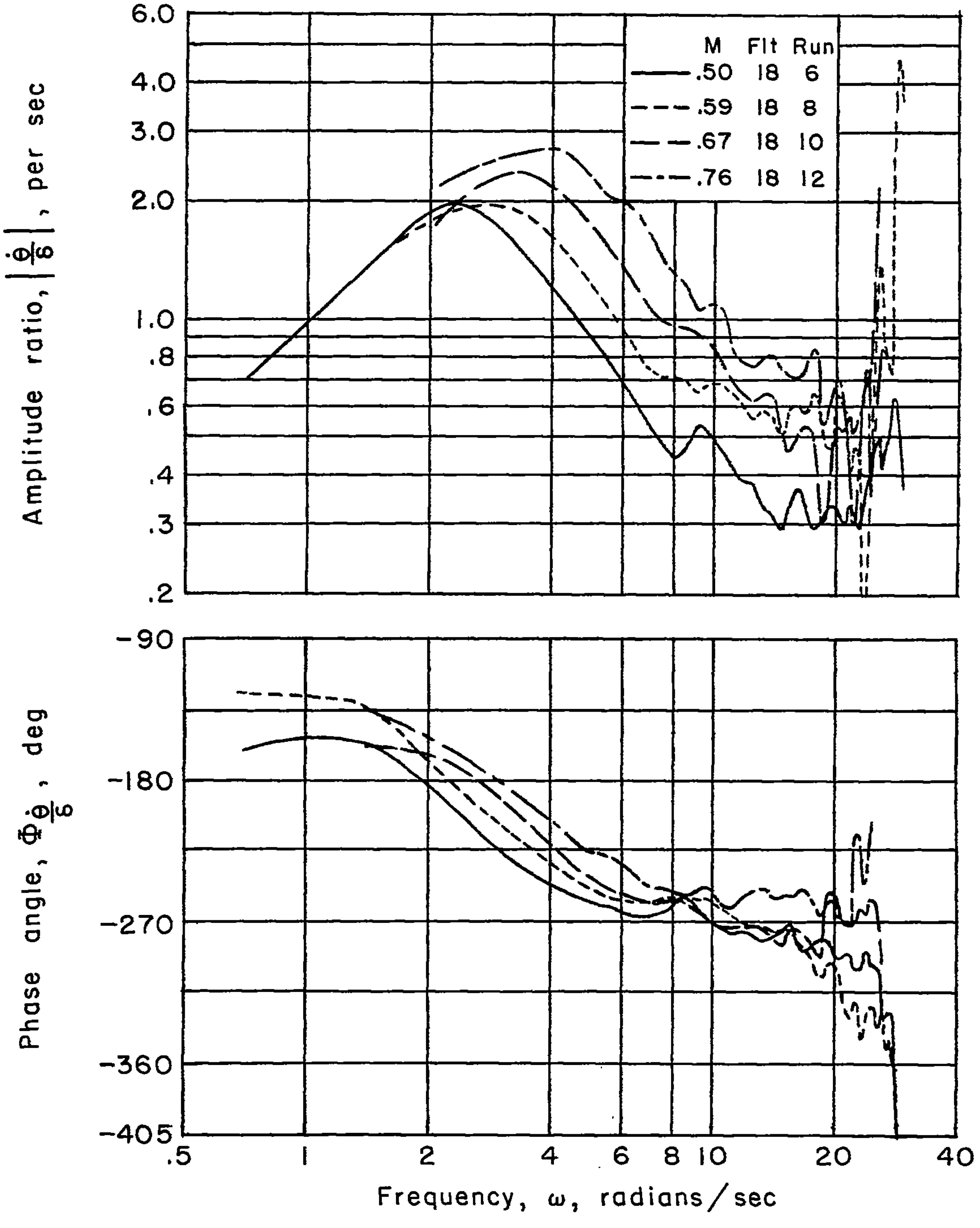

(a) Pitching velocity at center of gravity.

Figure 4.- Frequency response at an altitude of 15,000 feet.

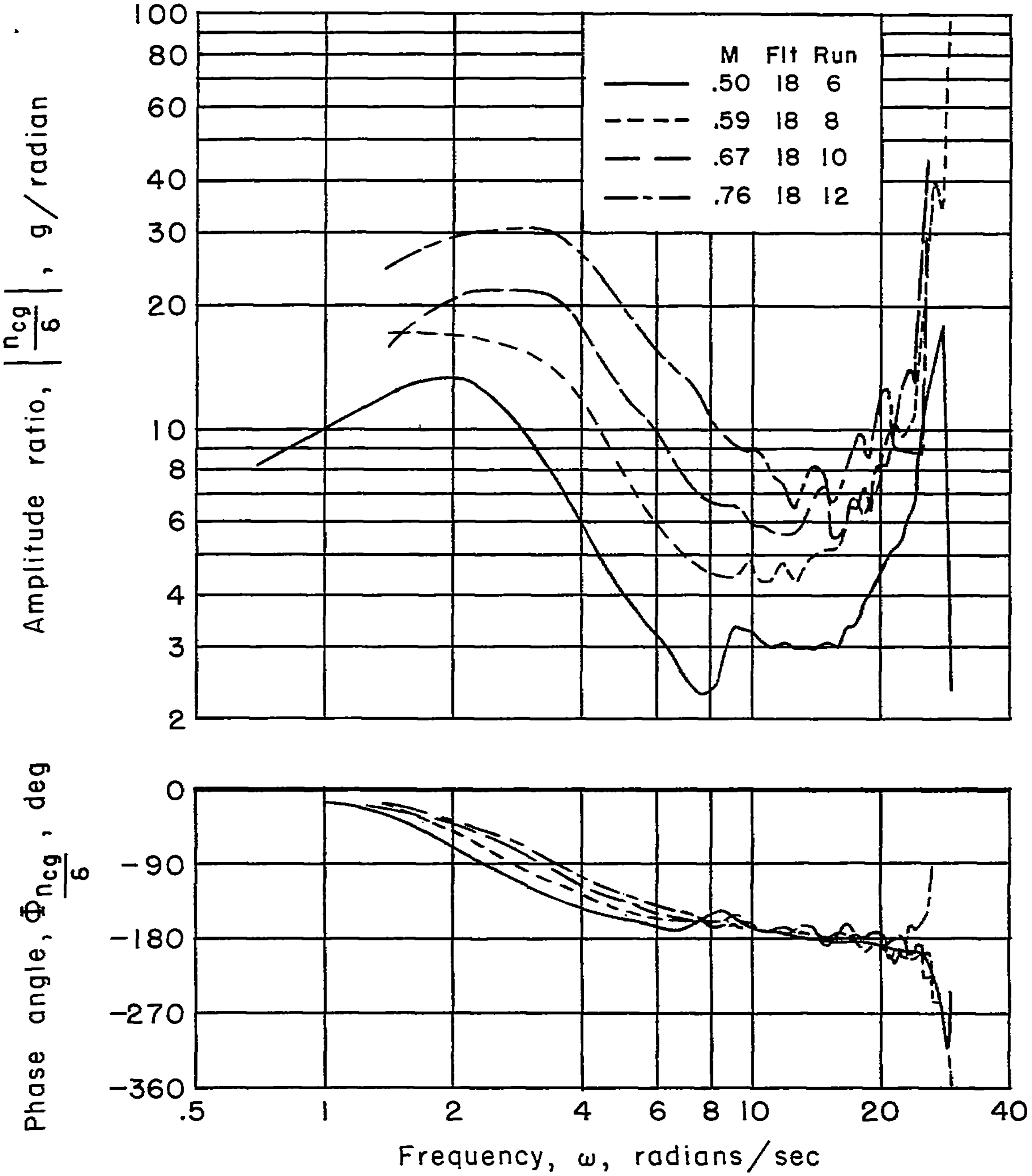

(b) Acceleration at center of gravity.

Figure 4.- Continued.

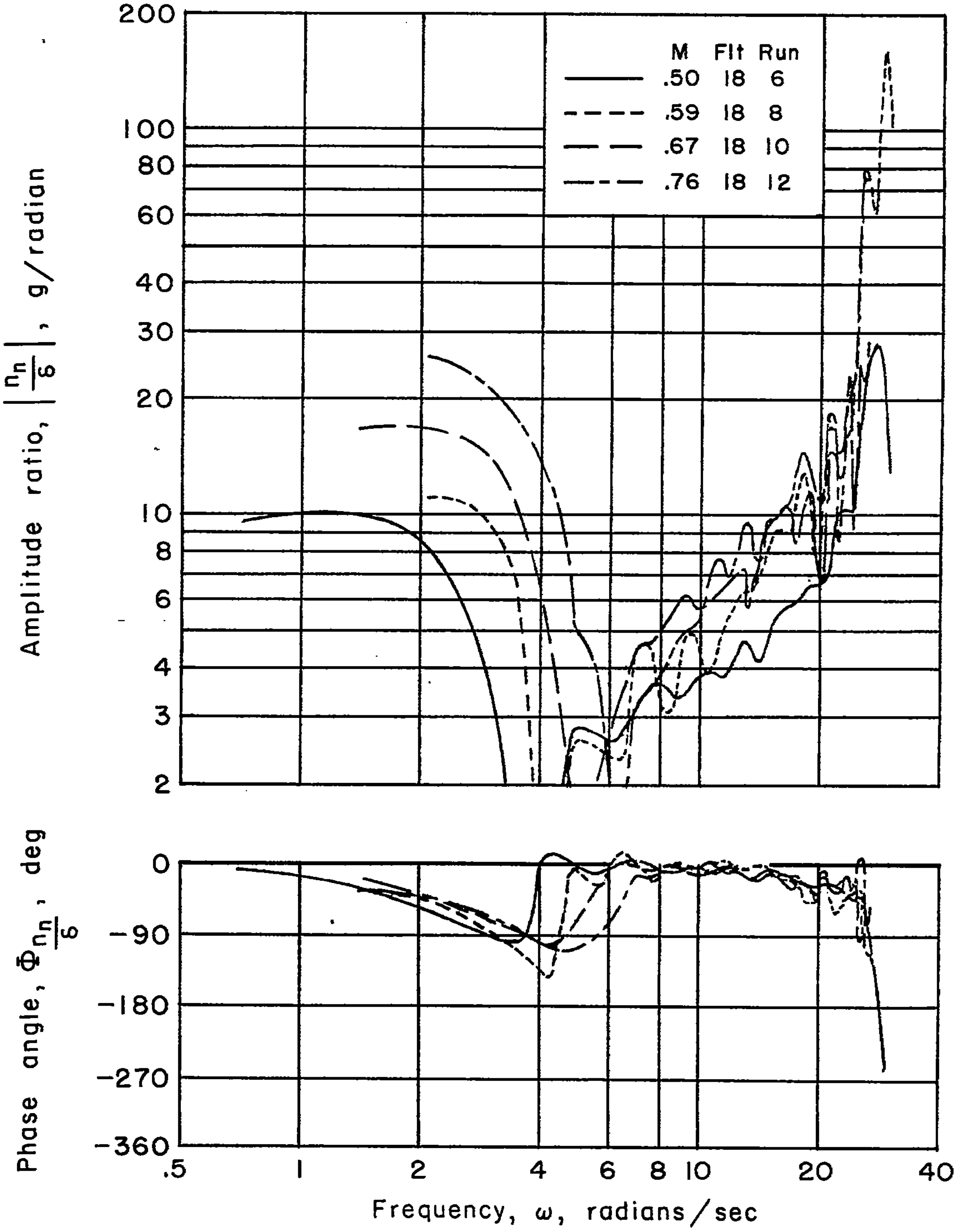

(c) Acceleration at nose.

Figure 4.- Continued.

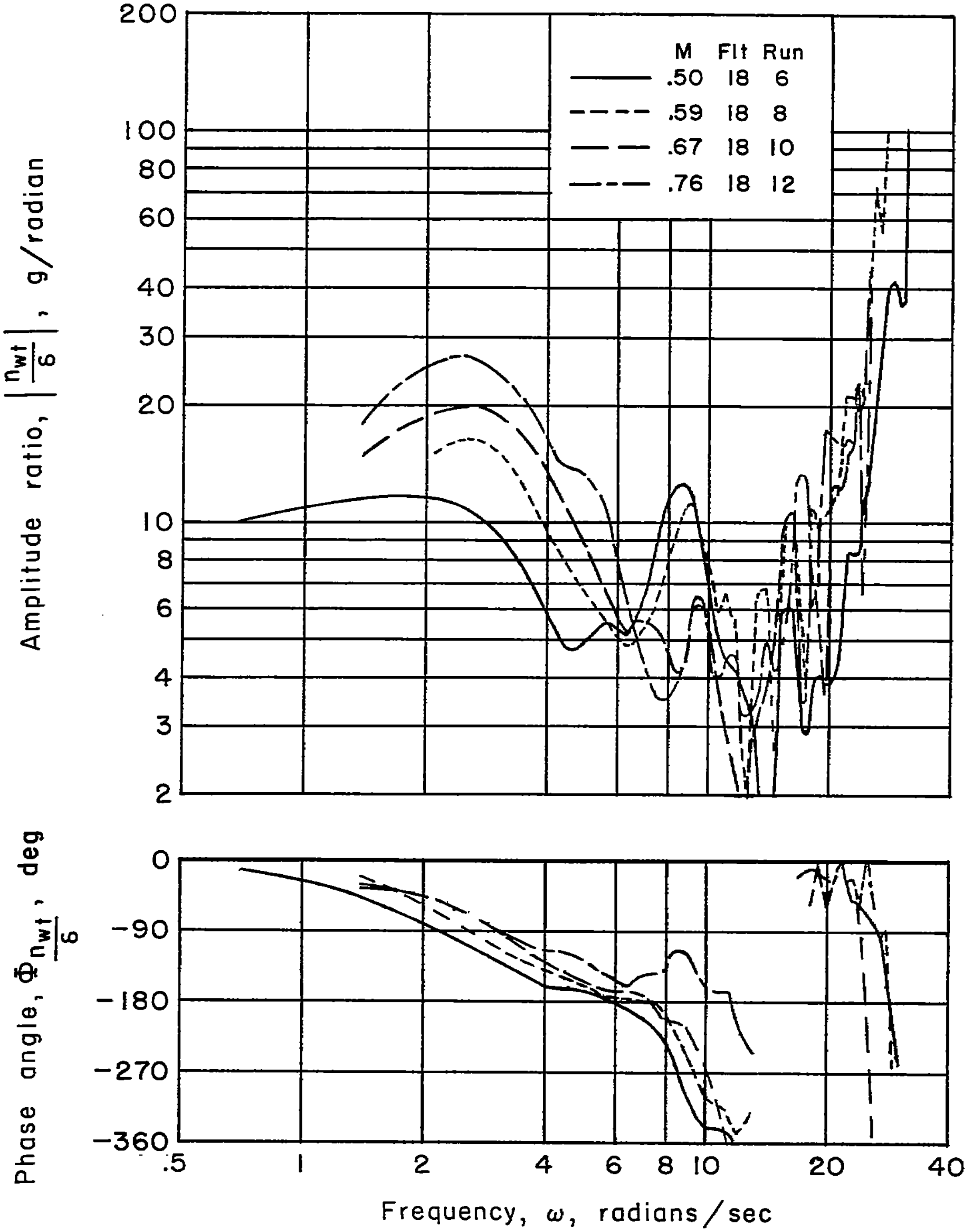

(d) Acceleration at wing tip.

Figure 4.- Continued.

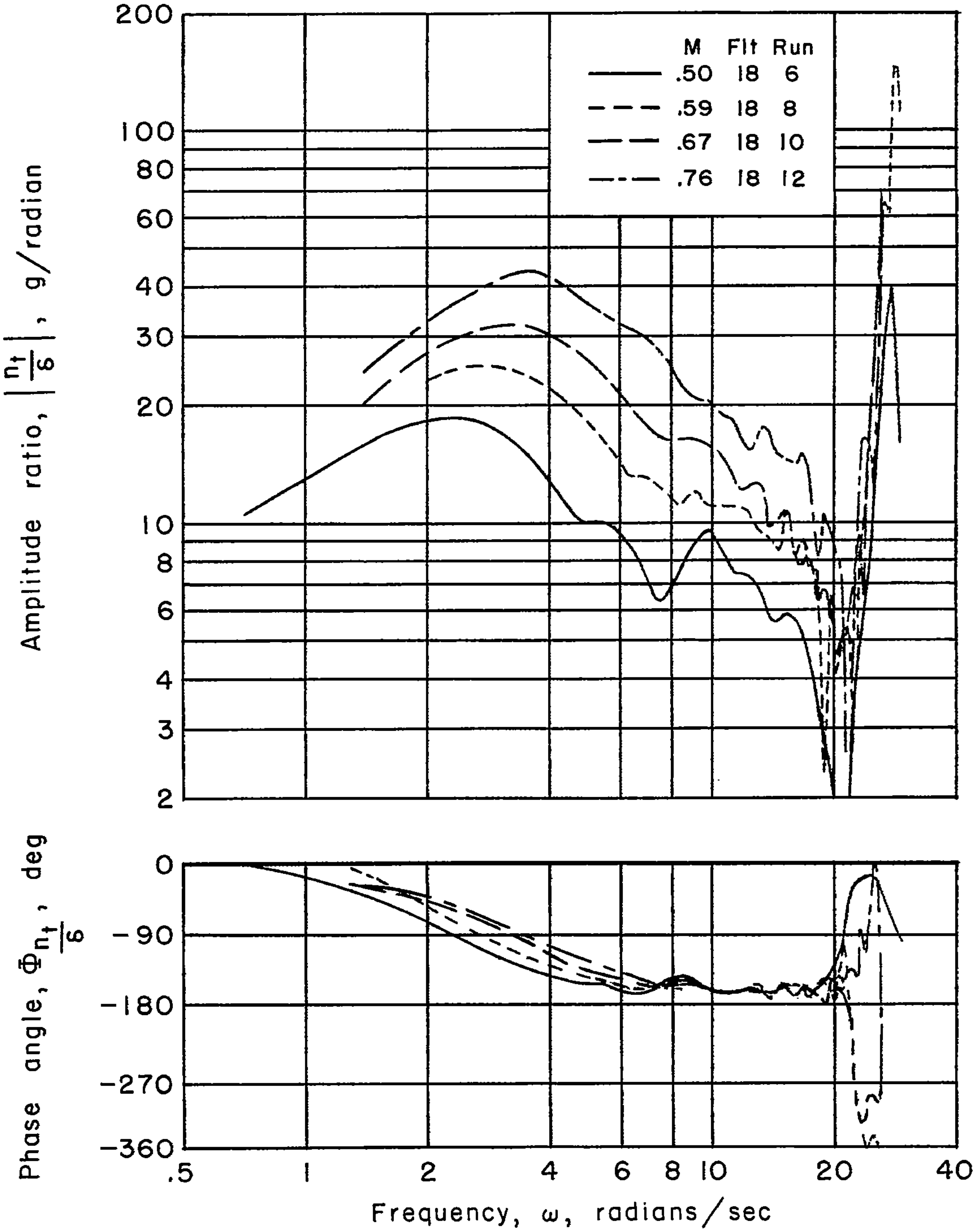

(e) Acceleration at tail.

Figure 4.- Concluded.

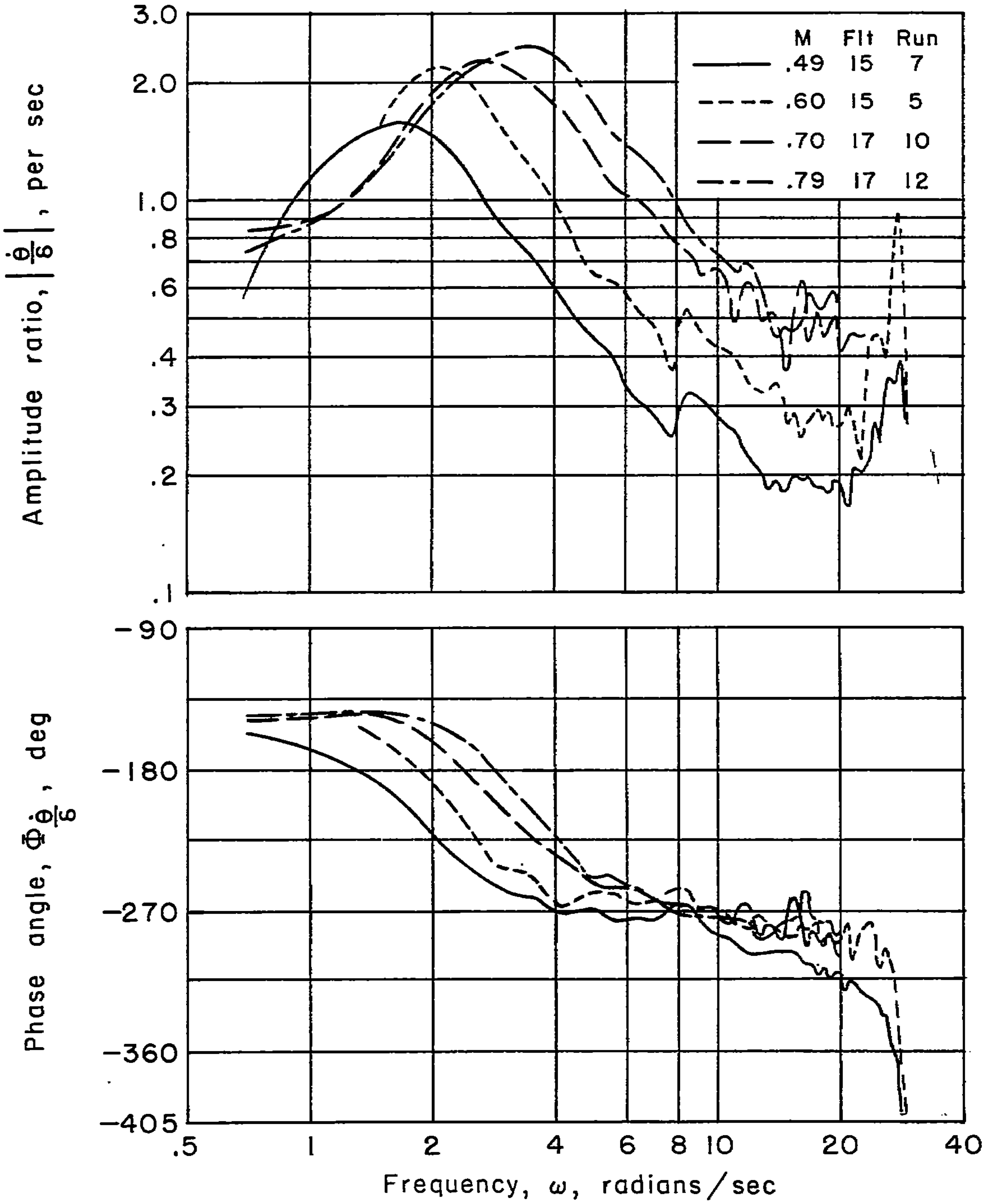

(a) Pitching velocity at center of gravity.

Figure 5.- Frequency response at an altitude of 25,000 feet.

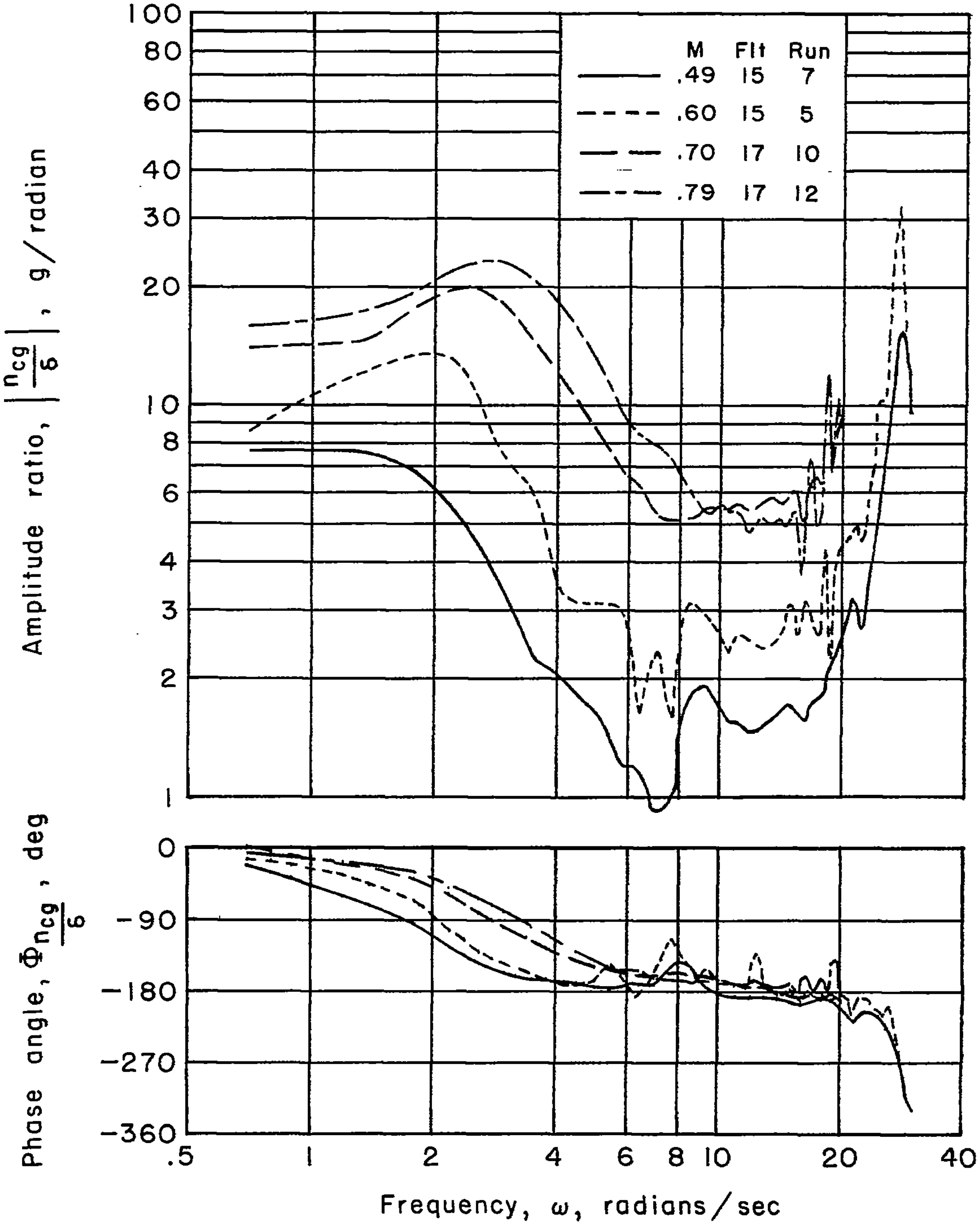

(b) Acceleration at center of gravity.

Figure 5.- Continued.

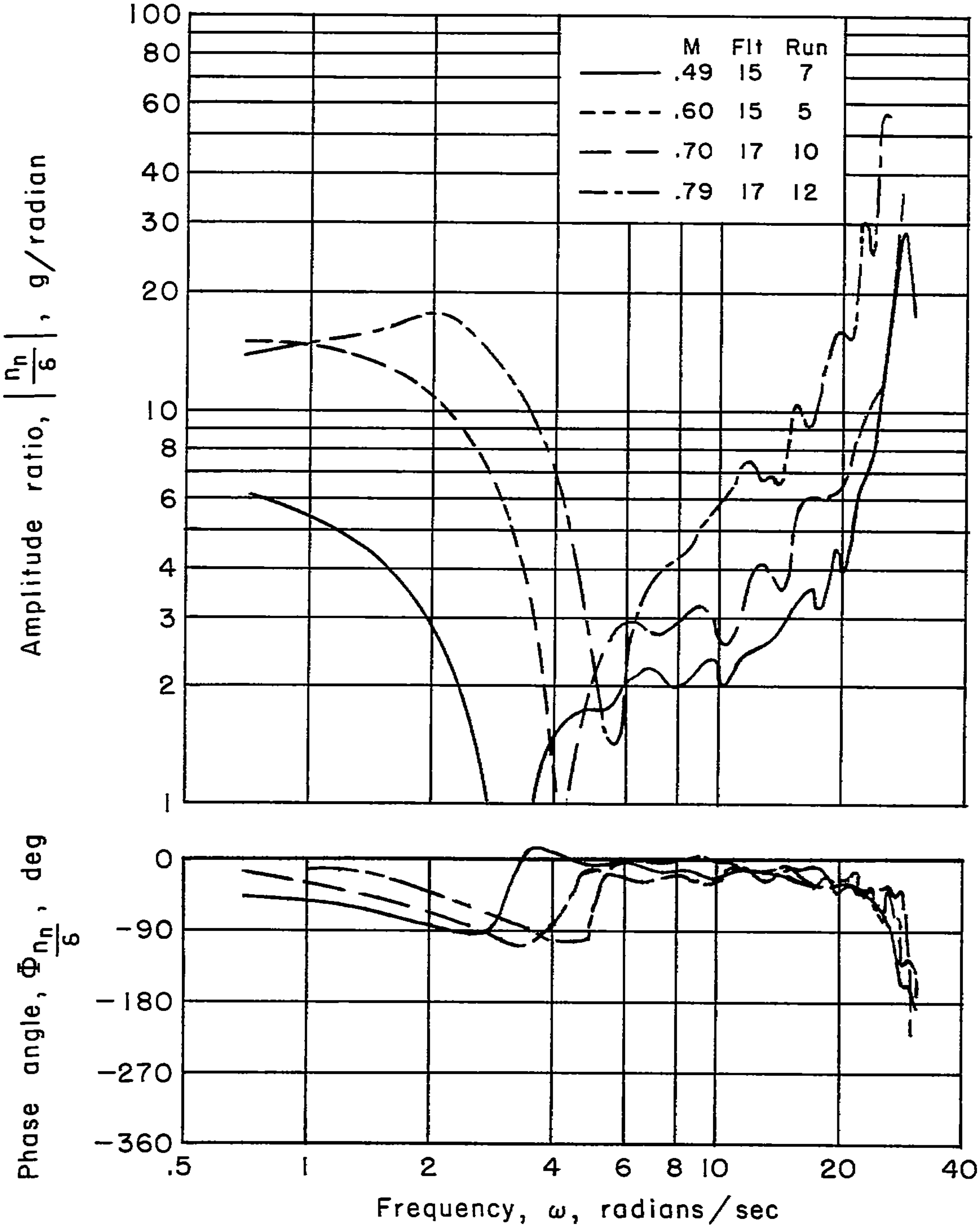

(c) Acceleration at nose.

Figure 5.- Continued.

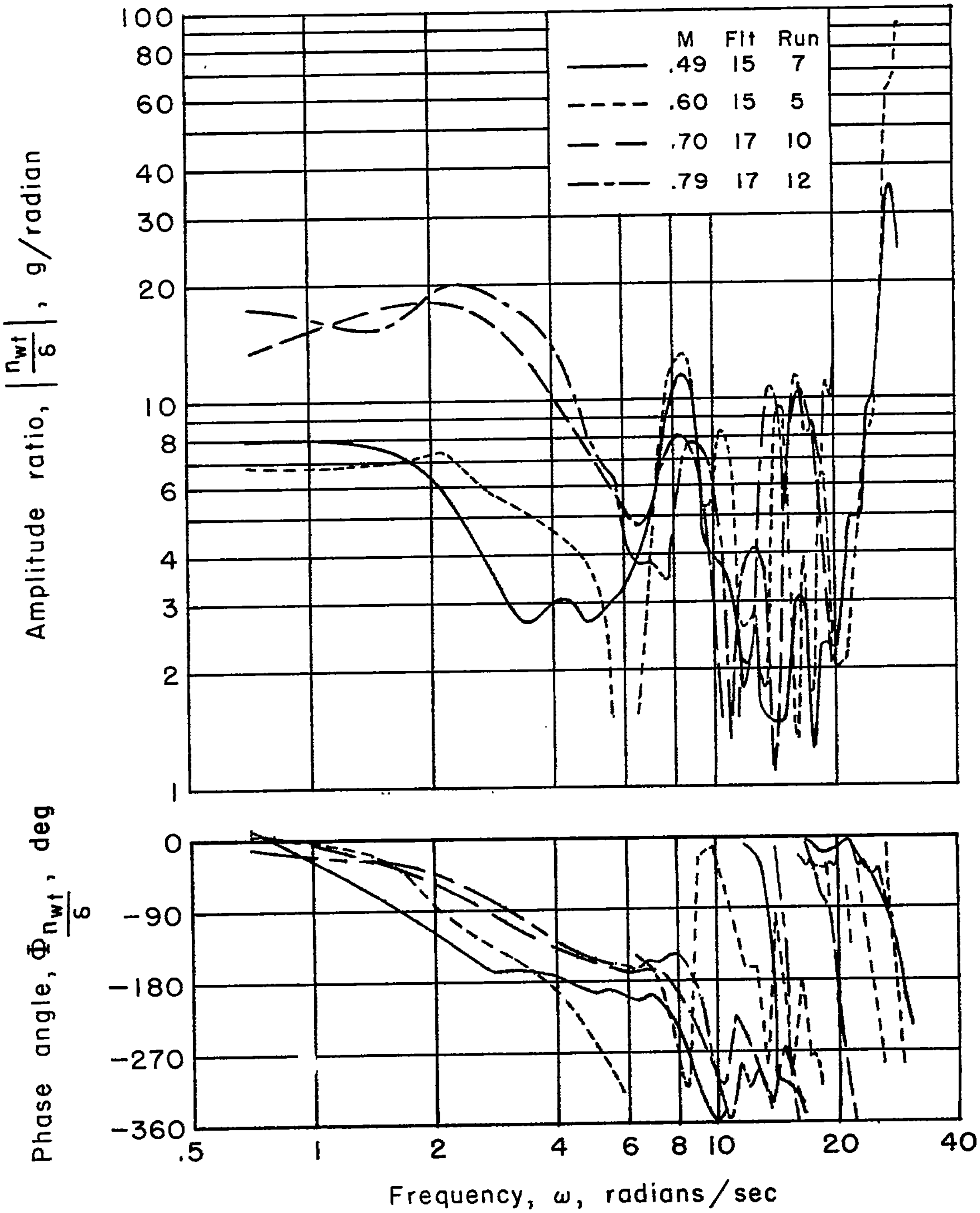

(d) Acceleration at wing tip.

Figure 5.- Continued.

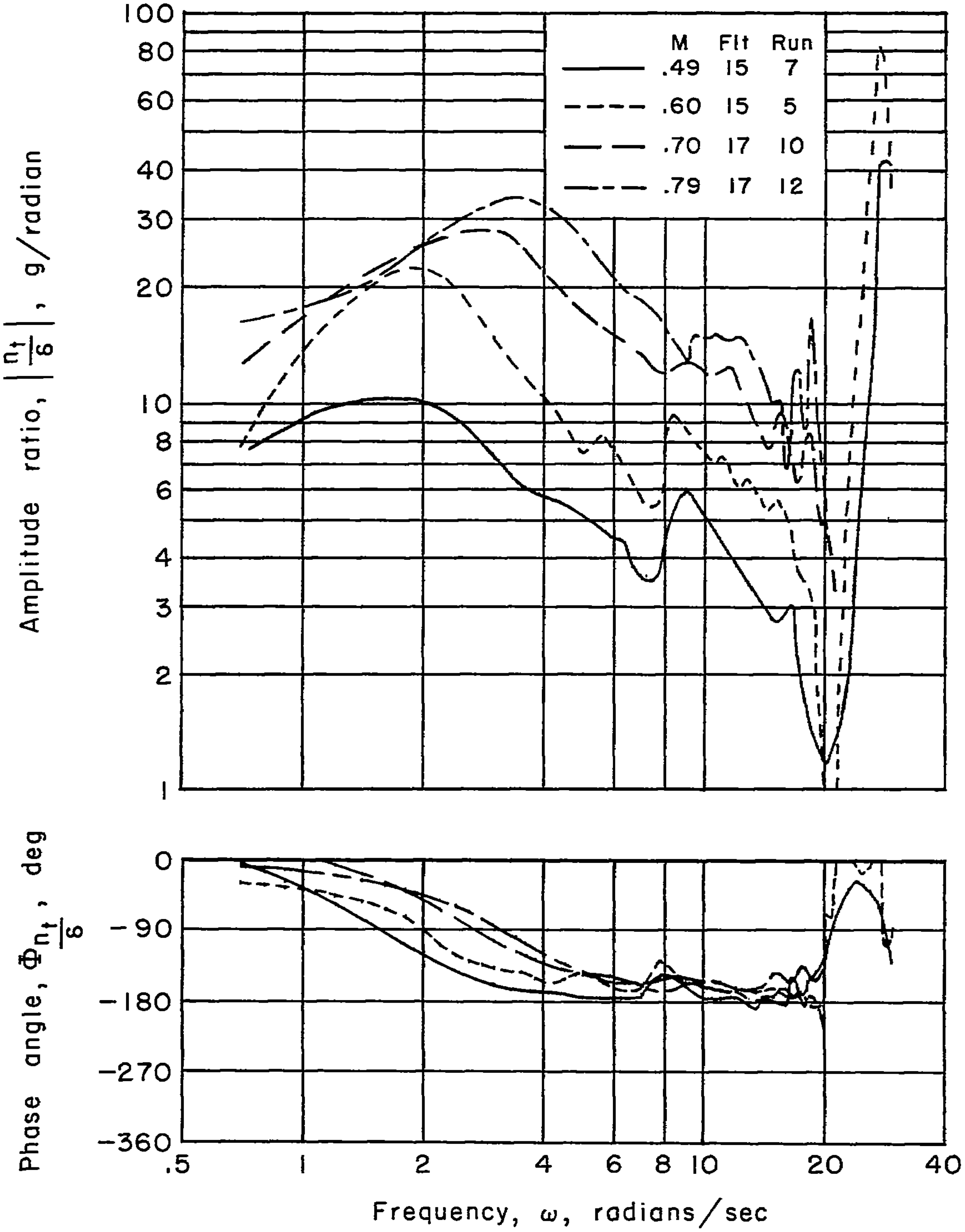

(e) Acceleration at tail.

Figure 5.- Concluded.

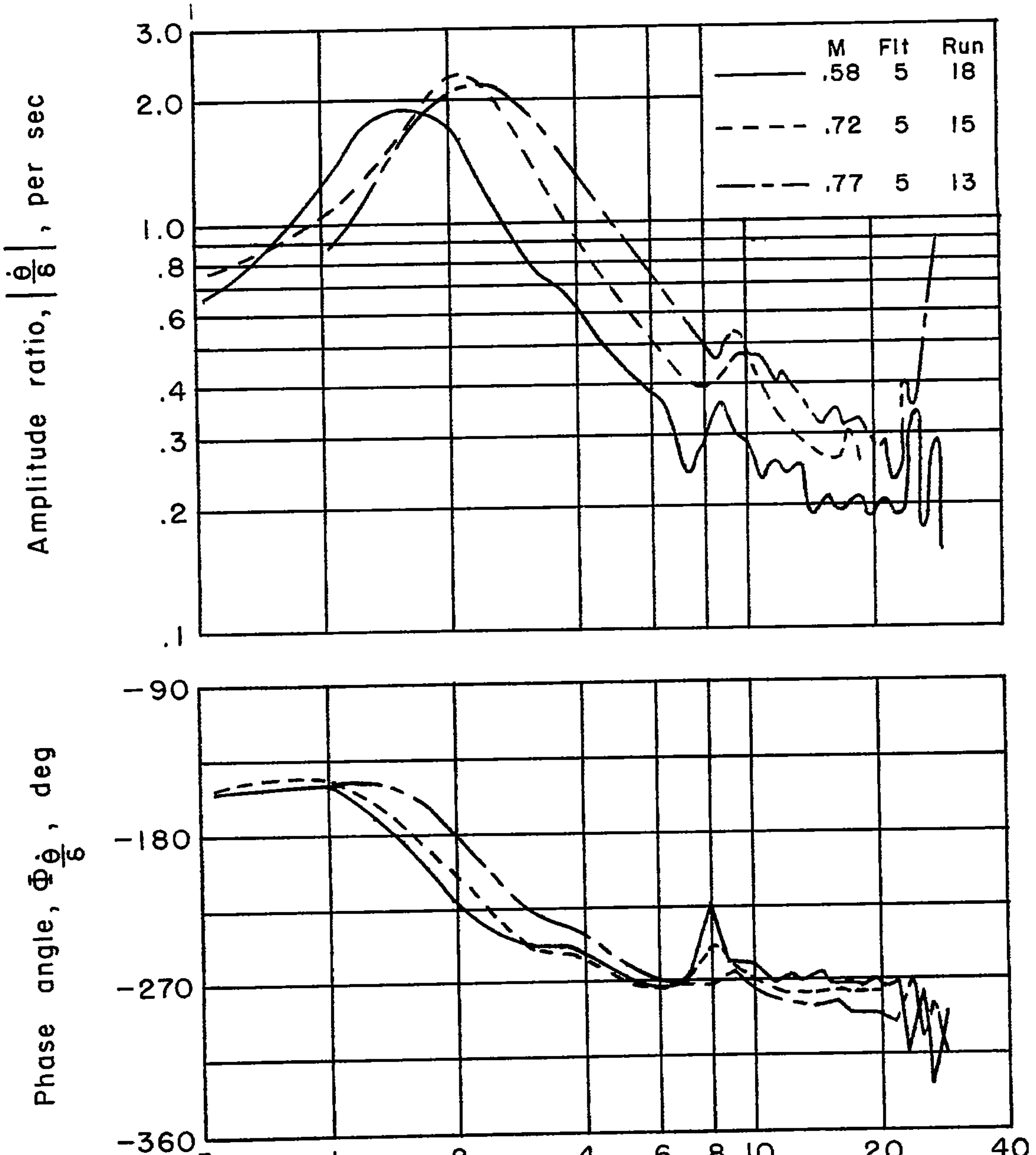

(a) Pitching velocity at center of gravity.

Figure 6.- Frequency response at an altitude of 35,000 feet.

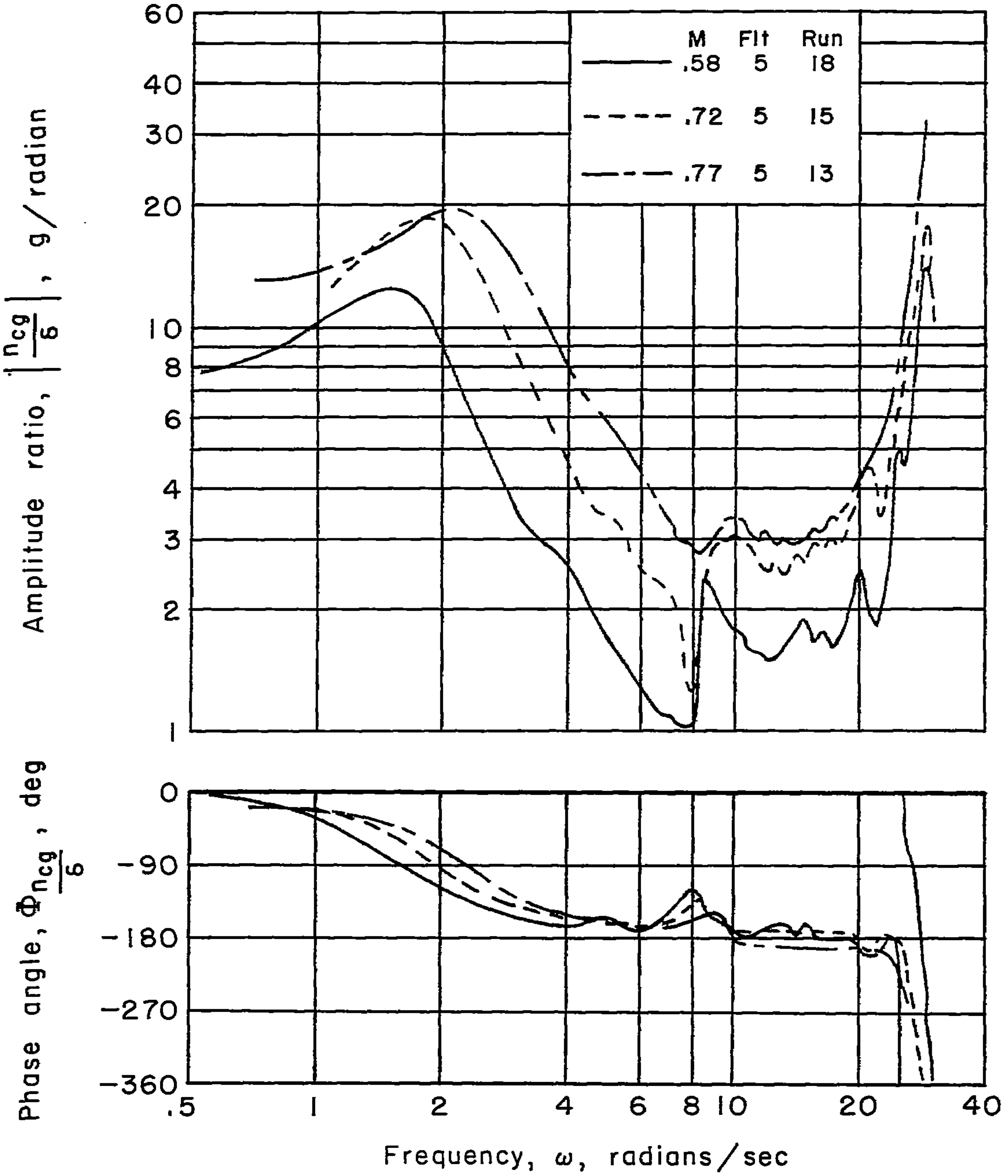

(b) Acceleration at center of gravity.

Figure 6.- Continued.

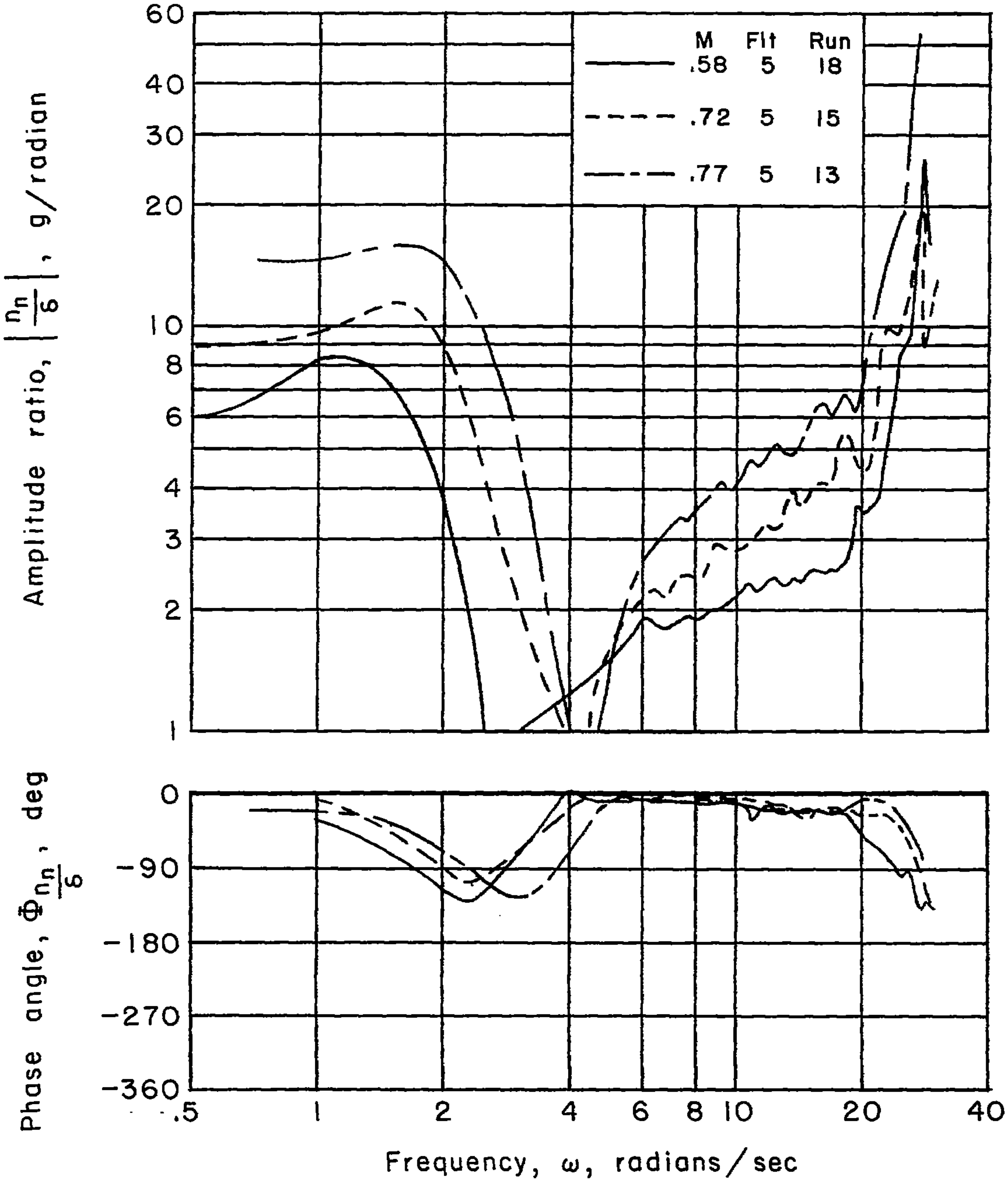

(c) Acceleration at nose.

Figure 6.- Continued.

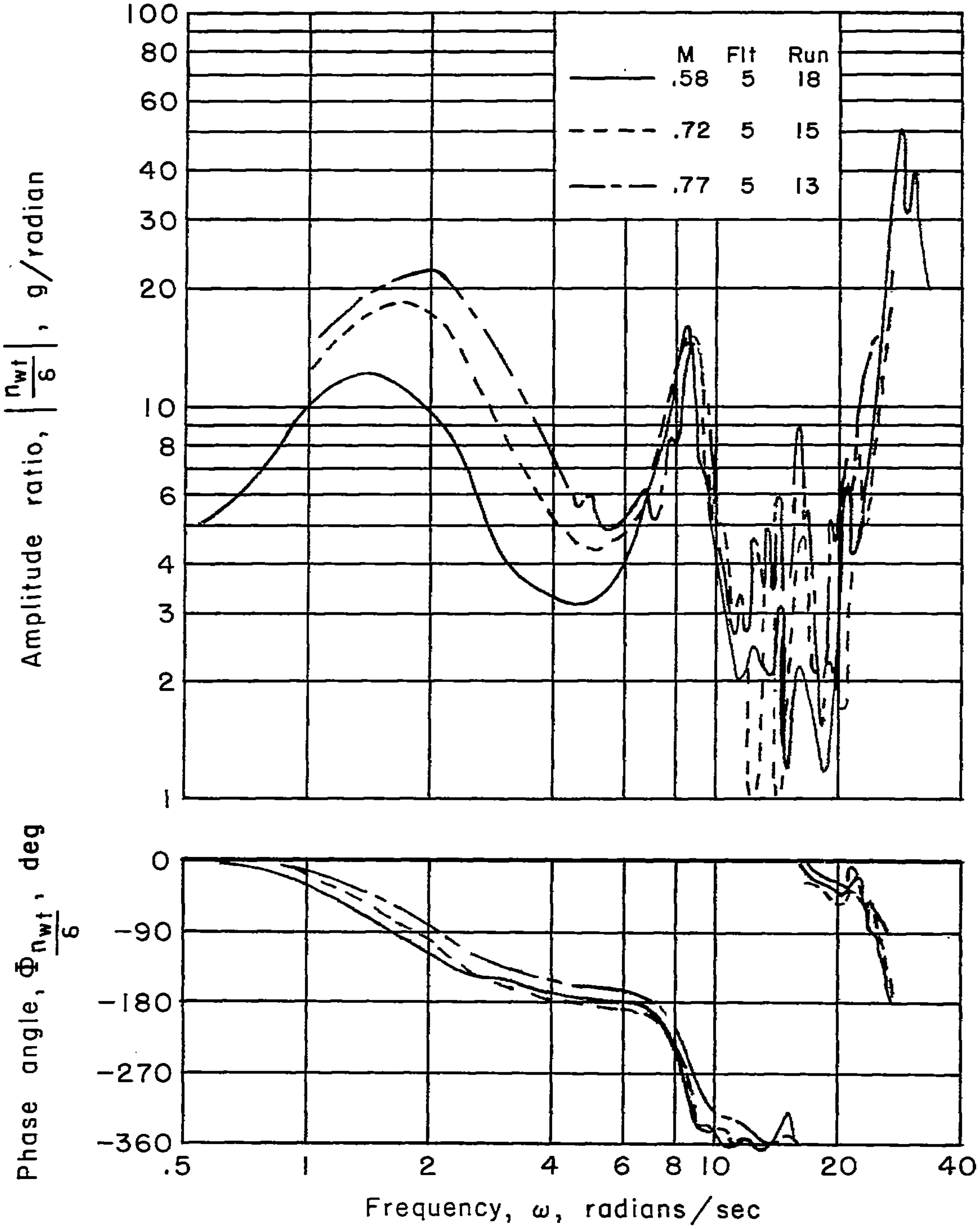

(d) Acceleration at wing tip.

Figure 6.- Continued.

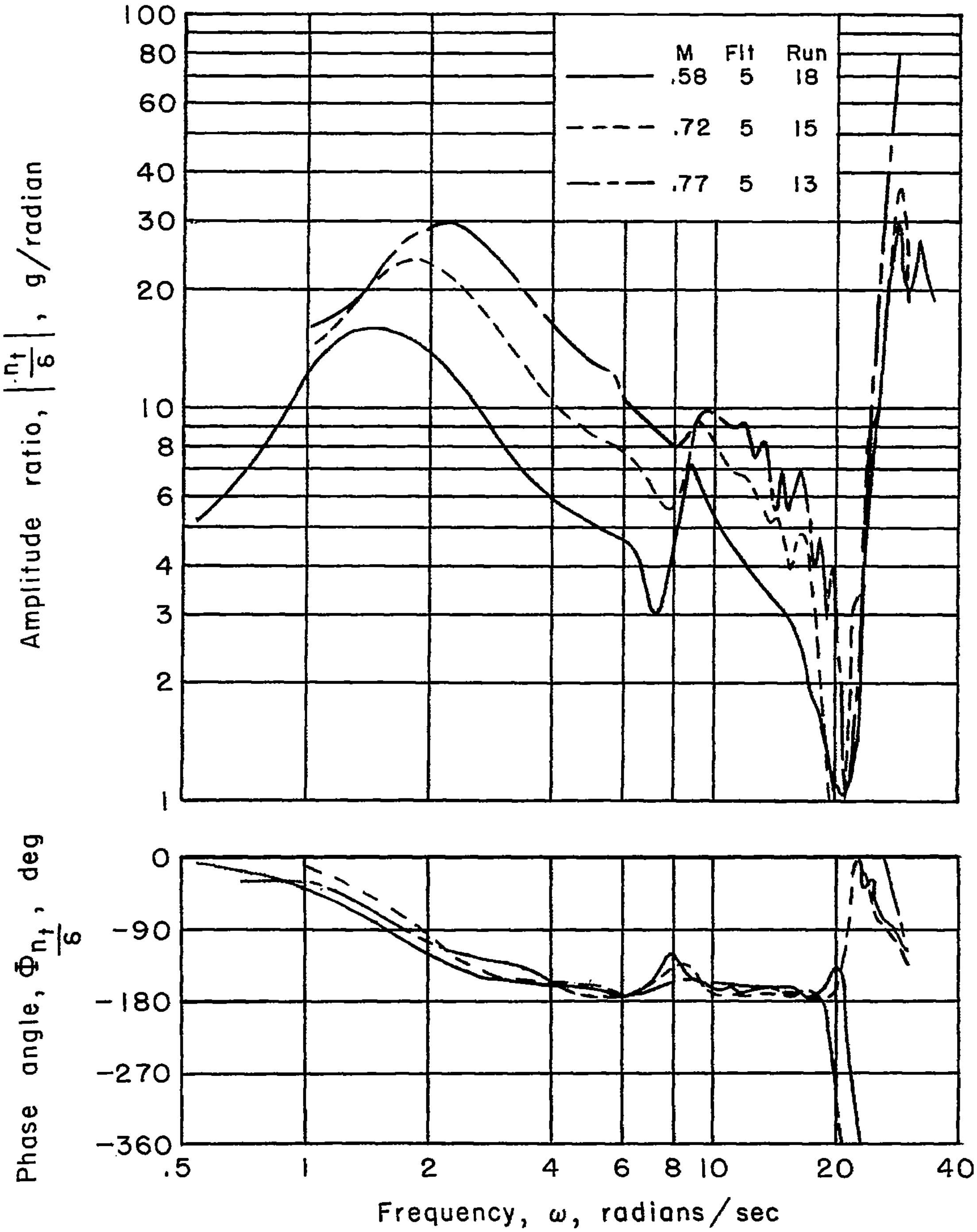

(e) Acceleration at tail.

Figure 6.- Concluded.

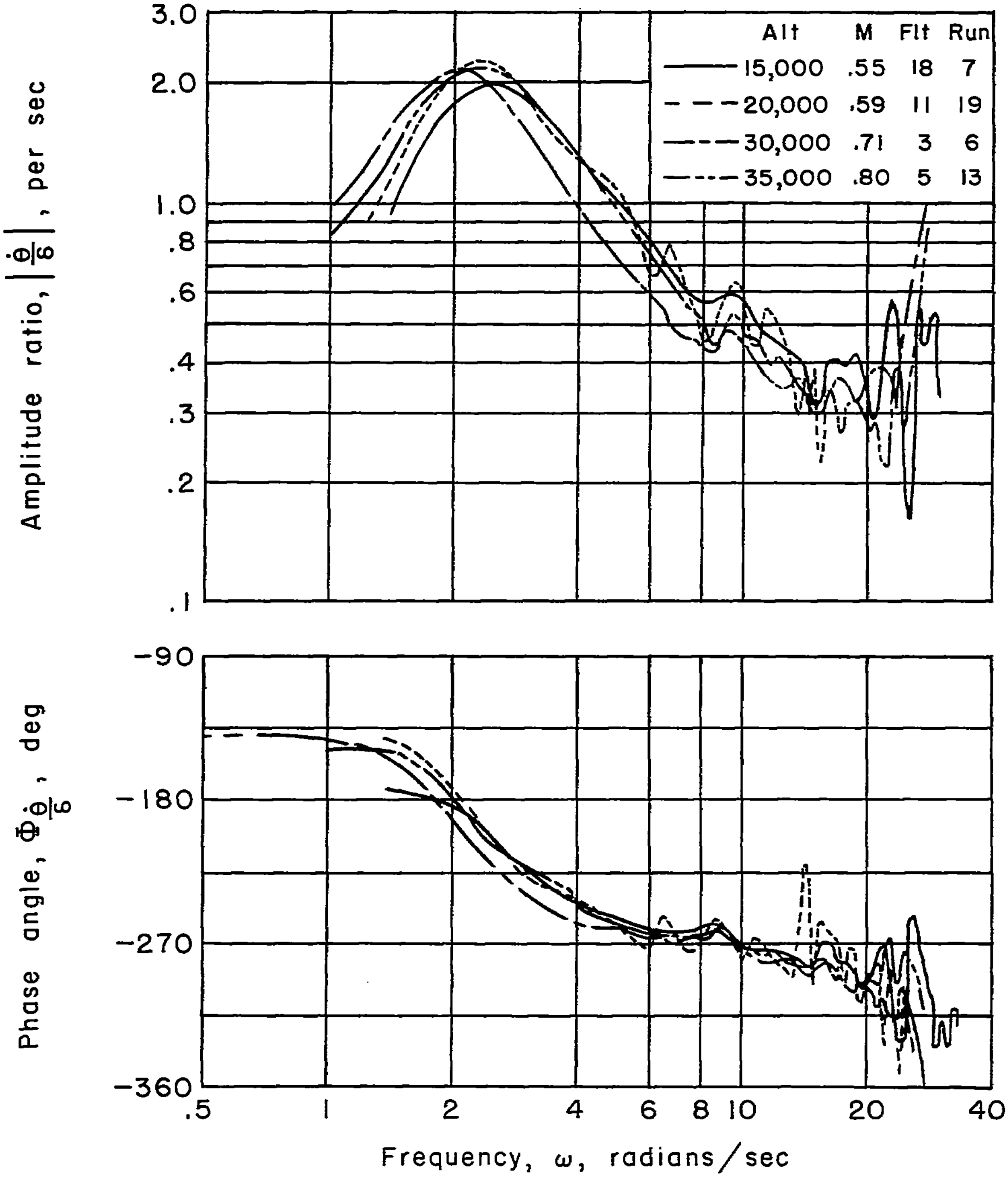

(a) Pitching velocity at center of gravity.

Figure 7.- Frequency response at a q/β of 280 pounds per square foot.

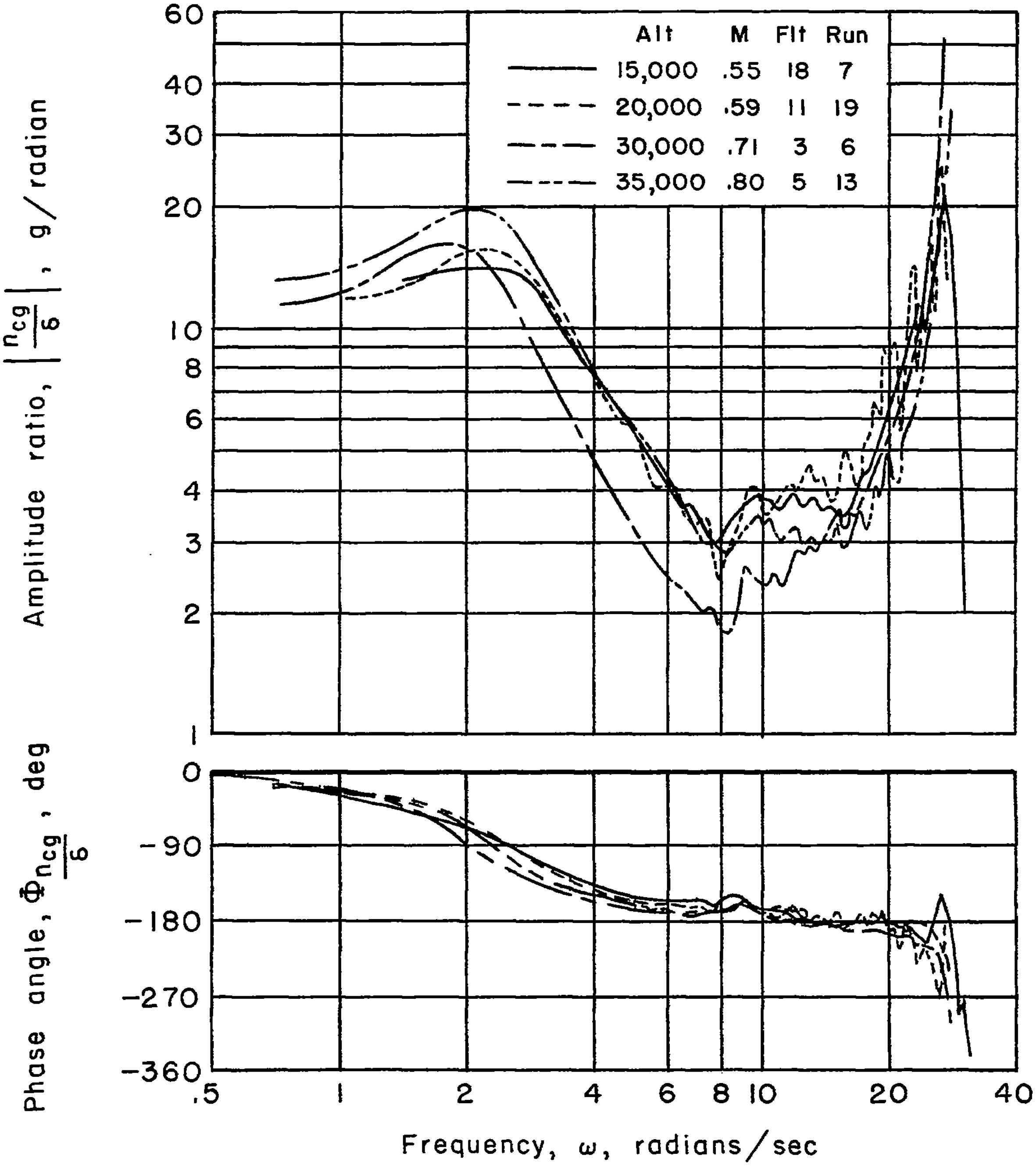

(b) Acceleration at center of gravity.

Figure 7.- Continued.

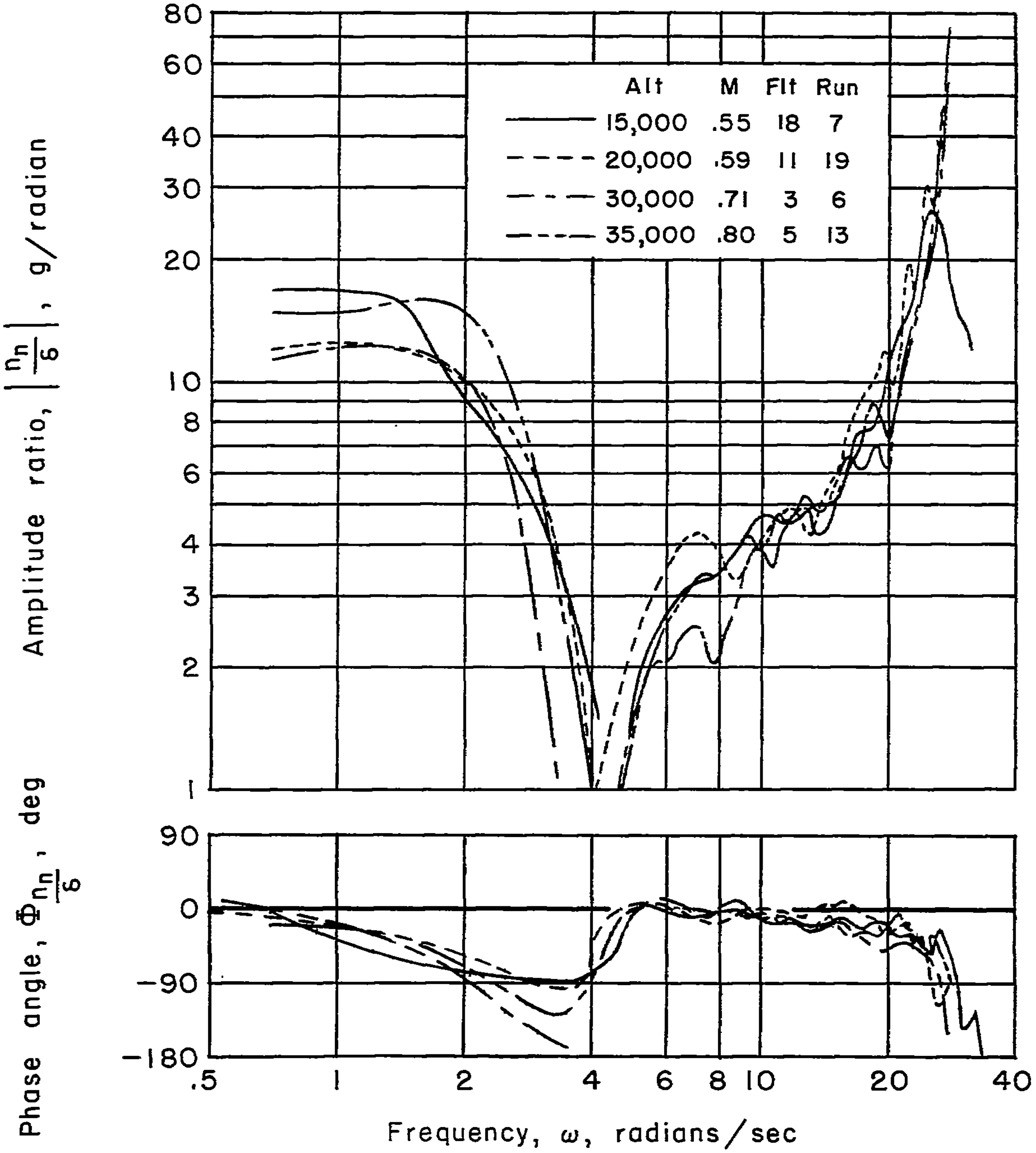

(c) Acceleration at nose.

Figure 7.- Continued.

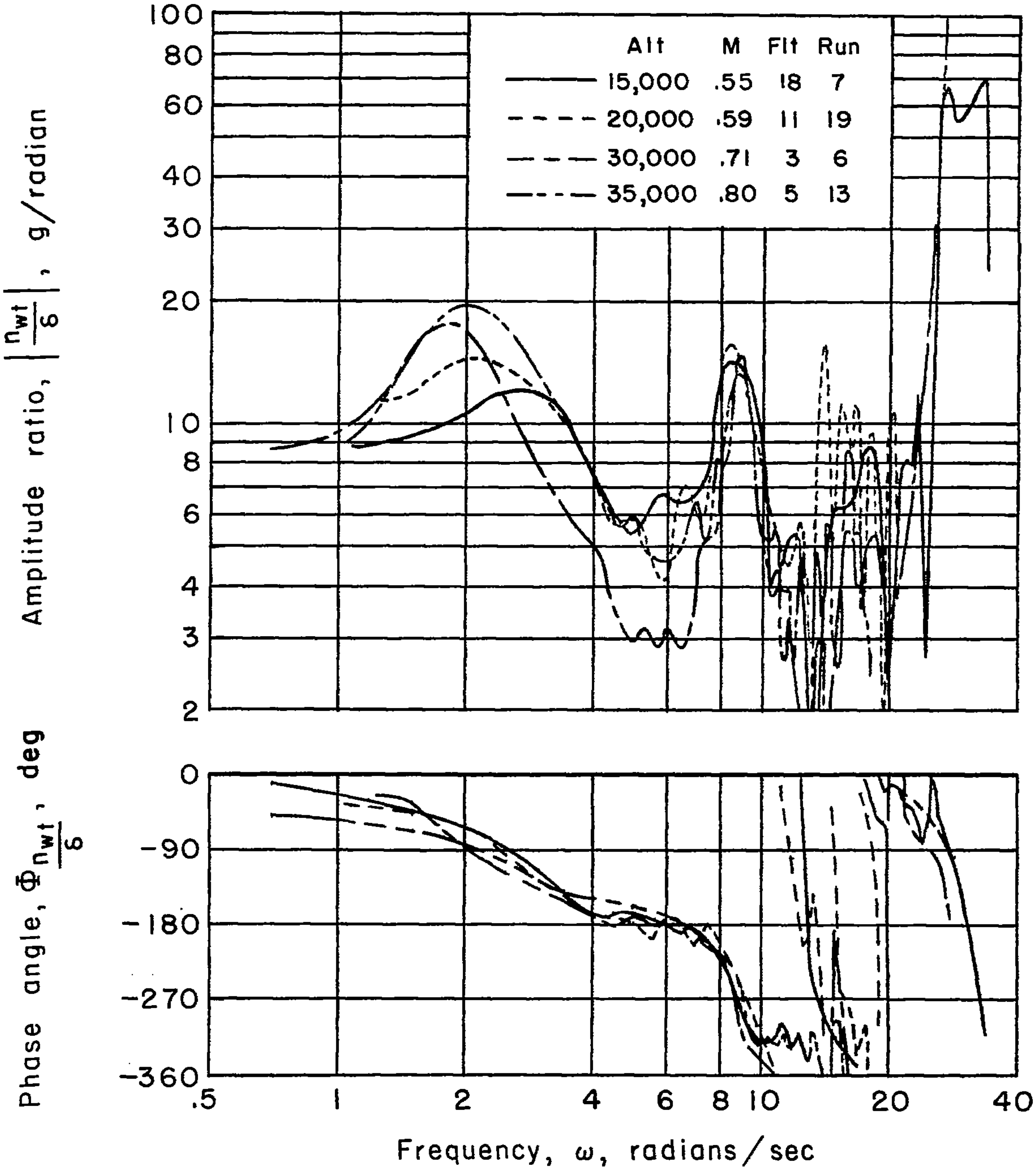

(d) Acceleration at wing tip.

Figure 7.- Continued.

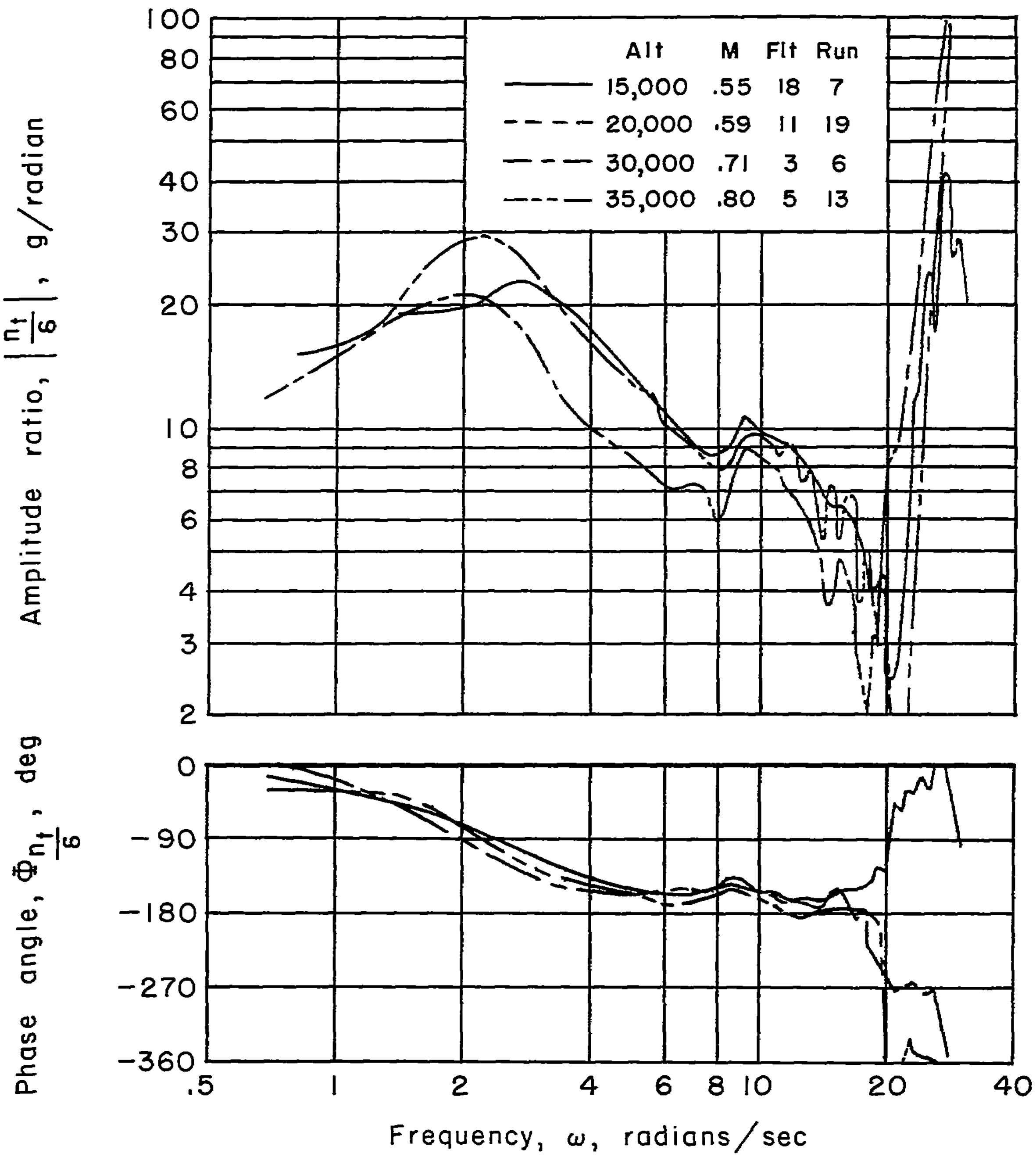

(e) Acceleration at tail.

Figure 7.- Concluded.

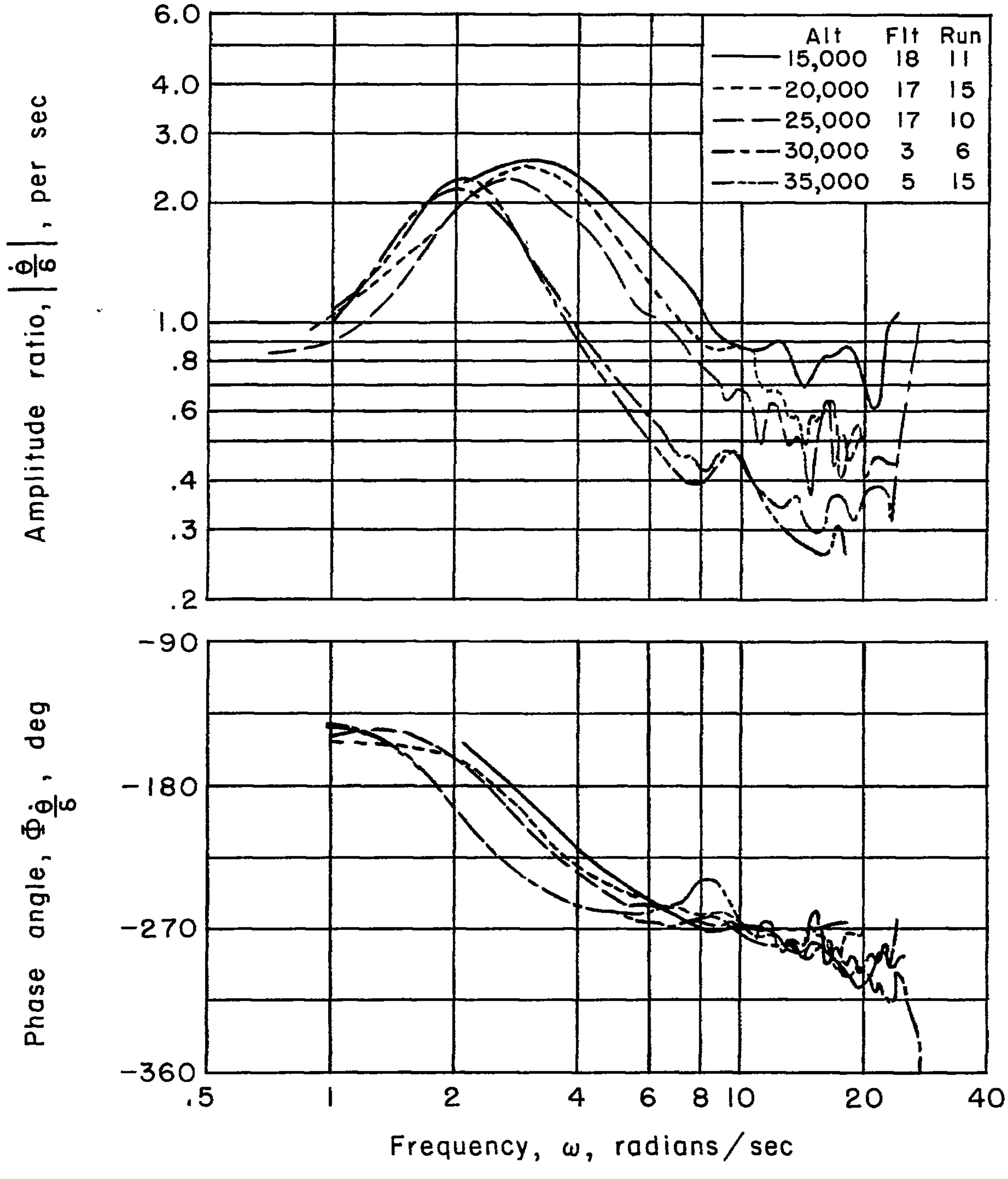

(a) Pitching velocity at center of gravity.

Figure 8.- Frequency response at a Mach number of 0.7.

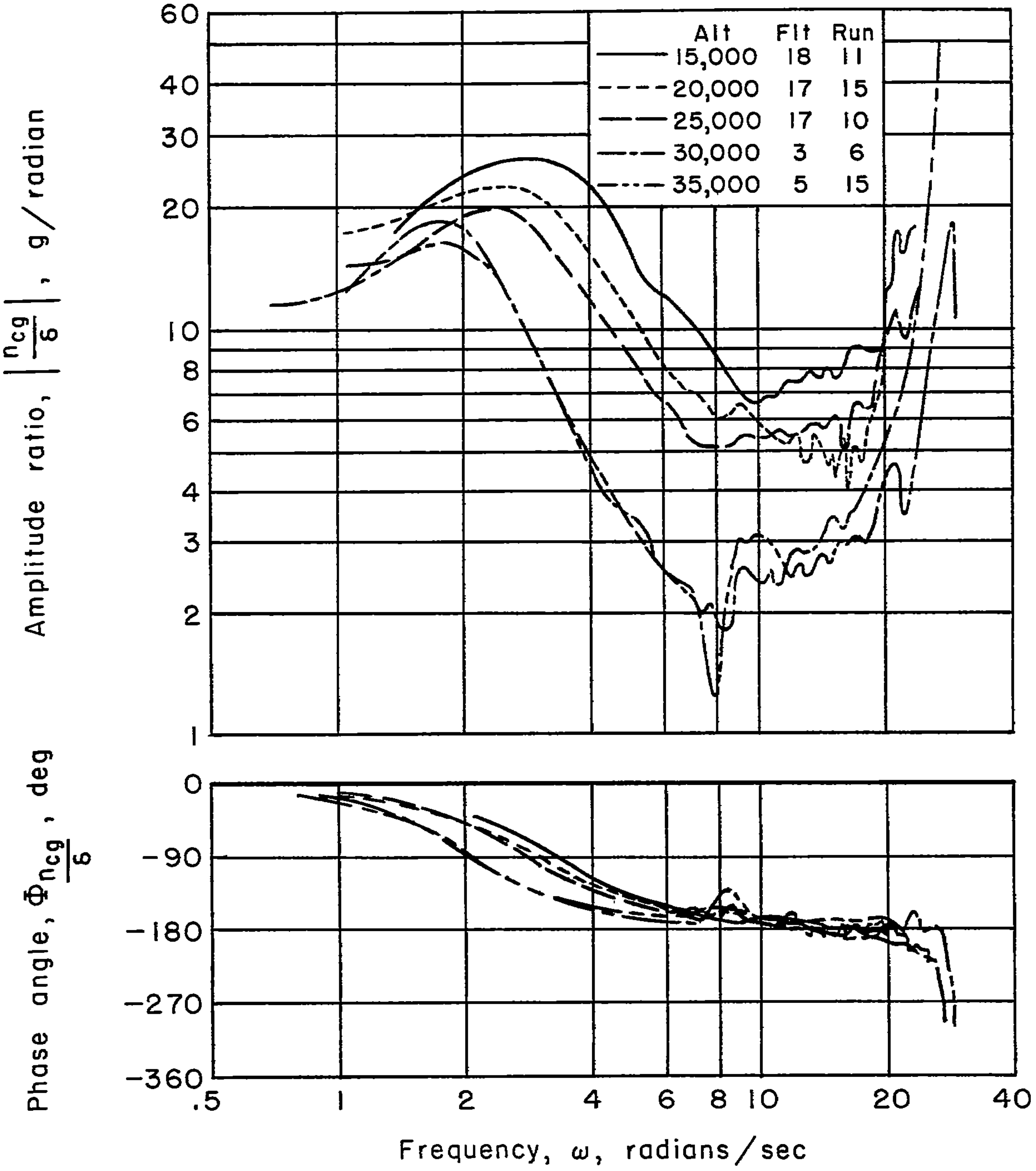

(b) Acceleration at center of gravity.

Figure 8.- Continued.

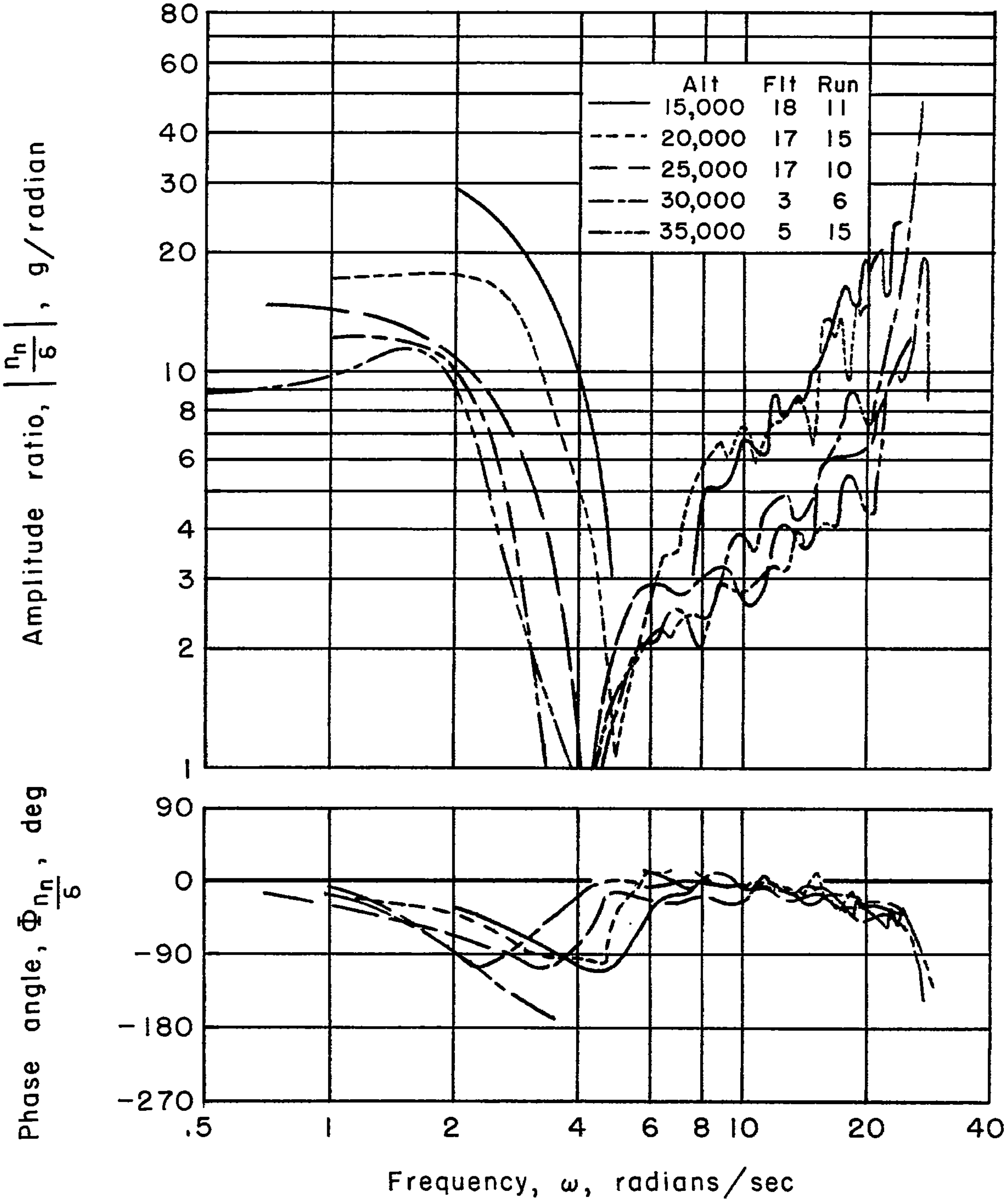

(c) Acceleration at nose.

Figure 8.- Continued.

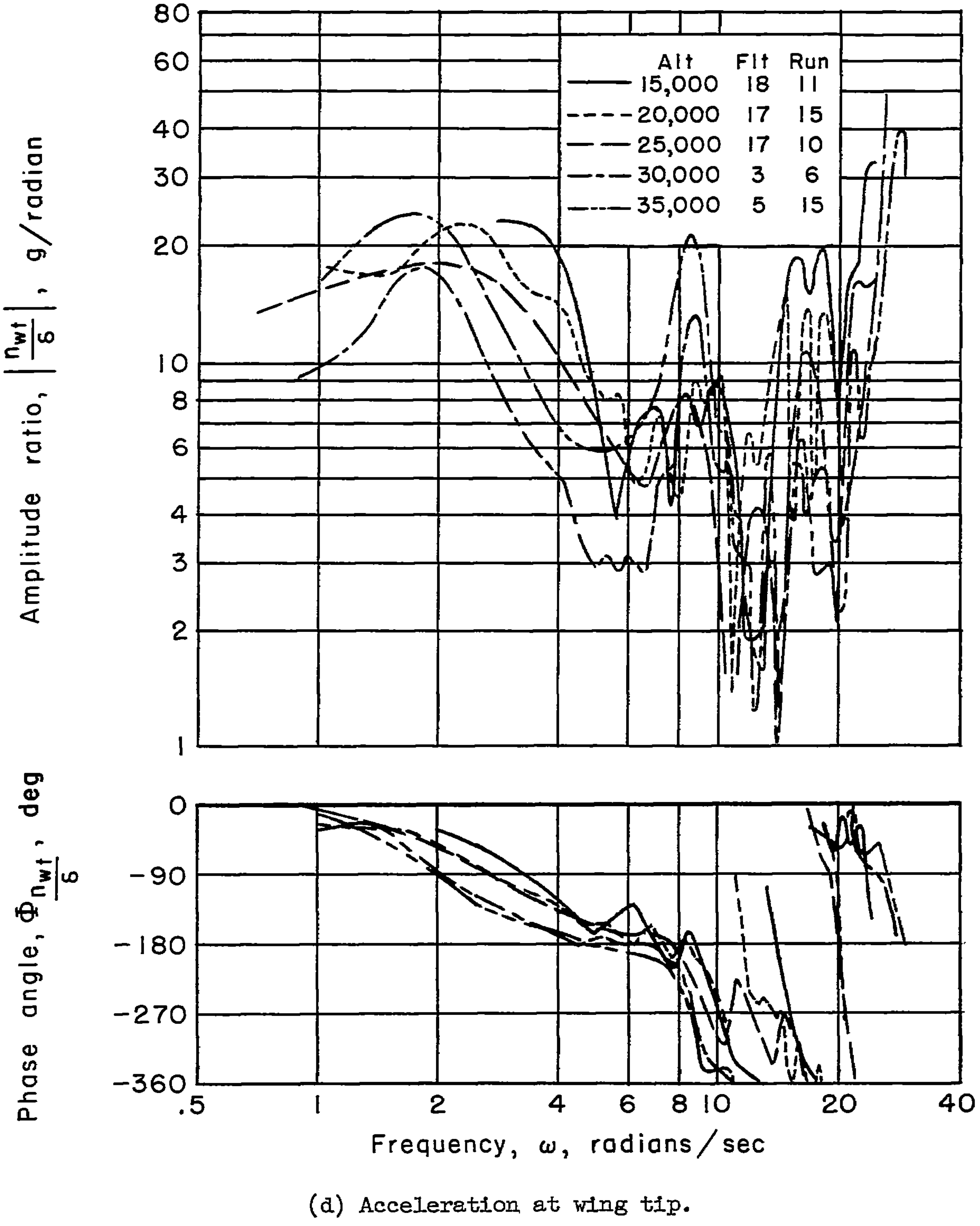

(d) Acceleration at wing tip.

Figure 8.- Continued.

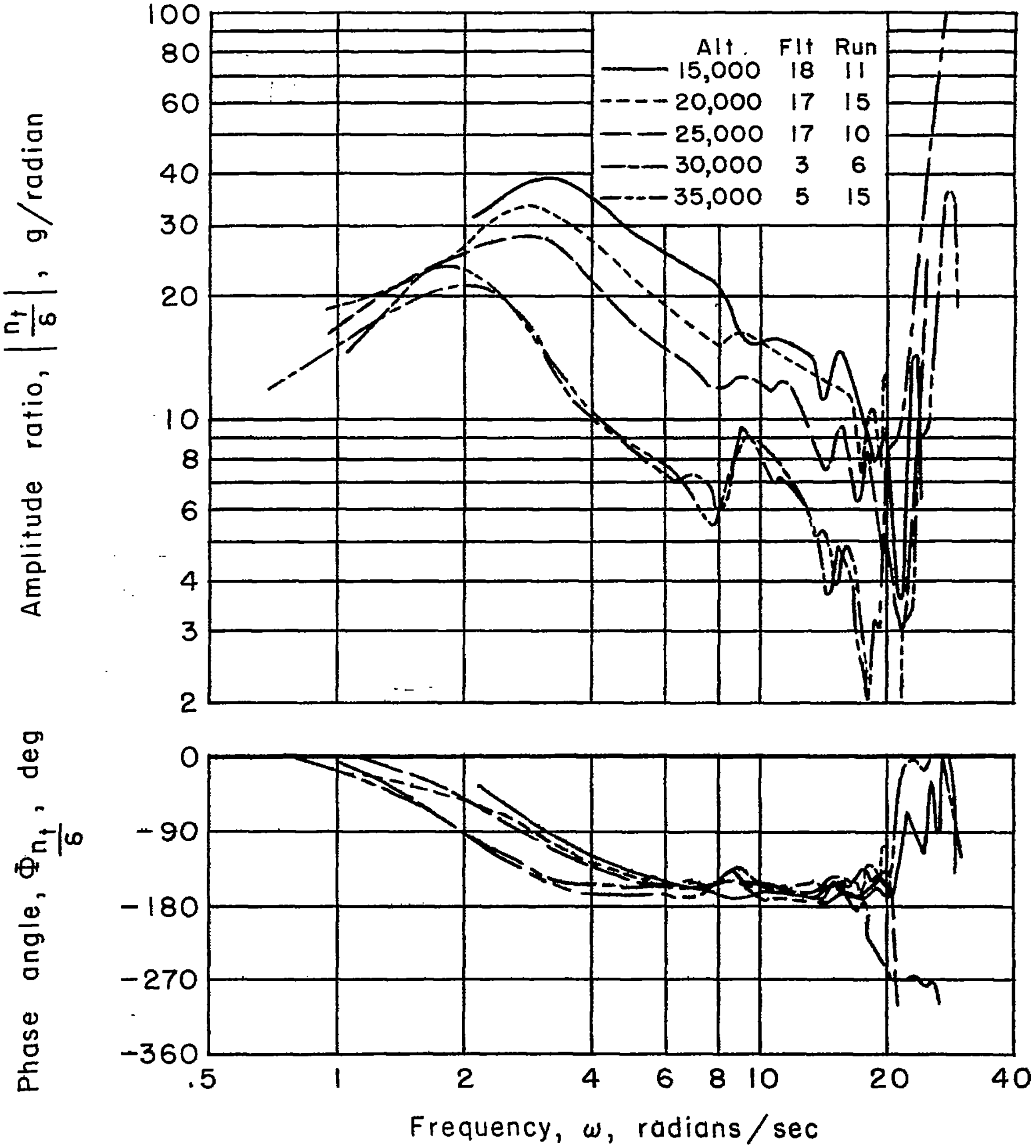

(e) Acceleration at tail.

Figure 8.- Concluded.

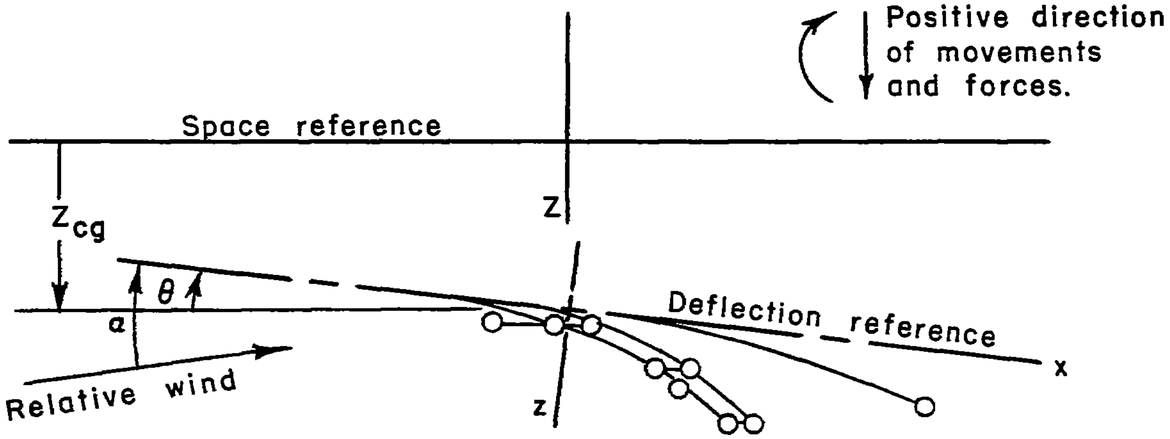
Positive direction of movements and forces.
Space reference
Z
Z_{cg}
θ
α
Relative wind
Deflection reference
x
z

Side view

Note:

Stations 1F, 1R, 2F, 2R, 3F, 3R, 5, 6, 7, a, and c.g. denote mass stations.

Stations 1, 2, 3, and 4, denote angle of attack stations at 0.924, 0.707, 0.383, and 0 fraction of semispan, respectively.

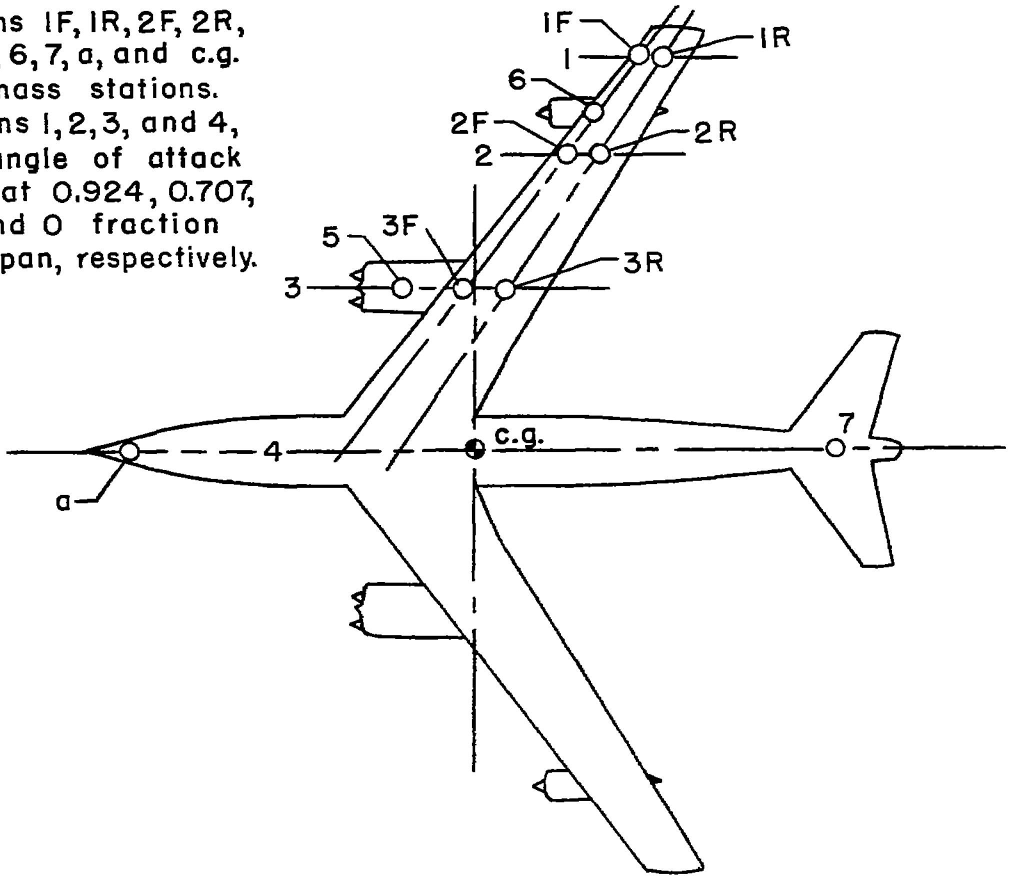
1F
1R
1
6
2F
2R
2
5
3F
3R
3
4
c.g.
7
a

Plan view

Figure 9.- Coordinate system.

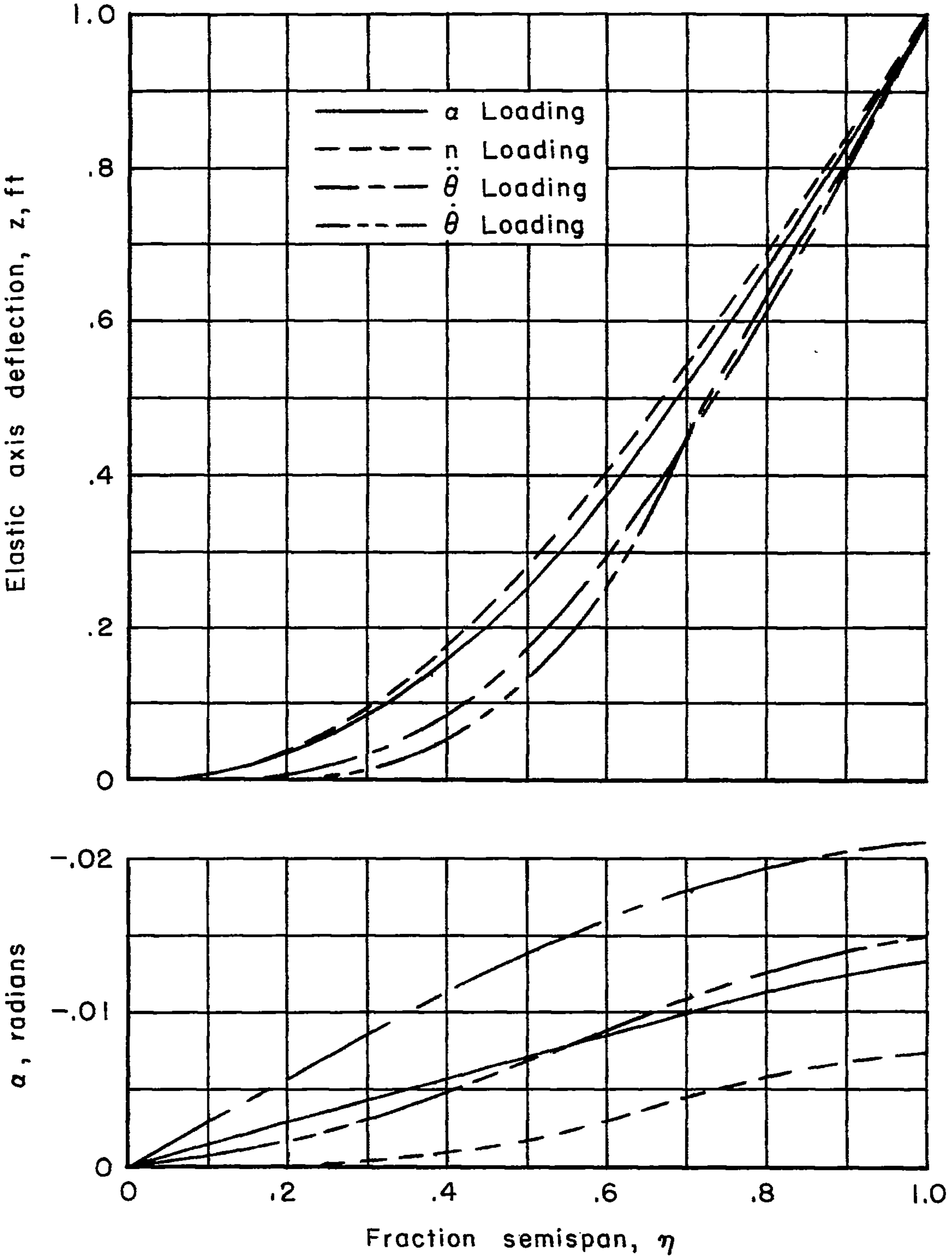

Figure 10.- Comparison of various pseudostatic deflection curves; $q/\beta = 209$, c.g. = 21 percent M.A.C.

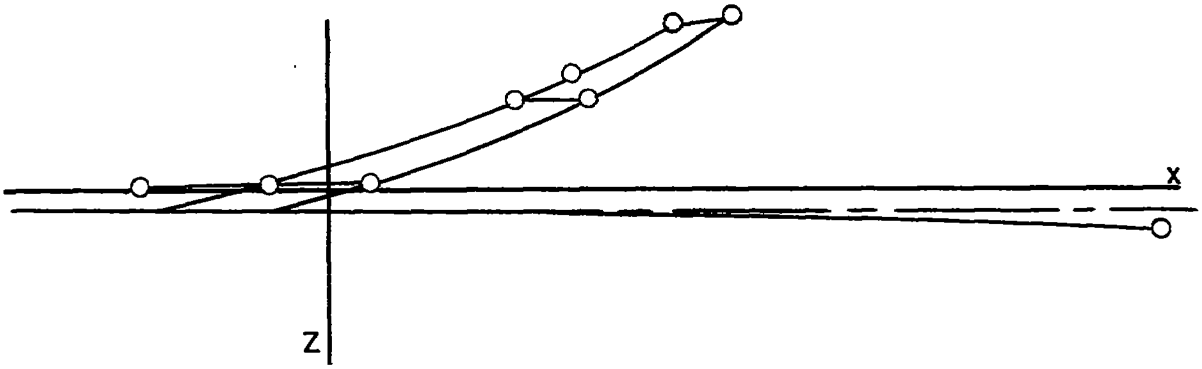

Dominant mode (ω_f = 8.1 radians/sec).

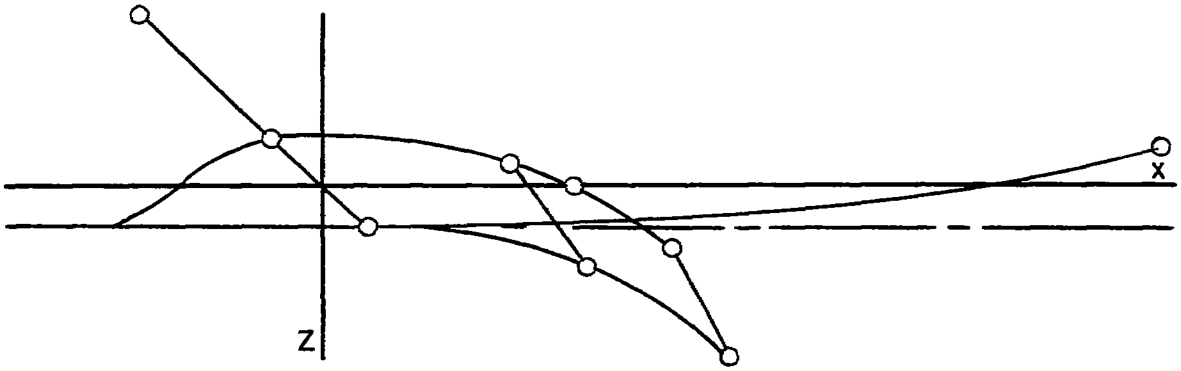

First subdominant mode (ω_f = 22.5 radians/sec).

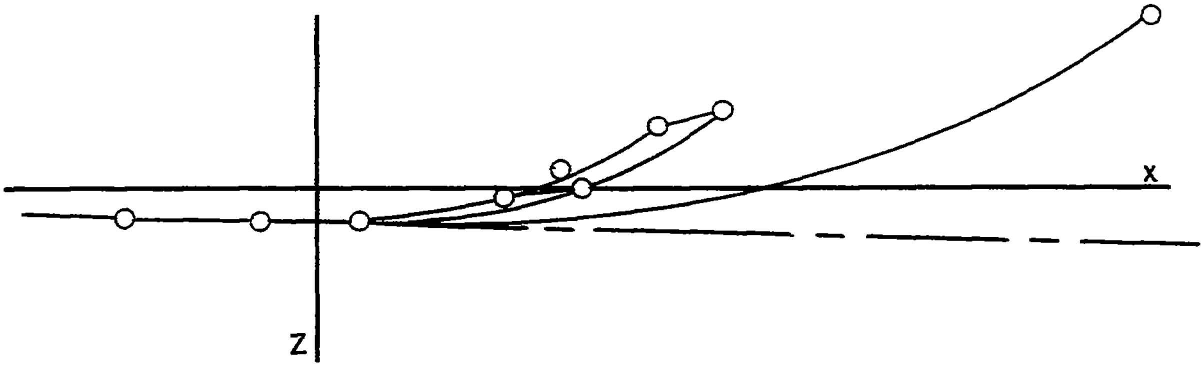

Second subdominant mode (ω_f = 25.0 radians/sec).

Figure 11.- Calculated free-free modes.

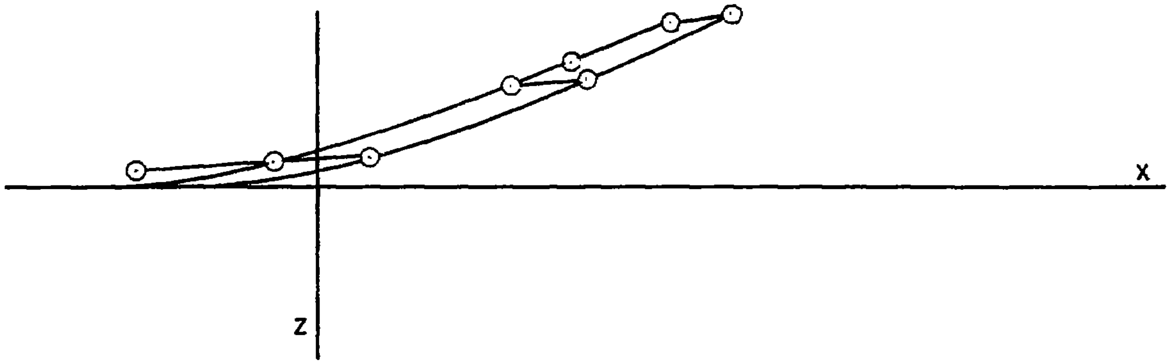

Wing first-bending mode, $\lfloor a_i \rfloor$

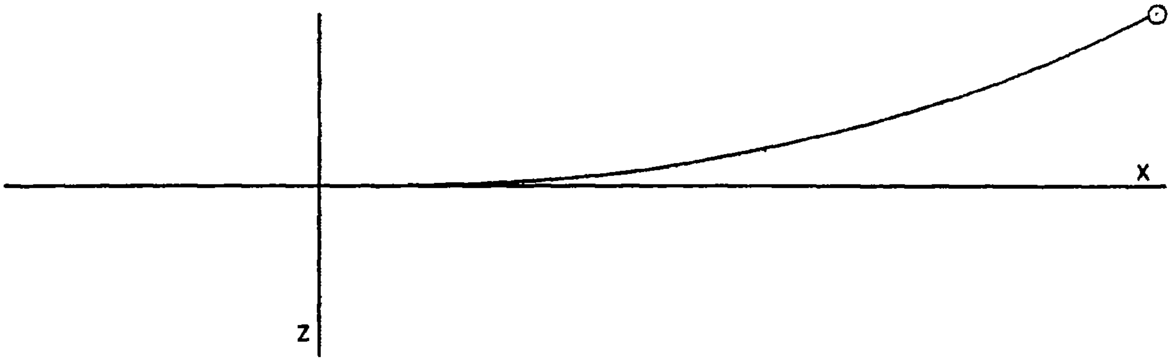

Fuselage first-bending mode, $\lfloor b_i \rfloor$

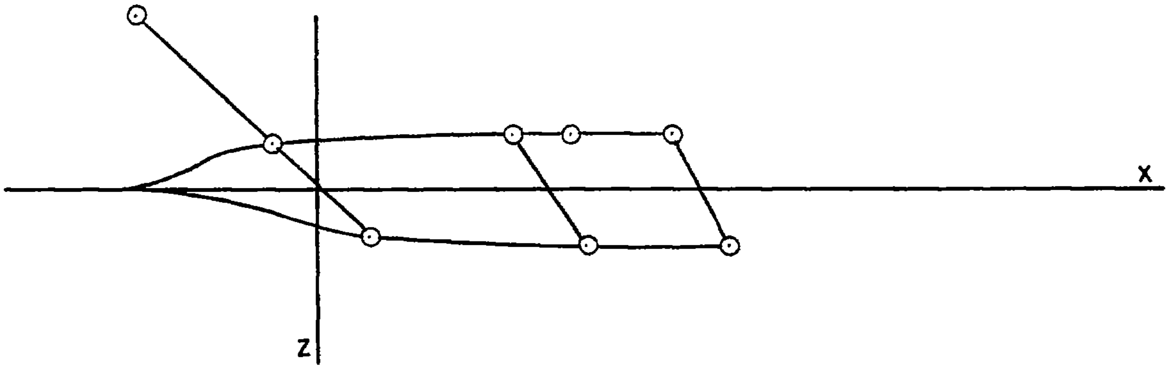

Wing first-torsion mode, $\lfloor c_i \rfloor$

Figure 12.- Deflection coordinates used in the analysis.

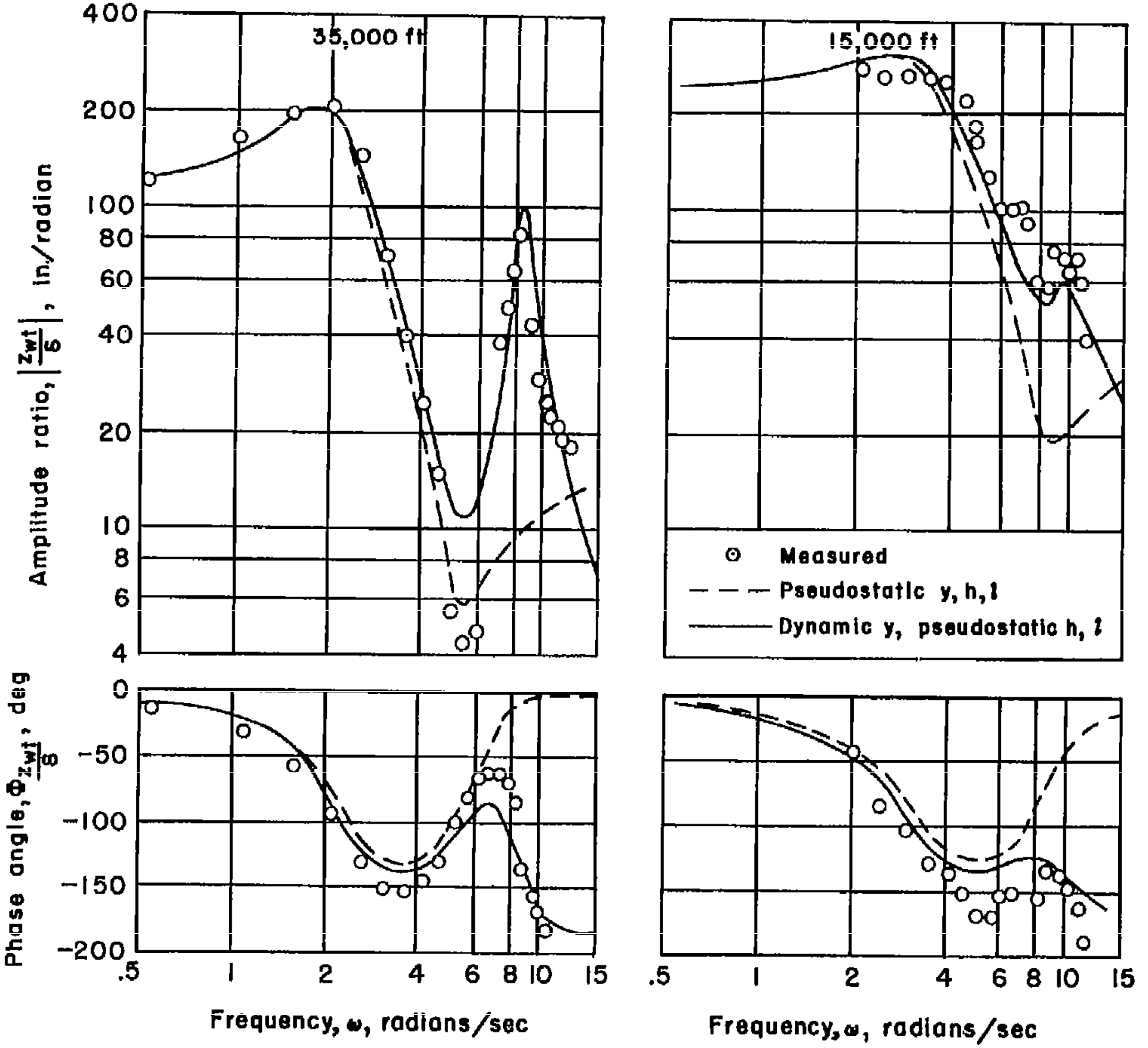

Figure 13.- Wing-tip-deflection frequency response at a Mach number of 0.7.

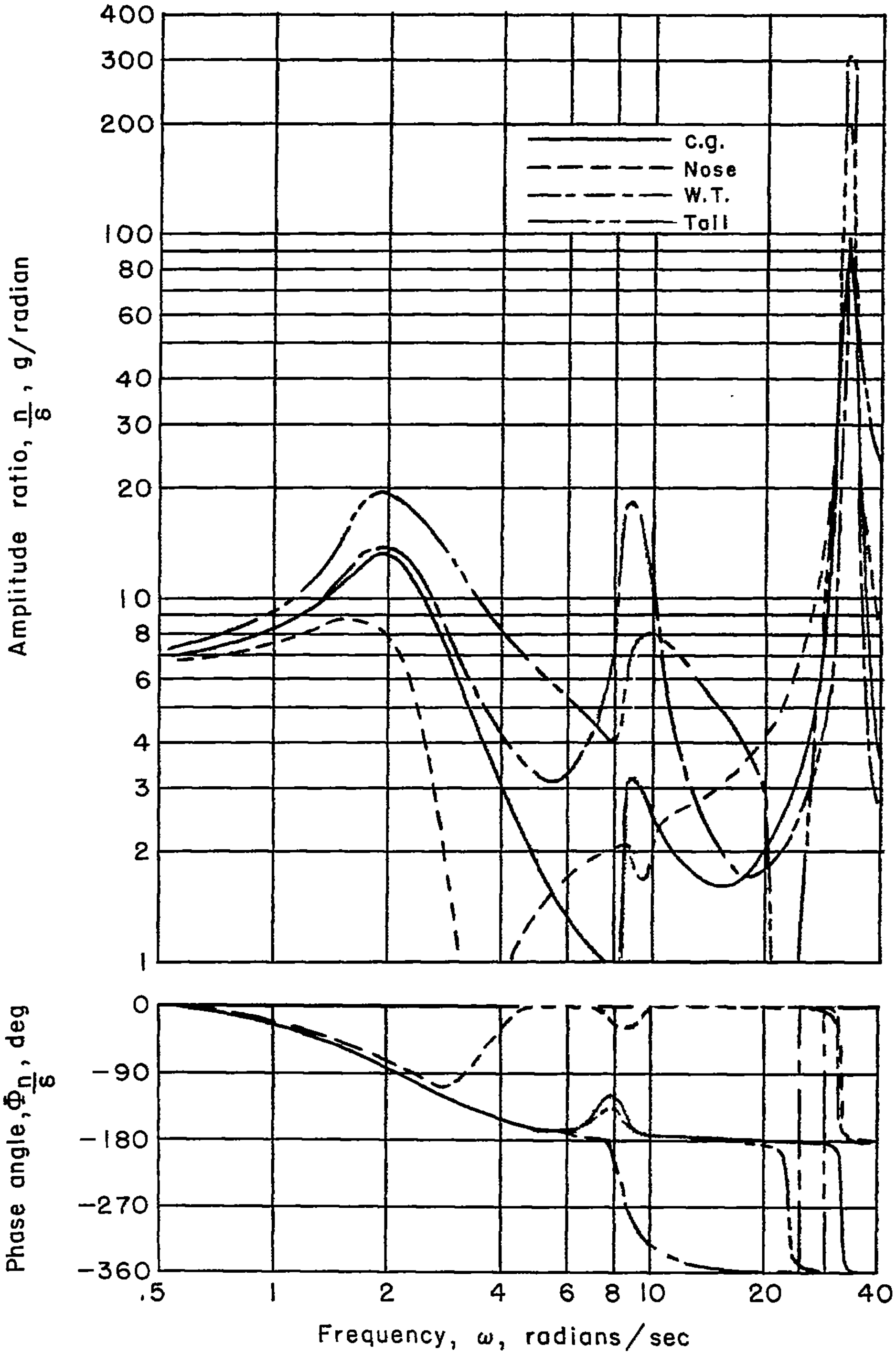

Figure 14.- Predicted frequency responses of acceleration at various points; W = 115,000 pounds, c.g. = 21 percent M.A.C., I_y = 1,450,000 slugs-ft^2, altitude = 35,000 feet, M = 0.7.

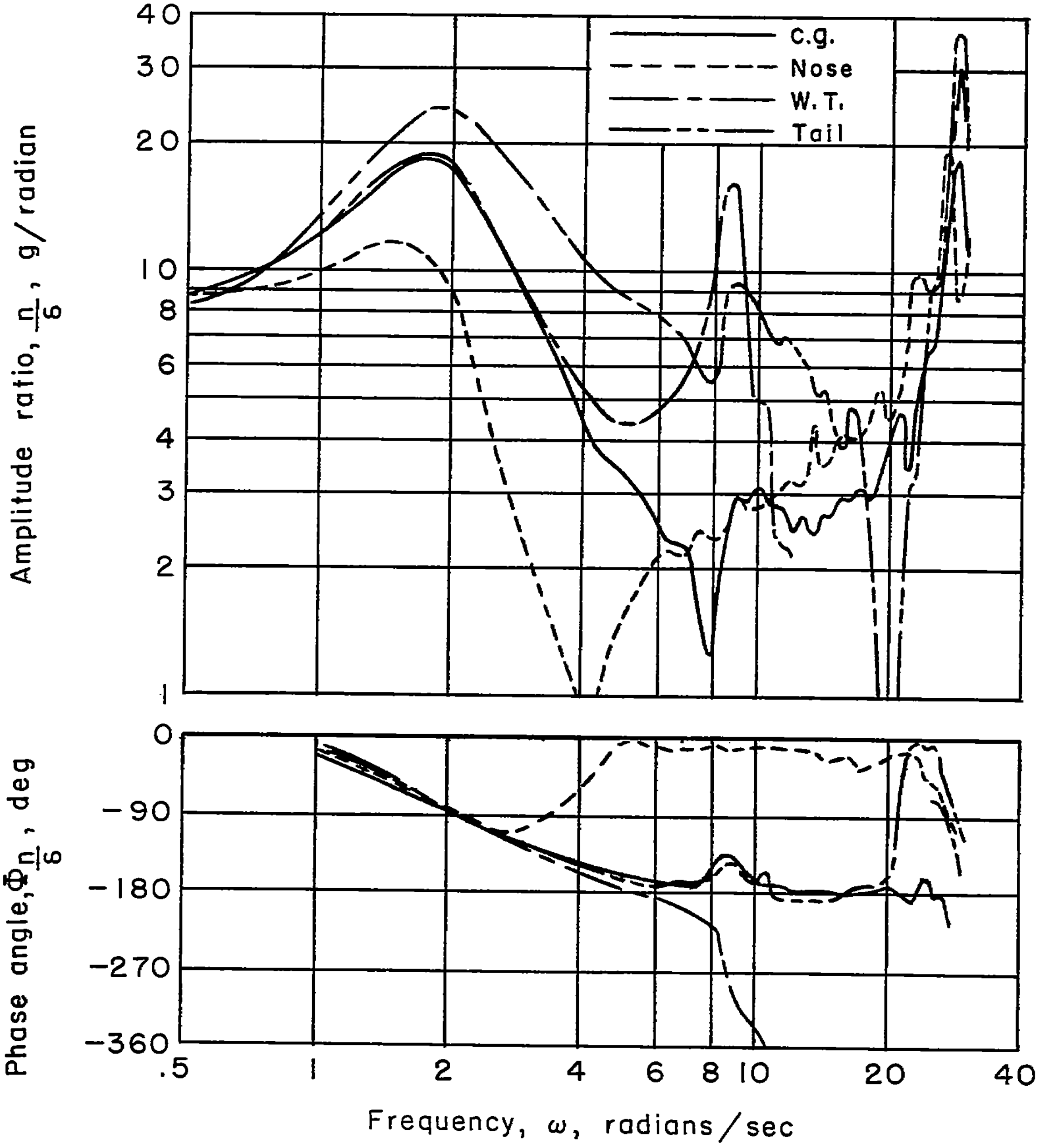

Figure 15.- Measured frequency responses of acceleration at various points; flight 5, run 15.

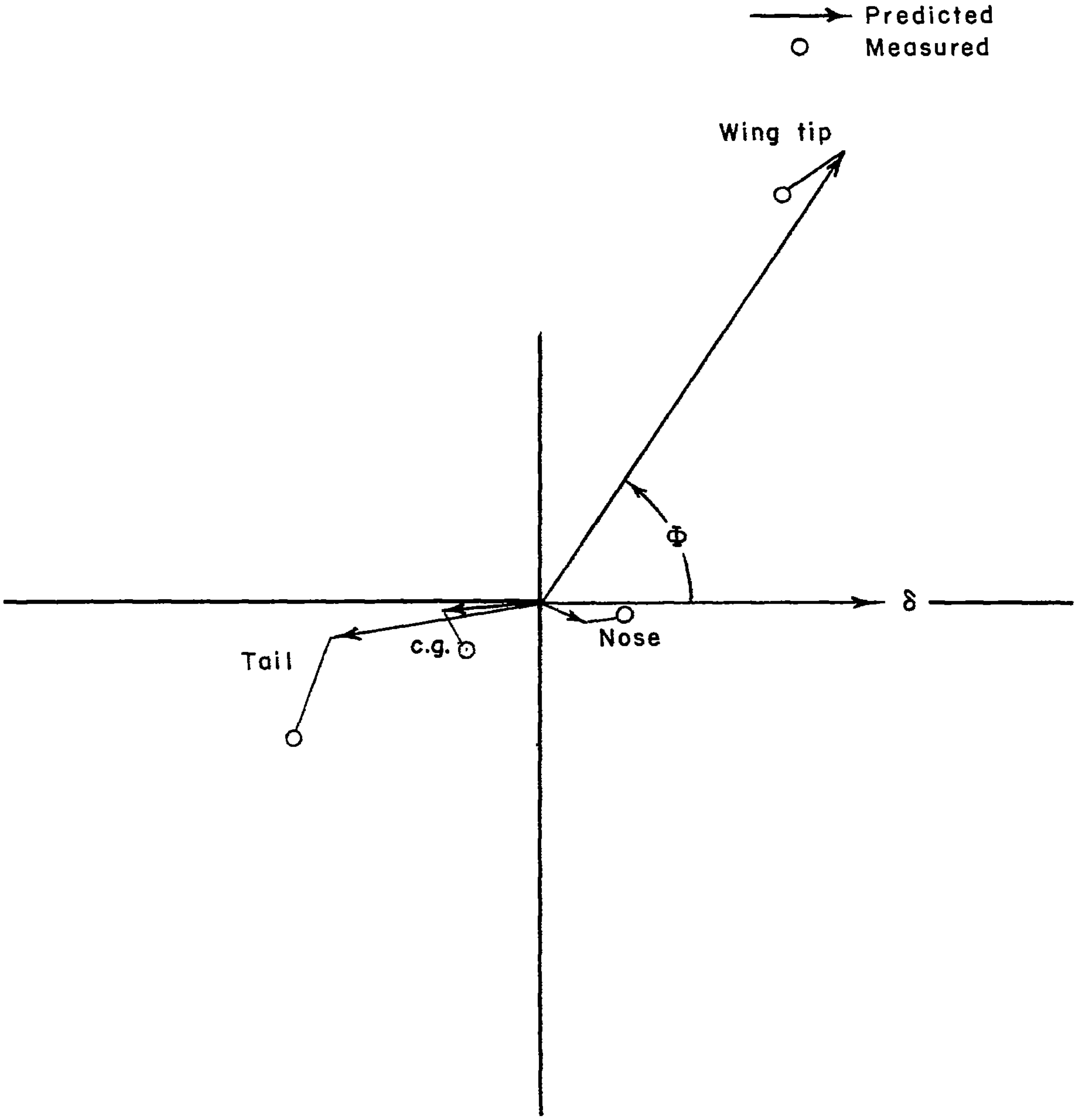

Figure 16.- Amplitude-phase plot of predicted and measured accelerations at wing first-bending mode frequency; ω = 8.9 radians/sec.

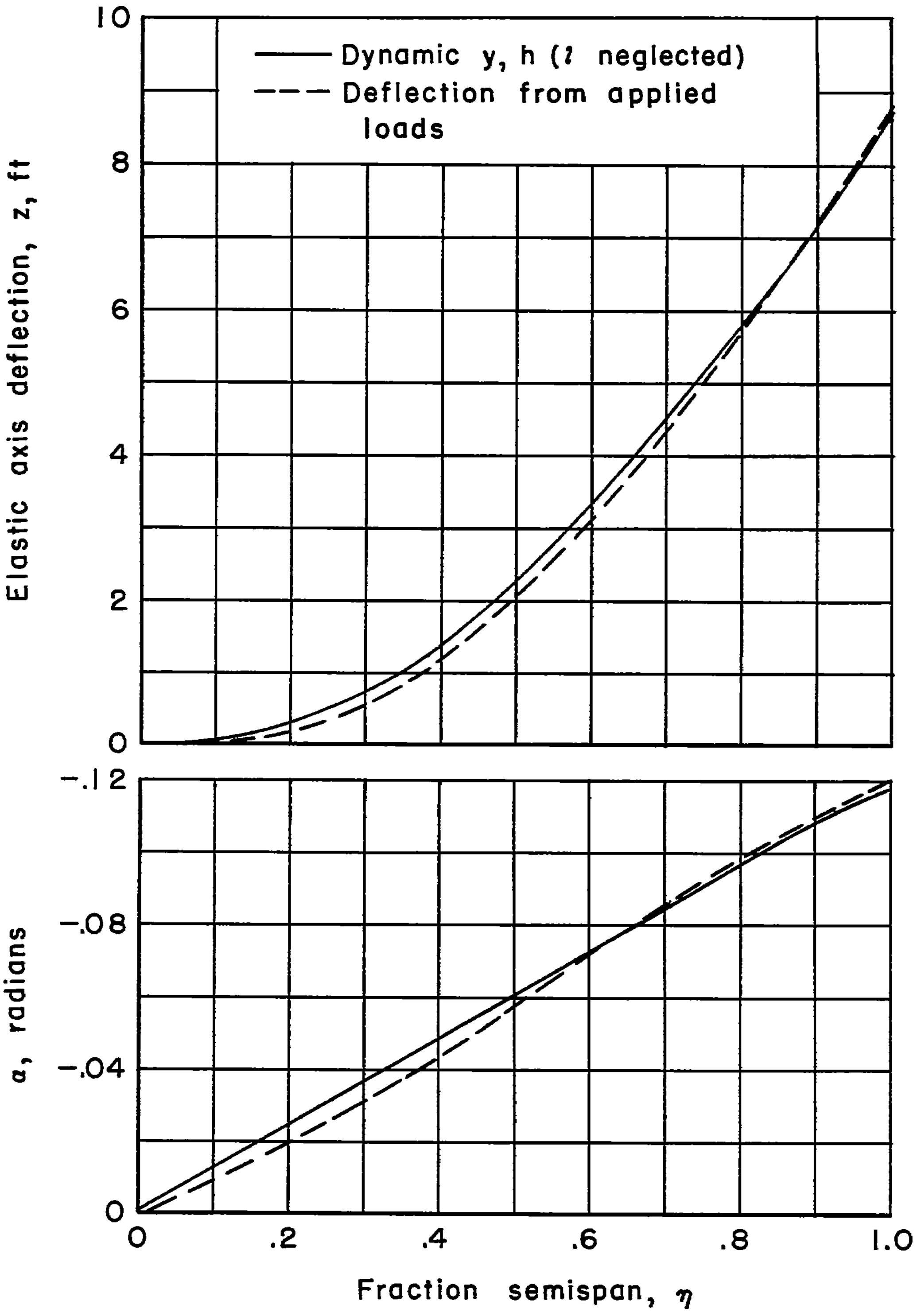

Figure 17.- Deflection check of components in phase with wing tip at wing first-bending mode frequency, per radian of elevator deflection.

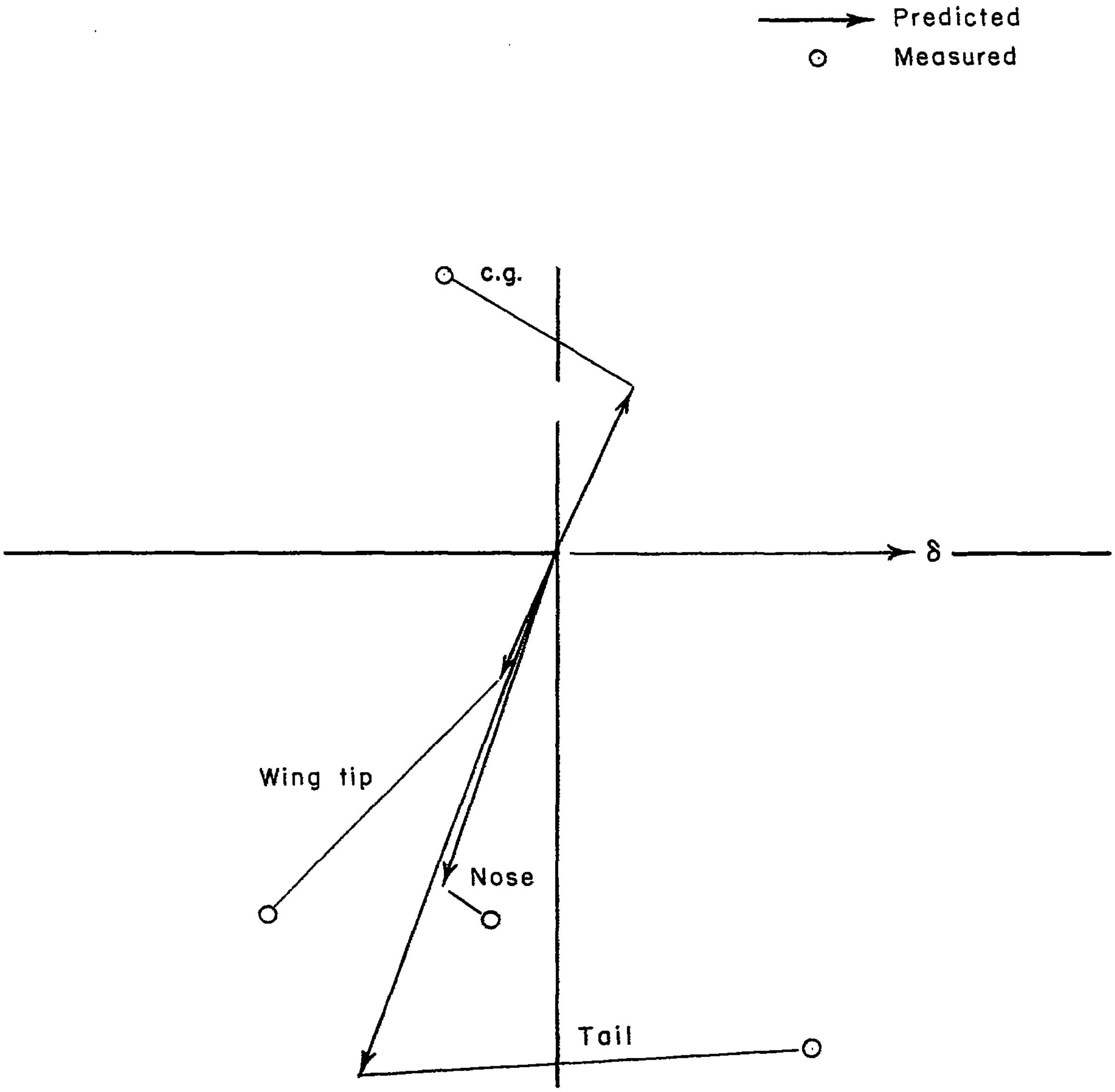

Figure 18.- Amplitude-phase plot of predicted and measured accelerations at fuselage first-bending mode frequency; $\omega = 28.3$ radians/sec.

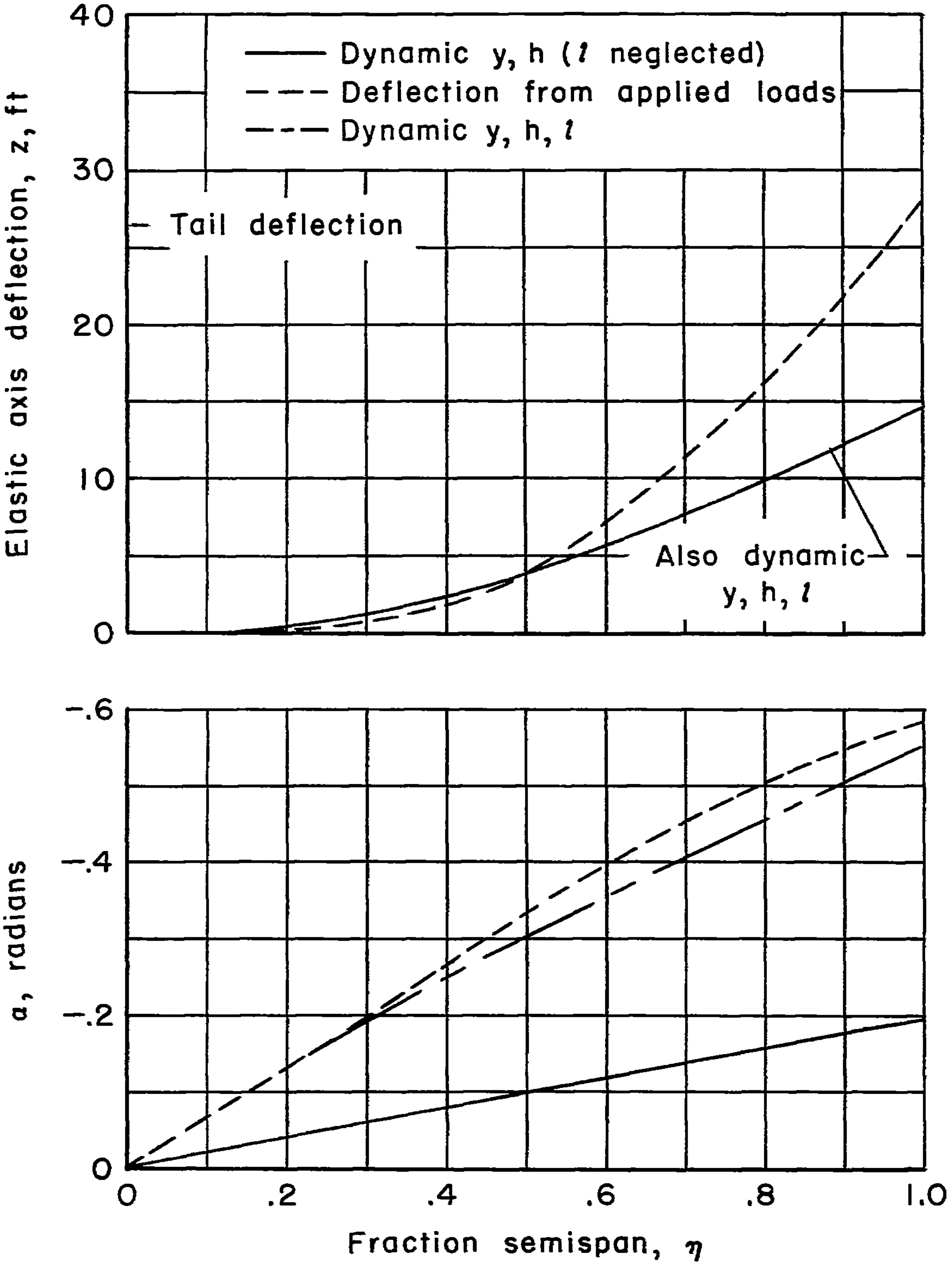

Figure 19.- Deflection check of wing components in phase with tail deflection at fuselage first-bending mode frequency, per radian of elevator deflection.

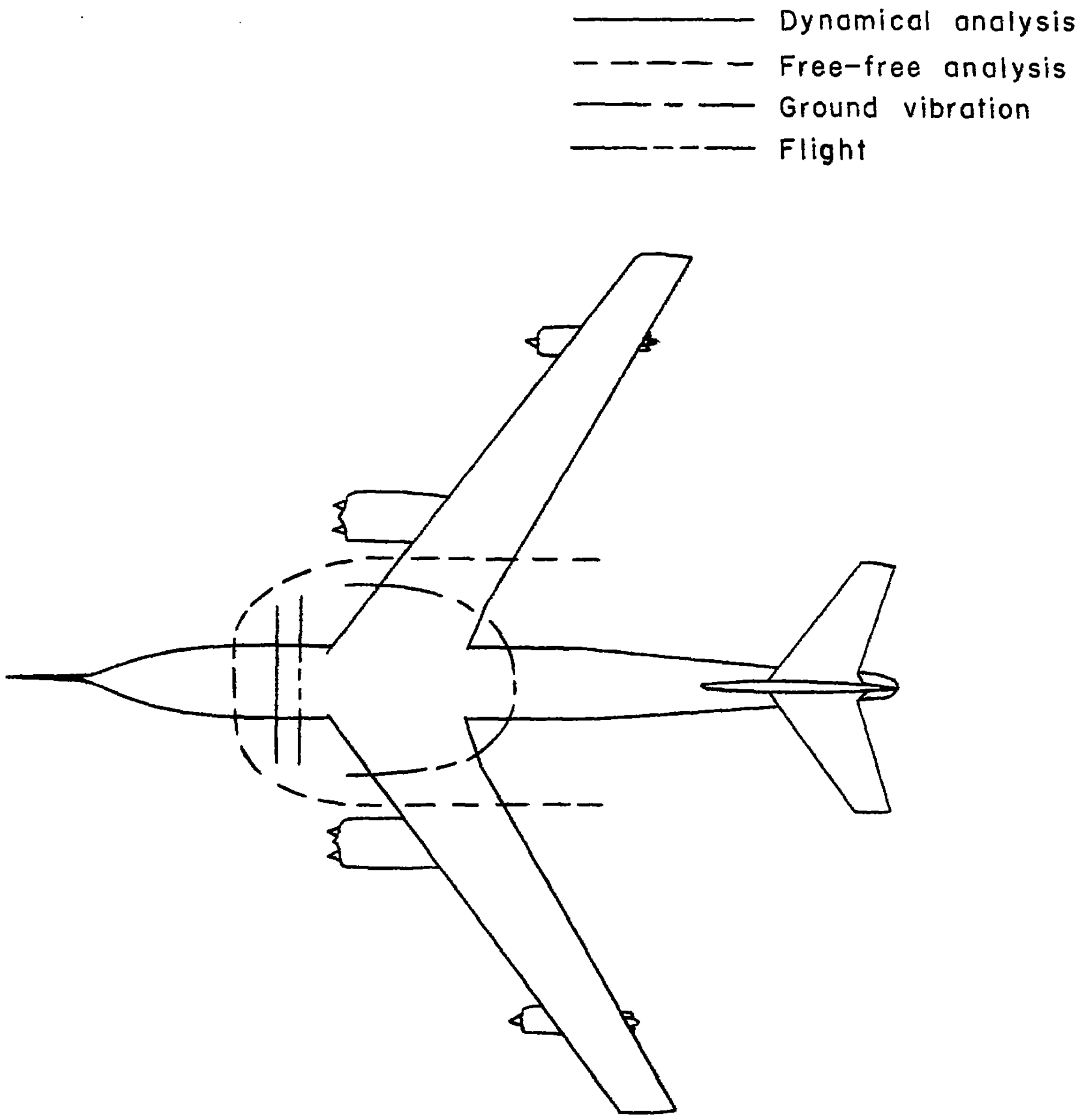
Dynamical analysis
Free-free analysis
Ground vibration
Flight

Figure 20.- Predicted and measured node lines and lines of low response of wing first-bending mode.

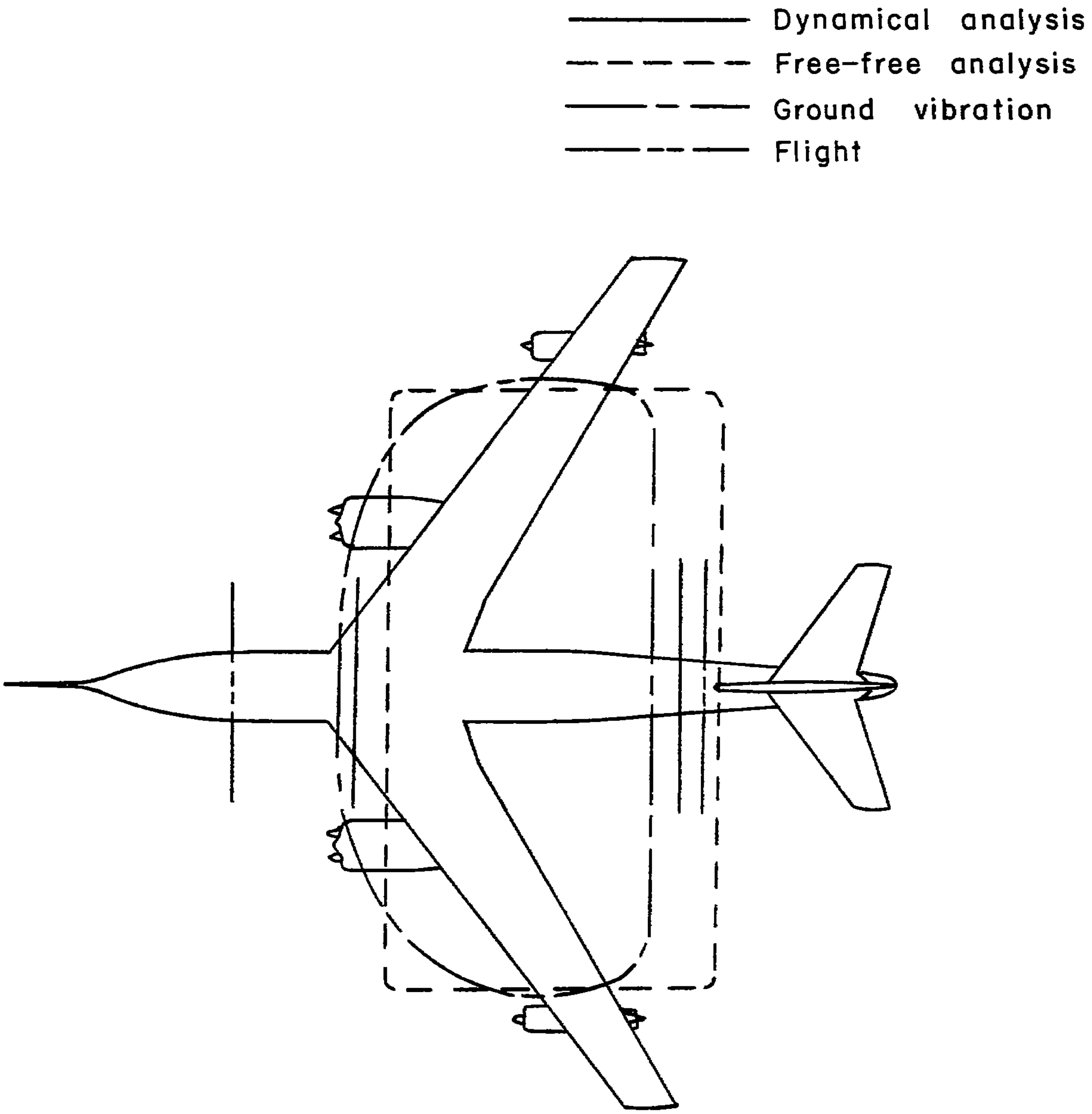
Dynamical analysis
Free-free analysis
Ground vibration
Flight

Figure 21.- Predicted and measured node lines and lines of low response of fuselage first-bending mode.

NACA - Langley Field, Va.